Novel connections between DNA replication, telomere homeostasis and the DNA damage response revealed by a genome-wide screen for *TEL1/ATM* interactions in *Saccharomyces cerevisiae*

Brian D. Piening

A dissertation

submitted in partial fulfillment of the

requirements for the degree of

Doctor of Philosophy

University of Washington

2013

Reading Committee:

Daniel Gottschling, Chair

Amanda Paulovich

Toshiyasu Taniguchi

Program Authorized to Offer Degree:

Molecular and Cellular Biology

University of Washington

Abstract

Novel connections between DNA replication, telomere homeostasis and the DNA damage response revealed by a genome-wide screen for *TEL1/ATM* interactions in *Saccharomyces cerevisiae*

Brian D. Piening

Chair of Supervisory Committee:
Professor Daniel E. Gottschling
Department of Genome Sciences

Tel1p is the budding yeast ortholog of the mammalian tumor suppressor and DNA damage response (DDR) kinase ATM. However, *tel1-Δ* cells, unlike ATM-deficient cells, do not exhibit sensitivity to DNA damaging agents, but do display shortened (but stably maintained) telomere lengths. Neither the extent to which ATM/Tel1p functions in the DDR nor the mechanism by which ATM/Tel1p contributes to telomere metabolism is well-understood. In this dissertation, I present our large-scale transcriptional profiling of normal and ATM-deficient lymphoblast cell lines in response to ionizing radiation (IR). From these results, we make the surprising observation that *ATM*-deficient cells exhibit no significant defects in IR-induced gene expression, which along with work from others suggests that significant redundancy exists in the DNA damage response, and may be an explanation for the relative DNA damage insensitivity in *tel1-Δ* yeast cells. To address this question, I performed a comprehensive genome-wide screen for genetic interactions with *tel1-Δ* that cause sensitivity to MMS and/or ionizing radiation, along with follow-up characterizations of the 13 interactions yielded by this screen.

Surprisingly, many of the *tel1-Δ* interactions that confer DNA damage sensitivity also exacerbate the short telomere phenotype, suggesting a connection between these two phenomena. Restoration of normal telomere length in the *tel1-Δ xxx-Δ* mutants results in only minor suppression of the DNA damage sensitivity, demonstrating that the sensitivity of these mutants must also involve mechanisms independent of telomere length. In support of a model for increased replication stress in the *tel1-Δ xxx-Δ* mutants, I show that depletion of dNTP pools through pre-treatment with hydroxyurea renders *tel1-Δ* cells (but not wild-type) MMS-sensitive, demonstrating that under certain conditions, Tel1p does indeed play a critical role in the DDR.

TABLE OF CONTENTS

TABLE OF FIGURES 6

TABLE OF TABLES 7

ACKNOWLEDGEMENTS 8

CHAPTER 1: Introduction 10

CHAPTER 2: Transcriptional profiling of the ionizing radiation (IR) response in normal and *ATM*-deficient human lymphoblasts. 18

ABSTRACT 18

INTRODUCTION 18

MATERIALS AND METHODS 21

RESULTS 27

DISCUSSION 37

CHAPTER 3: Results and characterizations from a genome-wide screen for TEL1/ATM interactions in *S. cerevisiae* 66

ABSTRACT 66

INTRODUCTION 66

MATERIALS AND METHODS 67

RESULTS 71

DISCUSSION 81

CHAPTER 4: Conclusions and future directions 103

OVERVIEW 103

SHORT TELOMERES AND DNA DAMAGE SENSITIVITY 104

EXPLORING THE ROLE OF Tel1p IN RESPONSE TO REPLICATION STRESS 105

CONSERVATION OF *ATM/TEL1* INTERACTIONS IN MAMMALIAN CELLS 106

REFERENCES 109

VITA 119

TABLE OF FIGURES

Figure 1. Western blotting for P53 phosphorylation in ATM+/+ and ATM-/- cells. 61
Figure 2. Radiation-repressed (RR) or radiation–induced (RI) gene signatures cluster breast cancer patients from the Netherland Cancer Institute according to clinical outcome. 62
Figure 3. Radiation-repressed (RR) or radiation–induced (RI) gene signatures cluster breast cancer patients from Loi *et al*. according to clinical outcome. 63
Figure 4. Comparison of tumor classification by gene expression signatures. 64
Figure 5. Parallels between the molecular stages of tumorigenesis and the DNA damage response. 65
Figure 6. Quantitative survival analysis for *tel1* interactions in MMS via colony-forming assay. 91
Figure 7. Quantitative survival analysis in IR. 92
Figure 8. Quantitative survival analysis using continuous low dose-rate IR. 93
Figure 9. Telomerase-null cells exhibit a progressive increase in MMS sensitivity. 94
Figure 10. Southern blot for telomere lengths of TLC1 and tlc1 haploid spores. 95
Figure 11. Telomere lengths for tel1-Δ MMS-sensitive interactions. 96
Figure 12. Repeated subculturing does not alter telomere lengths. 97
Figure 13. MMS sensitivity with or without the CDC13-EST2 fusion construct. 98
Figure 14. Suppression of MMS sensitivity in rad24-Δ tel1-Δ and rad17-Δ tel1-Δ by a CDC13-EST2 fusion plasmid. 99
Figure 15. HO-induced translocation frequency for tel1-Δ interactions. 100
Figure 16. Gross chromosomal rearrangement (GCR) frequency in 0.003% MMS. 101
Figure 17. MMS sensitivity following pretreatment with hydroxyurea 102
Figure 18. A model for Tel1p/ATM-mediated suppression of MMS sensitivity. 108

TABLE OF TABLES

Table 1. Radiation repressed genes in response to 5 Gy IR. 44
Table 2. Radiation-induced genes after IR. 48
Table 3. Enrichment of GO categories for the radiation-induced genes. 48
Table 4. Enrichment of GO categories in the unirradiated samples. 49
Table 5. Enrichment of clinical parameters in radiation-induced and radiation-repressed gene sets by GSEA. 50
Table 6. P53-dependent targets in the RI set. 51
Table 7. Differential expression of genes in breast tumor lines before and after 8 Gy of IR. 55
Table 8. Analysis of risk factors for death in breast cancer patients in the NKI study. 56
Table 9. Analysis of risk factors for death in breast cancer patients in the Loi *et al.* study. 57
Table 10. Overlap of RR and RI gene signatures with other breast cancer outcome signatures. 58
Table 11. Error rate and sensitivity from leave-one-out cross validation. 59
Table 12. Segregation of tumor samples into 4 groups based on their classification by gene expression signatures. 59
Table 13. P-values for the association between clinical variables and group labels in Table 12. 60
Table 14. *Saccharomyces cerevisiae* strains used in this study. 89
Table 15. Tabulation of phenotypes uncovered in this study. 90

ACKNOWLEDGEMENTS

A portion of the material in Chapter 2 appears in Piening *et al.* (PIENING *et al.* 2009) and includes contributions from Pei Wang and Aravind Subramanian (statistical analyses). In addition, cell culture and microarray data generation was performed by Amanda Paulovich. Western blots were generated by Richard Ivey. Permission to republish this work has been granted by the copyright holder.

A portion of the material in Chapter 3 appears in Piening *et al.* (PIENING *et al.* 2013) and includes contributions from Dongqing Huang (assistance with Synthetic Genetic Array technology and training at the bench) and Amanda Paulovich (mentorship & training). Permission to republish this work has been granted by the copyright holder.

I would like to thank the members of the Paulovich laboratory for many years of friendship, frequent collaboration, technical assistance and intellectual guidance. My utmost appreciation goes out to Richard Ivey and Dongqing Huang who have been fantastic mentors in the lab.

I would like to offer my sincerest gratitude to those who guided me during the initial steps of my training at the bench. This includes Toshiyasu Taniguchi, Celine Jacquemont, Sue Amundsen, Gerry Smith and Akiko Murakami-Sekimata; thank you for taking the time and effort to train a young scientist!

I wish to thank the labs that comprise the Seattle yeast community for an incredibly open and fertile exchange of ideas. Extra thanks goes out to members of the Gottschling, Brewer/Raghuraman, Davis, Smith and Biggins labs for allowing me to participate in lab meetings, sharing strains and equipment, help with experimental design and being such an all-around cordial group of colleagues. I feel very privileged to be part of this community.

My sincerest gratitude to my graduate committee, Dan Gottschling, Trisha Davis, Mary-Claire King, Toshiyasu Taniguchi and Pei Wang. You all have provided an incredible amount of guidance and support during my studies.

I wish to thank those responsible for funding me during my graduate study via the FHCRC dual mentor program and the Department of Defense Breast Cancer Research Program.

Many thanks to those who have shared strains and plasmids that were used in my experiments: Dan Gottschling, Vicki Lundblad, Elizabeth Blackburn and Sang-Eun Lee.

I owe a tremendous amount of gratitude to Pei Wang, who has been an incredible mentor for all things computational and statistical, and a frequent and productive collaborator.

To Norm McCormick, professor emeritus of Mechanical Engineering at UW, thank you for introducing me to academic research.

Thanks to the trio of intrepid undergraduate students I have had the privilege of mentoring during my time here, Corey Jones-Weinert, Jose Mendiola and Carolyn Chen; you will be successful in any endeavor you choose.

Thanks to my always-supportive wife Leah for her love and patience during my training; for often structuring our personal life around the exponential growth cycles of unicellular fungi and for uprooting your career and personal life so that I can continue to pursue this dream at Stanford.

Extra thanks go out to my parents Jeannette and Don Piening for their love and support and for spending so much time teaching me at a very early age. You gave me a tremendous head start. To my brother Kevin, for following his own dream!

Lastly, my utmost thanks goes out to Mandy Paulovich, who many years ago took a chance on hiring an inexperienced young undergraduate into a critical role in her lab. Mandy, your unbridled enthusiasm for science and your dogged pursuit of improvements on how we detect and treat cancer has provided inspiration to me from day one. It is amazing to think about how differently my career would have turned out had I not met you. If I can be half the scientist that you are today, I will have a very successful career!

CHAPTER 1: Introduction

ATM: spearheading the DNA damage response

The ATM tumor suppressor kinase is a major signaling component of the DNA damage response (DDR) pathway, and patients with homozygous *ATM* mutations are afflicted with the cancer-prone disorder Ataxia Telangiectasia (AT) (SAVITSKY *et al.* 1995; SHILOH 2003). It is estimated that as much as 3% of the population carry a mutant ATM allele (SWIFT *et al.* 1986), and carriers are at an elevated risk of developing breast cancer (RENWICK *et al.* 2006; THOMPSON *et al.* 2005). ATM frequently undergoes somatic mutation in cancer, and based on estimates of positive selection pressure, these mutations are thought to drive tumorigenesis (GREENMAN *et al.* 2007). *ATM*-deficient cell lines are sensitive to DNA damage, exhibit pronounced checkpoint and double-strand break (DSB) repair defects (KASTAN *et al.* 1992; KUHNE *et al.* 2004; PAINTER and YOUNG 1980) and exhibit significantly reduced phosphorylation levels of DDR targets (CANMAN *et al.* 1998). Cells from AT patients exhibit accelerated telomere shortening (METCALFE *et al.* 1996) and ATM is thought to play a role in telomere length regulation through interactions with telomere binding proteins (WU *et al.* 2007).

In the absence of DNA damage, ATM exists in the cell as an inactive dimer (BAKKENIST and KASTAN 2003). Following the generation of DSBs, ATM is recruited to sites of DNA damage by the Mre11-Rad50-Nbs1 DNA end-binding complex and its kinase function is activated (LEE and PAULL 2004; UZIEL *et al.* 2003). This activation requires ATM acetylation at K3016 by the histone acetyltransferase and tumor suppressor Tip60 (SUN *et al.* 2005; SUN *et al.* 2010; SUN *et al.* 2007). Following acetylation, ATM activation also requires autophosphorylation at multiple sites and monomerization (BAKKENIST and

KASTAN 2003; KOZLOV *et al.* 2006). Activated ATM then initiates an incredibly complex signaling cascade involving numerous targets in the coordination of checkpoint activation and DNA repair initiation (LAVIN 2008; SHILOH 2003). Our knowledge of the myriad ways by which ATM influences the DDR are simplistic at best, and in all likelihood the coming years will provide an immense increase in novel connections between ATM and diverse cellular mechanisms. As an example, work in the past few years has shown that in response to oxidative stress, an alternative form of active ATM is generated through the formation of a disulfide bridge targeting C2991; this activation does not require the MRN complex nor the presence of DNA DSBs (GUO *et al.* 2010a; GUO *et al.* 2010b). Moreover, recent work by Kastan and colleagues has shown that ATM is recruited to dysfunctional mitochondria and loss of *ATM* is associated with an increase in mitochondrial ROS through a defect in targeting mitochondria for mitophagy (VALENTIN-VEGA and KASTAN 2012; VALENTIN-VEGA *et al.* 2012). In all likelihood further characterization of these novel mechanisms will provide a significant increase in our understanding of how ATM prevents tumorigenesis.

TEL1 is the *Saccharomyces cerevisiae ATM* ortholog

The *Saccharomyces cerevisiae* ortholog for mammalian *ATM* is *TEL1* (GREENWELL *et al.* 1995; MALLORY and PETES 2000; MORROW *et al.* 1995). Like ATM, Tel1p is recruited to DSBs via an interaction with the Mre11-Rad50-Xrs2 DNA-binding complex (NAKADA *et al.* 2003) and Tel1 both facilitates efficient end-resection through an unknown mechanism and participates in phosphorylation of downstream DDR substrates (MANTIERO *et al.* 2007). Following DSB resection, the related kinase Mec1 (ATR in mammals (CIMPRICH *et*

al. 1996)) recognizes RPA-coated ssDNA at ssDNA-dsDNA junctions via an interaction with Ddc2, and the DNA damage checkpoint is activated (PACIOTTI *et al.* 2000). The distinct sensing of double-strand and single-strand damaged DNA structures by Tel1p and Mec1p bears a striking resemblance to the different roles of their ATM and ATR counterparts in mammalian cells (LEE and PAULL 2007; ZOU and ELLEDGE 2003). However, while the loss of *MEC1* results in severe sensitivity to DNA damaging agents (WEINERT *et al.* 1994), Tel1p is not functionally required for checkpoint activation in response to intrachromosomal DSBs, and the loss of *TEL1* does not significantly sensitize cells to DNA damaging agents (GREENWELL *et al.* 1995; MORROW *et al.* 1995). Despite this, a *mec1 tel1* double mutant is more sensitive to DNA damage than the *mec1* single mutant. These results demonstrate that although *MEC1* plays the predominant role at intrachromosomal DSBs, *TEL1* does play some role in response to DNA damage in a *mec1* background (MORROW *et al.* 1995).

TEL1/ATM functions in telomere maintenance

Telomeres are comprised of repetitive, G-rich DNA elements (300-400 bp in yeast; multiple kilobases in mammals) and bound proteins that prevent these ends from being recognized as DNA double-strand breaks (DSBs) by the DNA damage response (DDR). In order to counteract the progressive end-shortening associated with semi-conservative DNA synthesis, eukaryotes employ the reverse transcriptase ribonucleoprotein complex telomerase, which synthesizes new repeat DNA at chromosomal ends (GREIDER and BLACKBURN 1985). In most human tissues however, telomerase is not expressed and progressive telomere shortening confers a limit to replicative life span, termed the Hayflick

limit (HAYFLICK and MOORHEAD 1961); this is thought to serve as an antitumor mechanism (HANAHAN and WEINBERG 2000). However, cells that have entered replicative senescence due to excessive telomere shortening can in rare cases escape senescence and gain the ability to maintain telomeres via recombination, in a process dubbed Alternative Lengthening of Telomeres (ALT) (LUNDBLAD and BLACKBURN 1993; TENG and ZAKIAN 1999).

While Mec1p appears to be the primary responder to DNA damage (with Tel1p functioning in a back-up role), their respective roles are reversed at telomeres. In *Saccharomyces cerevisiae,* the telomerase enzyme preferentially associates with short telomeres for elongation through an interaction with Cdc13, and this preferential association is dependent on *TEL1* and the MRX complex (SABOURIN *et al.* 2007). MRX recruits Tel1p to DNA ends (FUKUNAGA *et al.* 2011), at which Tel1p phosphorylates one or more substrates to facilitate telomerase recruitment by Cdc13 via an as yet poorly understood mechanism (GAO *et al.* 2010; MARTINA *et al.* 2012). *tel1* mutant cells exhibit a decreased frequency of telomere elongation events and decreased telomerase processivity at telomeres (ARNERIC and LINGNER 2007; CHANG *et al.* 2007) that leads to progressive telomere shortening (GREENWELL *et al.* 1995; MALLORY and PETES 2000). Telomeres in *tel1* cells are shortened but are stably maintained; this depends on *MEC1* (RITCHIE *et al.* 1999). Telomere erosion in a *mec1 tel1* mutant leads to aneuploidy, senescence, and cell death (CRAVEN *et al.* 2002; MCCULLEY and PETES 2010; VERNON *et al.* 2008). Despite the requirement for *MEC1* in telomere homeostasis in the absence of *TEL1*, Mec1p is not detected at telomeres in wild-type or *tel1-Δ* cells, and the specific role

Mec1p plays in facilitating telomere maintenance in the absence of *TEL1* is not yet understood (MCGEE *et al.* 2010).

Unanswered questions regarding the role(s) of *ATM/TEL1*

Proteomic analyses have recently revealed that the substrate network targeted by ATM/Tel1 after DNA damage is vast. In a large scale screen of ATM/ATR substrates utilizing antibodies recognizing the characteristic –SQ/TQ motif, Matsuoka *et al.* described over 700 proteins that were phosphorylated in response to DNA damage (MATSUOKA *et al.* 2007). Accordingly, another recent screen in budding yeast uncovered a large number of novel Mec1/Tel1-dependent phospho-substrates (SMOLKA *et al.* 2007); taken together these results suggest that the cellular functions under ATM/ATR and Mec1/Tel1 control are numerous. In addition, while Mec1 has been shown to be the primary kinase responsible for phosphorylation of a number of Mec1/Tel1 substrates including the checkpoint kinase Rad53 (SUN *et al.* 1996), a Tel1-specific screen has not yet been performed and it is unknown whether a subset or perhaps different set of substrates are phosphorylated in a Tel1-dependent manner. Supporting this, loss of *TEL1* confers a defect in the MMS-dependent phosphorylation of the Ies4 subunit of the INO80 chromatin remodeling complex, while loss of *MEC1* does not (MORRISON *et al.* 2007).

For Tel1p's role in both the DDR and telomere metabolism, significant questions remain. While Tel1p is often thought to be functionally redundant with Mec1p in the DDR, recent studies have identified distinct Mec1-independent roles for Tel1p in checkpoint signaling (MANTIERO *et al.* 2007), replication fork stability (DOKSANI *et al.* 2009) and in the suppression of genome rearrangements (LEE *et al.* 2008). None of the mechanisms

underlying these roles are well-understood. At telomeres, the straightforward model consisting of Tel1p phosphorylation of Cdc13 leading to a conformational change that allows for recruitment of the Est1 subunit of telomerase has recently given way to more complex interactions potentially involving multiple kinases, rates of telomere end-resection and other, possibly novel intermediates (GAO *et al.* 2010; MARTINA *et al.* 2012; WU *et al.* 2013). Moreover, the mechanism(s) by which MRX and Tel1 are targeted to short telomeres is poorly understood but likely involves constituents of the shelterin complex (MARCAND *et al.* 1997; TEIXEIRA *et al.* 2004).

Aim and significance of my dissertation research

Despite recent characterizations of Mec1-independent roles for Tel1p in the DDR, these roles are apparently either non-essential, infrequently utilized or redundant with other pathways as the fact remains that the loss of *TEL1* alone does not confer sensitivity to DNA damaging agents. Thus, it remains a formal possibility that in addition to a strong genetic interaction with *MEC1* in response to DNA damage (GREENWELL *et al.* 1995; MALLORY and PETES 2000; MORROW *et al.* 1995; RITCHIE *et al.* 1999), additional genetic backgrounds exists in which Tel1 function is required. In this dissertation, I describe first the results of data analysis I performed (along with work from my colleagues Pei Wang and Aravind Subramanian) of a large microarray dataset consisting of normal and *ATM*-deficient cell lines treated with IR (Chapter 2). From this, we made the surprising observation that *ATM*-deficient cells, despite significant radiosensitivity, do not exhibit a significant defect in the transcriptional response to IR. Despite this, we culled from these data a set of radiation-responsive transcripts that as a signature for gene expression show

significant prognostic capability for outcome in breast cancer patients. Our microarray data further support the hypothesis that genetic interactions may suppress the effects of loss of *ATM/TEL1.*

Following these additional observations, I generated a genome-wide genetic interaction library for *tel1-Δ* interactions in the budding yeast and screened for interactions that cause IR- and MMS-sensitivity (Chapter 3). From these screens, I found that a diverse set of mutants interact with *tel1-Δ* to cause synergistic DNA damage sensitivity. Due to the diversity of the identified *tel1-Δ xxx-Δ* interactions, I was surprised to find that the vast majority of these interactions also contributed to further shortening telomeres in *tel1-Δ* cells. This work has revealed a surprisingly complex interplay between DNA metabolism, cellular dNTP levels and telomere lengths that underlie the DNA damage sensitivity of *tel1-Δ* interactions.

An overarching goal of this work and related work in the Paulovich laboratory is to uncover the so-called “missing-heritability” underlying genetic susceptibility to breast cancer. In short, despite prior success stories in identifying individual highly-penetrant breast cancer susceptibility loci such as *BRCA1* and *BRCA2* (MIKI *et al.* 1994; WOOSTER *et al.* 1995), these cases represent a minority of breast cancer incidence. While twin and family studies reveal a strong genetic component for risk to so-called “common” forms of breast cancer (PETO and MACK 2000), large-scale GWAS efforts to map out this missing genetic component have been largely unsuccessful. While work is currently being undertaken to pursue exceedingly rare variants using next-generation sequencing-based approaches, an alternative hypothesis is that the genetic component underlying cancer susceptibility is due to gene-gene interactions, either due to the cumulative effect of

additive interactions of perhaps many mutant alleles or due to a strong synergistic effect between a small number of alleles (MANOLIO *et al.* 2009). Due to the combinatorial problem of accounting for two or more interacting variants genome-wide, even the large sample sizes associated with current GWAS and next-gen studies are ill-suited to this approach. Recent work from the Kruglyak lab has demonstrated that *Saccharomyces cerevisiae* is an ideal model system for mapping out such interactions, as large numbers of segregants can be rapidly genotyped and interacting QTLs can be efficiently mapped (BLOOM *et al.* 2013; EHRENREICH *et al.* 2012; EHRENREICH *et al.* 2010). Applying this methodology across a large number of quantitative traits, Bloom *et al.* observed both multi-gene additive effects and two-gene synergism for a variety of traits (BLOOM *et al.* 2013). Alternatively, one may take a more directed approach and screen for genetic interactions in yeast with one or more fixed gene deletions. The Synthetic Genetic Array (SGA) approach, developed by the Boone laboratory (TONG and BOONE 2006; TONG *et al.* 2001), leverages the non-essential yeast gene deletion collection to generate via a series of massively parallel mating and sporulation steps a set of double-knockout strains for identifying additive or synthetic interactions. This is the approach we have taken in the lab and the *ATM/TEL1* interaction screen is part of a larger, ongoing project in which we have performed MMS-dependent interaction screens for the *BRCA1/53BP1* ortholog *RAD9* (MURAKAMI-SEKIMATA *et al.* 2010) and the *XRCC3* ortholog *RAD57* (HUANG *et al.* 2013). While there is significant ongoing work in the lab to detect these gene-gene interaction effects via a targeted approach in large breast cancer datasets, we have shown that at least a subset of these DNA-damage-sensitive interactions can be recapitulated in human breast epithelial cells (Hu HM *et al.,* in preparation).

CHAPTER 2: Transcriptional profiling of the ionizing radiation (IR) response in normal and *ATM*-deficient human lymphoblasts.

ABSTRACT

Tumor-derived gene expression signatures have recently shown utility for predicting clinical outcome in patients afflicted with a variety of cancer types. Studies have shown that activation of the DNA damage response pathway is a hallmark for early tumorigenesis, while loss of the DNA damage checkpoint is associated with disease progression. As such, we hypothesized that the transcriptional DNA damage response may serve as a prognostic signature for outcome in cancer patients. We comprehensively characterized the transcriptional DNA damage response in normal and *ATM*-deficient human lymphoblast cells, using γ-irradiation to induce DNA lesions. We observed a robust transcriptional response to IR in lymphoblasts; this response was surprisingly not dependent on *ATM* status. From these data, we developed a radiation-response signature, which we used to screen a panel of cancer datasets for the ability to characterize long-term survival of cancer patients. We demonstrate that genes induced or repressed by ionizing radiation predict clinical outcome in two independent breast cancer datasets and we compare the radiation signature to previously described gene expression-based predictors. While genes repressed in response to radiation likely represent the well-characterized proliferation signature predictive of outcome, genes induced by radiation likely represent other deregulated biological properties of tumors such as checkpoint or apoptotic responses.

INTRODUCTION

For patients afflicted with breast cancer, there is considerable diversity in both the response to treatment and long term survival. Despite the availability of some individual markers for tumor classification (e.g. Her2, P53, estrogen and progesterone receptors), our ability to predict outcome or apply tailored therapy regimens remains limited. Efforts to develop new tumor classification assays, especially those based on panels of markers rather than individual markers, seek to provide better discrimination of clinically important subtypes of breast cancer. Gene expression arrays have shown considerable utility in this area, and early applications have identified highly stratified subtypes in multiple human cancers, extending the classification of tumors beyond that defined by traditional histological analysis and single biomarker measurements (KAPP *et al.* 2006; LAPOINTE *et al.* 2004; PEROU *et al.* 2000).

Complementarily, recent research has focused on the development of multi-gene expression signatures that correlate with patient outcome and that can be applied clinically to identify the most aggressive individual tumors. Such signatures have emerged for multiple tumor types (BARRIER *et al.* 2005; BEER *et al.* 2002). Specifically for breast cancer, no less than 8 different expression signatures have been proposed for predicting clinical outcome (reviewed in Sotiriou & Piccart, 2007) (SOTIRIOU and PICCART 2007). The first among these was developed by a group at the Netherlands Cancer Institute, and commonly referred to as the “Amsterdam signature”. This 70-gene signature has shown significant prognostic capabilities (VAN 'T VEER *et al.* 2002; VAN DE VIJVER *et al.* 2002), culminating in the development of a custom-made microarray for high-throughput clinical screening and ongoing clinical trials (GLAS *et al.* 2006). Other signatures have followed, each introducing minor variations on the derivation of the signature or the exact type of

prediction. These include a model based on breast cancer recurrence (PAIK *et al.* 2004), a 76-gene signature developed for predicting distant metastasis (WANG *et al.* 2005), a signature based on expression subtypes known as the genomic grade index (SOTIRIOU *et al.* 2006), and a signature that is associated with loss of the PTEN suppressor and that has shown applicability to carcinomas from multiple tissues (SAAL *et al.* 2007).

One underlying commonality among these breast cancer outcome signatures is that all were developed from gene expression datasets derived from tumor samples. In contrast, Chang *et al.* utilized a gene expression signature representing the "wound response" to accurately discriminate survival outcome in breast cancer patients (CHANG *et al.* 2005; CHANG *et al.* 2004). This signature, derived from human fibroblasts stimulated with serum, represents the first predictor developed completely independent of cancer patient samples or tumor cell lines. Instead, the signature was developed based on a hypothesis exploiting the similarities between cancer progression and wound healing. Genes upregulated in fibroblasts in response to serum stimulation were also shown to be upregulated in poor-prognosis tumors (CHANG *et al.* 2004). This study represents a novel methodology in cancer prediction: developing a prediction signature based on our understanding of the cellular mechanisms underlying tumorigenic progression.

In 2005, two different research groups revealed that human precancerous (and early stage cancerous) lesions show constitutive activation of the DNA-damage response (DDR) pathway (BARTKOVA *et al.* 2005; GORGOULIS *et al.* 2005). It has been hypothesized that replication stress due to abnormal cell cycle progression activates the DNA damage checkpoint directly or through the sensing of DNA double-strand breaks (DSBs). Notably, this activation is associated with the induction of oncogene-induced senescence, which

is dependent on the DSB sensor kinase ATM (BARTKOVA *et al.* 2006; DI MICCO *et al.* 2006). As such, activation of the DNA damage checkpoint may act as a first line defense to halt tumor progression, and further mutations (*P53*, for example) may allow tumors to evade this mechanism. Thus, evaluating the activity of the DDR pathway and downstream effectors in human tumors may offer significant prognostic capabilities, similar to what has been shown for the wound response.

In this study, we utilize microarrays to assay human lymphoblast cell lines with different *ATM* genotypes to identify radiation-responsive genes. We extend the current literature by reporting a number of transcripts not previously implicated as being radiation-responsive and report that *ATM*-deficient cell lines do not exhibit a discernible defect in the transcriptional response to IR. Using the radiation-responsive genes as bait for Gene Set Enrichment Analysis (SUBRAMANIAN *et al.* 2005), we identified a number of significant connections to human cancer, including correlation to clinical outcome in breast cancer. Following this observation, we demonstrate that our radiation-responsive signature serves as an effective predictor of survival outcome in two independent breast cancer datasets. We compare the radiation-response signature to previously developed outcome signatures, and show similar prognostic capability, despite varying degrees of gene/gene overlap. Like the wound-response signature, the radiation-response signature is an effective tumor outcome classifier derived from a biological hypothesis based on known tumor physiology (i.e. abnormal checkpoint function and chromosomal instability).

MATERIALS AND METHODS

Cell lines and growth conditions

Human lymphoblast (LBL) cell lines used in this study were obtained either from the Coriell Cell Repository (http://ccr.coriell.org/) or were kindly provided by Dr. Daniel Haber and Daphne Ball at the M.G.H. Charlestown Navy Yard. Fresh aliquots of cells were thawed and grown in RPMI 1640 + 15% FBS (Sigma, heat-inactivated) + 100 units/ml penicillin + 100 ug/ml streptomycin in a humidified incubator at 37°C and 5% CO2. Cells were fed by addition of fresh, pre-warmed medium 2-3 times per week as required to maintain culture density at 2-7 x 10^5 cells/mL until sufficient quantities of cells for the experiment were present (10-14 days). At this point, 2 x 10^7 cells were harvested by centrifugation and resuspended in 30 mL of fresh medium. Resuspended cells were then aliquotted into 3 x 10 mL identical samples in T25 Falcon tissue culture flasks and returned to the incubator where they were allowed to return to baseline following this manipulation. Specifically, the cultures were placed on the same shelf within the incubator, and the incubator door was not opened until the cells were irradiated 36-40 hours later.

LCL Irradiation

Following the 36-40 hour recovery period described above, all cultures were removed *en masse* from the incubator, and transported on a cart to the Gamma-cell 40 source. One aliquot of each culture was mock-irradiated whereas a second aliquot was exposed to 5.0 Gy using a ^{137}Cs gamma-Cell source operating at a dose rate of 96.1 cGy/minute. Following exposure or mock exposure, all cultures were then returned to the incubator for 5 hours, after which they were harvested by centrifugation. The cell cycle

distribution (assessed by flow cytometry) of the lymphoblasts was not significantly altered during the relatively short response period following exposure to IR (data not shown).

RNA Isolation, hybridization, washing, scanning Affymetrix U133A and U133B chips

Total RNA was extracted using a standard Trizol (Gibco BRL) extraction (CHOMCZYNSKI and SACCHI 1987; CHOMCZYNSKI and SACCHI 2006). RNA samples were quantified by absorbance at 260 nm, and purity was assessed by determining ratios of A260/A280. For first strand cDNA synthesis, 1 ml 100 pmol/ml T7-(T)24 primer (Genosys; GGCCAGTGAATTGTAATACGACTCACTATAGGGAGGCGG-(T)24) was hybridized to 15 ug total RNA (65º C for 10 minutes, then transfer to ice) and subsequently incubated with 400U Superscript II reverse transcriptase (Gibco BRL) in 1X buffer for 1 hour at 42ºC. Second strand cDNA synthesis was carried out using 40U DNA Polymerase I (Gibco BRL), 10 U DNA ligase (Gibco BRL), 2 U RNase H (Gibco BRL), and 0.23 mM dNTPs (Gibco BRL) in 1X buffer at 16ºC for 2 hours. The resultant cDNA was cleaned-up by phenol extraction (PLG Phase-Lock Gel tubes, 5'-3') and ethanol precipitation. *In vitro* transcription (IVT) was carried out according to the manufacturer's recommendations (Ambion T7 MegaScript Kit) in the presence of Bio-11-CTP and Bio-16-UTP (Enzo). Resultant cRNAs were cleaned-up using Qiagen's RNeasy Mini Kit and fragmented in 1X RNA Fragmentation Buffer (5X stock: 200 mM Tris-Acetate, pH 8.1, 500 mM KOAc, 150 mM MgOAc) for 35 minutes at 95ºC. Fragmented cRNAs were hybridized to Affymetrix U133a and U133b arrays in MES Hybridization Buffer (100 mM MES, 1M [Na+], 20 mM EDTA, 0.01% Tween 20) at 45º C, 60 RPM, 16 hours. Control Oligo B2 (5'-Bio-

GTCAAGATGCTACCGTTCA-3') was included. After hybridization, the probe arrays were washed (100 mM MES, 0.1 M [Na+], 0.01% Tween 20), and the remaining biotin-labeled target was then stained with a Streptavidin R-Phycoerythrin (Molecular Probes). The signal was then amplified with a Biotinylated anti-Streptavidin Ab (goat; Vector Lab), followed by a second staining with the streptavidin-conjugated fluorescent stain prior to scanning. 1X Stain Buffer contained 100 mM MES, 1 M [Na+], 0.05% Tween 20, 0.005% Antifoam. Arrays were scanned using a Hewlett Packard (HP) scanner using MAS5 software (www.affymetrix.com), and the final dataset was normalized using RMA (quantile norm, default settings) (IRIZARRY *et al.* 2003).

Microarray Data Analysis

To search for genes differentially expressed between the irradiated group and unirradiated group, the Signal to Noise Ratio (SNR) was calculated for each of the 44760 probe sets as follows:

$$SNR_i \equiv \frac{\mu_{o,i} - \mu_{1,i}}{\sigma_{0,i} + \sigma_{1,i}} \quad (1)$$

where $\mu_{0,i}$ and $\sigma_{0,i}$ are the mean and variance of the *i*th probe set of the irradiated experimental group and $\mu_{1,i}$ and $\sigma_{1,i}$ are the mean and variance of the unirradiated grouping. (i ranges from 0 to 44759). The dateset was permuted 5000 times to generate a null distribution from which the q-value statistic was applied to correct for multiple hypothesis testing (STOREY and TIBSHIRANI 2003; TUSHER *et al.* 2001).

Pathway analysis using GSEA (SUBRAMANIAN *et al.* 2005) was done in two different ways. First, *a priori* defined Gene Sets were tested against the radiation response for discrimination between the irradiated and unirradiated states. Gene Sets were compiled

from the Gene Ontology consortium (ASHBURNER *et al.* 2000). Ontologies were separated at top level categories (Biological Process, Cellular Component and Molecular Function) and Gene Sets were created by iteration over all subcategories and placing all genes common to a subcategory in a Gene Set representing that subcategory. Gene Sets containing <25 or >500 genes were excluded from the analysis. Other parameters used as input for the GSEA program were as follows: the algorithm was Signal2Noise, normalization method was meandiv, permutations were done by phenotype, the scoring scheme was weighted, and 1000 permutations were used for each analysis.

Curation of Expression Datasets from the Literature

The NKI expression data set and patient clinical information (VAN DE VIJVER *et al.* 2002) were downloaded from the Stanford University public repository (http://microarray-pubs.stanford.edu/). There are 244 arrays in total with 24136 clones on each array. Global normalization was performed (center mean was set to zero and MAD (median absolute deviation) was set to 1). A second expression data set described in Loi *et. al.* (LOI *et al.* 2007) was downloaded from the Gene Expression Omnibus database (http://www.ncbi.nlm.nih.gov/geo/query/acc.cgi?acc=GSE6532). There are 277 arrays (from patients who received adjuvant tamoxifen treatment) with 44928 clones on each array. The dataset representing irradiated mammary tumor epithelial cells and lymphoid tumor cells was extracted from a larger dataset published by Amundson *et al.* (AMUNDSON *et al.* 2008), and the raw measurements were quantile normalized (R package "DNAMR").

Analysis of Expression Signatures in Curated Expression Datasets

Statistical analysis was conducted using the open source program R (http://lib.stat.cmu.edu/R/CRAN/). For hierarchical clustering, each gene was standardized to mean=0 and MAD=1. Euclidean distance was used with complete linkage in the R function *hclust* to derive hierarchical clustering. For survival analysis, the R package *survival* was used to plot Kaplan-Meier survival curves. Log-rank tests were performed for comparing Kaplan-Meier curves of two different groups. The RI (or RR) signature of a sample was defined as the projection of measurements of the RI (or RR) genes on the first principle component direction of the RI (or RR) gene set across all the samples. These RI (or RR) signatures were then used in various Cox proportional hazard models fitted with the R function *coxph*. The Fisher exact test was performed using the R function *fisher.test*. To identify genes serving as the key drivers of the clustering, we used a two-sided t-statistic. We controlled for multiple hypothesis testing by deriving q-values (R packages *testp*, and *qvalue*).

In the classification analysis, patients were first separated into two groups: the poor clinical outcome group (deceased within 10 years of follow-up) and the good clinical outcome group. Then, for each gene signature, leave-one-out cross validation was performed as follows: (1) For a selected test sample, we treated the rest of the data as the training set.; (2) We calculated the mean expression level for the training samples in the good- and bad-survival groups, and computed the distance between the expression level of the test sample and the centroids of the good- and poor-survival groups:

$$d(X^*) = \sum_{i=1}^{p} \frac{(x_i^* - \bar{x}_{ik})^2}{(s_i + s_0)^2} - 2\log \pi_k$$

where $X^* = \{x_i^*\}_i$ is the expression of the test sample; p is the total number of genes in this gene list; $\{\bar{x}_{ik}\}_i$ is the centroid of class $k(=1 \text{ or } 0)$; s_i is the standard deviation of x_i;

s_0 is set to be 0.01 here; π_k is the proportion of samples in class k. (3) We then classified the test sample into the class with the smallest distance. (4) Lastly, we repeated the process with a new test sample until we had iterated over all samples.

Based on the classification results of the 8 gene signatures, we further divided the patients into 5 groups based on both the true outcomes and the classification by the expression signatures. We then compared the distribution of other known clinical variables in group 1 (good survival and classified as "good") vs. 3 (bad survival but classified as "good"), and group 2 (poor survival but classified as "good") vs. group 4 (poor survival and classified as "poor").

RESULTS

Normal human lymphoblast cells exhibit a robust transcriptional response to ionizing radiation

To comprehensively characterize the human transcriptional response to γ-irradiation in human cells with a functional *ATM* gene or lacking one or two copies of *ATM*, we profiled 12 different *ATM+/+* lymphoblast cell lines (LBL), 10 different *ATM+/-* lines and 10 different *ATM-/-* cell lines at 5 hours following exposure to 5 Gy irradiation. Control samples were mock-irradiated. From this transcript array dataset, we first asked whether a robust transcriptional response was observable in normal human lymphoblasts (i.e. *ATM+/+*). By discriminant analysis, we determined 160 genes were induced by radiation (211 probe sets) and 59 genes repressed by IR (70 probe sets) at FDR ≤ 0.05 (Table 1 and 2). This large study identified known radiation-responsive transcripts (*e.g. GADD45A*, *XPC*, *PPM1D*, *FAS*, *etc*.) as well as many genes not previously implicated in the radiation

response (*e.g. ZNF79*, *C11orf24*, *CSNK1G1*, *KCNN3*, *etc*.). The radiation-induced (RI) genes function in a number of different cellular pathways including apoptosis signaling and cell cycle arrest, as determined by Gene Ontology (GO) (ASHBURNER *et al.* 2000) category enrichment; radiation-repressed (RR) genes function predominantly in cell division (Table 3 and 4).

ATM-deficient cells mount a normal transcriptional response to IR

As cells lacking *ATM* are highly sensitive to IR, we next hypothesized that *ATM-/-* cells from AT patients would manifest a transcriptional defect compared to the wild-type cell lines. However, discriminant analysis between the 12 irradiated *ATM+/+* cell lines and the *10 ATM-/-* cell lines did not reveal any significant differences at an FDR of 1%, showing that *ATM-/-* lymphoblast cell lines mount a normal transcriptional response to IR. Accordingly, *ATM+/-* cell lines also did not exhibit any transcriptional differences after IR when compared to wild-type cells at an FDR of 1%. Additionally, comparisons between the *ATM+/+*, *ATM+/-* and *ATM-/-* in the mock-irradiated samples did not reveal any significant differences in basal transcription levels. From these data, we conclude that despite a radiosensitive phenotype, *ATM-/-* lymphoblast cells exhibit a transcriptional response to 5 Gy IR at 5 hours that is indistinguishable from *ATM+/+* cells.

ATM-deficient lymphoblasts exhibit a defect in DDR signaling that is exacerbated by treatment with the PI3-like kinase inhibitor caffeine

The fact that *ATM-/-* lymphoblast cells did not exhibit a transcriptional defect in response to 5 Gy of IR was surprising given the fact that *ATM-/-* cells have a well-characterized

defect in phosphorylating the DNA damage responsive transcription factor TP53 (BANIN *et al.* 1998; CANMAN *et al.* 1998) in response to similar doses. Thus we asked whether in the cell lines utilized in this study, we observe a defect in TP53 phosphorylation at the dose and time utilized in the microarray experiments. As seen in Figure 1, the treatment of normal lymphoblasts with ionizing radiation results in a significant increase in TP53 phosphorylation in a dose- and time-dependent manner (Figure 1 a&b). However, in the *ATM-/-* line, we observe a both a delay in radiation-induced TP53 phosphorylation as well as a significant decrease in overall TP53 phosphorylation levels relative to the *ATM+/+* lymphoblasts. Of note, at the 5 hour timepoint, we observe a significant amount of residual phosphorylation in *ATM-/-* cells that may be sufficient to activate TP53 transcription factor activity. This residual activity is likely due to substrate overlap with other DDR signaling kinases such as ATR and DNA-PK (YANG *et al.* 2003). As such, we hypothesized that treating *ATM-/-* cells with the PI3-like kinase inhibitor caffeine would completely abolish this residual activity. As expected (Figure 1c), treatment of irradiated *ATM-/-* cells with increasing doses of caffeine completely abolished TP53 phosphorylation. From these data we conclude that redundancy in the DDR kinase-substrate network suppresses the signaling defect in *ATM-/-* cells and may contribute to the lack of transcriptional differences between irradiated *ATM+/+* and *ATM-/-* lymphoblasts.

Radiation Signature in Human Cancer Datasets

Due to the vital role of the DNA damage response pathway as a mechanism for resistance to tumorigenesis (BARTKOVA *et al.* 2006), as well as the importance of radiation therapy in treating human cancer, we next explored the prognostic capabilities of

radiation-responsive genes in human cancer datasets. We initially used the GSEA algorithm (SUBRAMANIAN *et al.* 2005) to screen the list of 160 radiation-induced (RI) genes and 59 radiation-repressed (RR) genes for correlation with a series of clinical traits in a panel of cancer microarray datasets curated from the literature. These traits included: clinical outcome in multiple cancer types (BEER *et al.* 2002; BHATTACHARJEE *et al.* 2001; MONTI *et al.* 2005; NUTT *et al.* 2003; POMEROY *et al.* 2002; SINGH *et al.* 2002; VAN DE VIJVER *et al.* 2002), estrogen receptor status in breast cancers (VAN DE VIJVER *et al.* 2002; WEST *et al.* 2001), *BRCA1* status in breast cancers (VAN 'T VEER *et al.* 2002), and *P53* status in multiple cancer cell lines (RAMASWAMY *et al.* 2001). The results of this screen are presented in Table 5. The breast cancer datasets yielded particularly interesting results, including correlation of a radiation-derived gene set with clinical outcomes as well as both estrogen receptor and *BRCA1/2* mutant status.

Following these observations from the initial screen, we further assessed the prediction capabilities of the radiation signature in breast cancer using a more thorough analysis. We focused on the clinical outcome dataset consisting of 244 breast cancer patients from the Netherland Cancer Institute (NKI) (VAN DE VIJVER *et al.* 2002). After applying a stringent filter to minimize false positives in the radiation signature (q-value ≤ 0.02, SNR ≥ 1.2), we identified 50 RI genes and 68 RR genes. We cross-mapped the radiation-induced and radiation-repressed signatures to the NKI dataset (15 RI genes + 31 RR genes overlapped) and clustered tumor samples in the space of the genes repressed by radiation (the RR gene set) or the space of genes induced by radiation (the RI gene set). As shown in Figure 2A, by applying hierarchical clustering, the RR gene set naturally separated the tumor samples into two distinct clusters based solely on the

expression of RR genes. We next performed Kaplan-Meier survival analysis on the two clusters (Panel 2B), and observed that primary tumors from the left cluster (Fig. 2A) were significantly more likely to progress to death than tumors from the right cluster ($p = 2.13 \times 10^{-7}$, log rank test). To determine the probability that this separation could be due to random chance, we repeatedly sampled a gene set of the same size (31 genes) from the original expression data set and again clustered the data and performed the log rank test. In 3 out of the 500 iterations, the log rank test p values were smaller than our calculated p-value; hence, the possibility of observing this association by chance was 0.006. We repeated the analysis using the RI signature, which also separated the tumor samples into good- and poor-outcome clusters (Figure 2 C&D). The log rank test for the difference in outcome between the clusters yielded a p-value of 0.0006, which corresponds to an error rate of 0.034 based on random sampling (17 out of 500 iterations have the same or smaller p-value).

We also tested for an association between tumor clusters (separated by radiation genes, Figure 2 A & C) and tumor grade and ER status, which are represented visually above the heatmaps in Figure 2 A & C. Tumor Grade was strongly correlated to the RR and RI gene sets, with the two clusters accurately separating poorly- and well-differentiated tumors (the p-value for RR 2.58×10^{-12}, p-value for RI was 0.00092). Estrogen receptor status was also correlated with the RR set (p-value = 2.05×10^{-8}) but not significantly correlated with the RI signature (p-value = 0.074). We conclude that the RR and RI signatures show a strong correlation with tumor grade, and the RR signature shows correlation with estrogen receptor status.

To extend and validate these results, we tested the prognostic power of the radiation-repressed and induced gene signatures in an additional independent breast cancer microarray dataset providing survival annotation (LOI *et al.* 2007). For the recently published Loi *et al.* dataset (LOI *et al.* 2007), we again cross-mapped the RI and RR genes to this dataset (41 RI + 51 RR genes overlapped) and performed clustering analysis in the space of either the RR or RI genes (Figure 3A & C). As before, the RR signature yielded two distinct clusters (Figure 3A), with the left cluster showing significantly higher mortality (Figure 3B, p-value=0.009). The left cluster was also significantly associated with grade 3 tumors (44/47 patients, p=1.0e-09). As was observed in the NKI dataset, the RI signature separated the samples into two distinct clusters (Figure 3C), which showed significant differences in clinical outcome (Figure 3D). The log rank test for the difference in outcome between the clusters yielded a p-value of 0.023, which corresponds to a random chance of 0.05 based on random sampling (27 out of 500 iterations have the same or smaller p-value). The clustering by RI genes was again correlated with tumor grade, with the left cluster enriched for poor-outcome tumors (Figure 3C, p-value = 0.0057). We conclude that the RR and RI signatures are prognostic for breast cancer, which has been demonstrated in two independent patient populations.

TP53 is a major factor controlling the transcriptional response to ionizing radiation (JEN and CHEUNG 2005), and TP53 status is associated with poor outcome in breast cancer (THOR *et al.* 1992). Hence, we hypothesized that aberrant regulation of the RI genes (predictive of poor outcome) could be a result of altered TP53 activity in the poor outcome tumors. To test this hypothesis, we determined whether genes that were the key drivers of the outcome clustering were known transcriptional targets of TP53. Genes that

exhibit the largest expression difference between the two clusters are the key drivers of the clustering of breast tumors (Figures 2 & 3). We ranked the 41 RI genes by their differential expression between the good vs. poor outcome clusters in the Loi *et al.* dataset and asked if these genes are known to be regulated by P53 (Table 6). Many of the key drivers for this clustering are not known P53-regulated genes (Table 6), suggesting that either these are novel p53 targets or that the RI genes are not entirely p53-regulated. Moreover, when we removed the non-P53 regulated genes from the RI signature and repeated the clustering, there was no significant discrimination between good- and poor-outcome tumors (data not shown), demonstrating that the genes not known to be p53-responsive are important for discriminating outcome. We conclude from these results that the predictive power of the RI signature is not entirely dependent on known P53-responsive genes. Moreover, we compared our RR and RI signatures with a previously published 32 gene P53 signature derived from transcriptional differences between P53 mutant and wildtype breast tumors (MILLER *et al.* 2005). Neither the RR nor RI signatures showed any overlap with the 32 genes in this P53-derived signature. We conclude that the tumor-derived P53 signature is not similar to the radiation response signature derived from non-tumor cells. This is perhaps not surprising as breast tumors commonly have a defective DNA damage response.

The radiation response signature was derived from lymphoblast cell lines. Because the radiation response may vary amongst cell types of origin, we sought to observe whether a signature derived from irradiated breast epithelial cell lines would prove to be a stronger predictor. To do this, we analyzed a subset of samples from a recently published study looking at gene expression across a panel of tumor cell lines derived

from a variety of tissues (AMUNDSON *et al.* 2008). From this dataset, we analyzed microarray data from the 5 breast cancer cell lines untreated versus 8 Gy IR. Analysis of this dataset yielded 66 induced and 10 repressed genes at a FDR ≤ 0.02 (Table 7). None of these genes overlapped with our lymphoblast-derived radiation gene sets. (Of note, this breast tumor line dataset represents a small number of tumor lines on a custom array platform of < 7000 genes, so its power to derive a predictor may be poor.) Unlike the radiation signature derived from the lymphoblast study, the gene set derived from the mammary epithelial tumor cell lines was not able to significantly distinguish good- from poor-outcome tumor samples (data not shown). Because tumors harbor known defects in the DNA damage response, it is perhaps not surprising that radiation signatures derived from tumor cell lines do not predict outcome in breast cancers. It is still conceivable that a radiation signature derived from primary mammary epithelial cells could yield a stronger predictor than that derived from lymphoblasts, but no such dataset is currently available to test this hypothesis.

Comparison of Outcome Signatures

Next, we used a Cox proportional hazard model to determine the relationship between the radiation signatures and known clinical parameters (and the wound response signature) in the NKI dataset. First, we generated a univariate Cox model to assess the predictive capabilities of the radiation and wound response signatures in the NKI dataset. In a univariate analysis (Table 8, left panel), the RI signature, RR signature, wound response, and five clinical variables (age, lymph node status, tumor grade, vascular invasion, and ER status) are significant risk factors for poor clinical outcome (p

value<0.05). Additionally, the combined RI and RR gene set yielded a significant hazard ratio, with a p-value of 3e-9. Next we performed multivariate analysis to determine the performance of the RR and RI signatures combined with clinical parameters and the wound response signature (Table 8). This was performed both with the RR and RI signatures separately (Model 1), and combined (Model 2). In the first model, both the RR signature and the age of the patient yielded significant hazard ratios, but notably the RI signature did not. However, using the combined RR and RI signature yielded a significant p-value in the multivariate model (p=0.021) that was marginally lower than the RR signature alone (0.030) (Table 8 model 2). As the combined radiation signature yielded a significant hazard ratio in the multivariate model, we conclude that this signature offers additional information with other clinical variables and the wound response signature.

The Cox analysis was then repeated for the Loi *et al.* dataset (Table 9). Once again, both the RR and RI sets (separately or combined) are strong risk factors in the univariate analysis. In the multivariate analysis with other clinical parameters (Table 9, Model 1), ER status was the predominant risk factor in the model using RR and RI as separate sets (p-value = 0.015). However, as with the NKI dataset, when the RR and RI are combined into a single set (Table 9, Model 2), the radiation signature is highly significant, with a p-value of 0.009 (ER status has a p-value of 0.019 in this model). This strongly suggests that the combined radiation gene signature offers significant potential in predicting outcome, and provides additional information about the tumor in combination with known clinical factors and the wound response signature.

We next compared the RR and RI signatures to previously published signatures in terms of gene overlap and prognostic power. Other signatures used in this comparison

were the Amsterdam 70 gene (VAN DE VIJVER *et al.* 2002), the wound response (CHANG *et al.* 2004), the 76-gene metastasis signature (WANG *et al.* 2005), the recurrence score (PAIK *et al.* 2004), the Genomic Grade Index (GGI) (SOTIRIOU *et al.* 2006), and the PTEN signature (SAAL *et al.* 2007). We first computed the overlap in gene membership between the RR and RI signatures and the other outcome signatures. We observed that the GGI and PTEN signatures showed some overlap with the RR signature (34 and 11 genes, respectively), while the other signatures yielded minimal overlap (Table 10). The overlap with the GGI signature includes 14 of the top RR genes (ranked by p-value), which are comprised mostly of cell cycle and mitosis-related factors. The lesser overlap with some of the other signatures is perhaps due to design, as the authors of the Wound Response and PTEN signatures specifically excluded cell cycle-related genes from the final list. (Indeed, matching the RR signature to the 193 genes removed from the Wound Response signature yielded an overlap of 28 genes.)

Next, we compared the prognostic capability of the radiation-repressed signature to previously published breast outcome signatures using the NKI dataset (VAN DE VIJVER *et al.* 2002). This comparison was done using the leave-one-out cross validation procedure, which consisted of calculating the mean expression of each signature with respect to the good and poor outcome groups, and comparing the distances of the left-out sample with the centroid of each group (see Methods). The results for each signature are reported in Table 11. Despite differences in the size of the gene sets, the signatures showed similar error rates and sensitivity for classifying patients for outcome.

To examine if a subset of tumors was commonly misclassified by all of the gene signatures, we plotted a heatmap of classification status for each sample as determined

by each of the 8 prediction signatures (Figure 4). Each signature was used to predict the classification of patients into groups representing survival past 10 years (the good clinical outcome group), and those which died prior to 10-years (the poor clinical outcome group). Most patients are generally grouped into the same clusters by each signature, demonstrating good concordance amongst the signatures (Figure 4). Interestingly, there exists a subset of tumors that are misclassified by all or most of the gene signatures. For example, in the poor-outcome group, there is a subgroup of 10-20 patients that are commonly misclassified as “good” by most signatures. Conversely, in the good-outcome group, a similarly sized subset of samples has been misclassified as “poor” by most signatures. We next examined whether misclassification of tumors was associated with the other known clinical parameters for which annotation was available (age, diameter, lymph node metastasis, tumor grade, vascular invasion, ER status, mastectomy, and chemotherapy; see Tables 12 and 13). For poor-outcome patients that were misclassified as “good outcome” by the majority of expression signatures, both ER- status ($p=1.0E-05$) and high Tumor Grade ($p=0.03$) were enriched. In contrast, no clinical variables were significantly enriched in tumors associated with good outcome but misclassified as poor outcome. We conclude that all gene expression signatures perform very similarly in tumor classification, and that there are subsets of both poor- and good-outcome samples that are commonly misclassified by all of the signatures.

DISCUSSION

Questions that arise from this study are why a transcriptional signature of the cellular radiation response shows prognostic capabilities in breast cancer, and how is the radiation-derived predictor different from other known predictors in breast cancer? There

are interesting parallels between tumorigenesis and the radiation response (Figure 5). Key drivers of tumorigenesis are the activation of oncogenes (stimulating deregulated proliferation) and the inactivation of tumor suppressor genes (leading to defects in checkpoint function and apoptotic responses) (Figure 5A). Similarly, in response to radiation, there is a rapid transcriptional response consisting of both up- and down-regulation of genes, wherein down-regulated genes are involved in driving progression through the cell cycle (proliferation) and up-regulated genes are involved in checkpoint inhibition of cell cycle progression and apoptosis (Figure 5B).

The majority of outcome signatures for breast cancer essentially detect the same property: the high potential for proliferation in poor outcome tumors (SOTIRIOU and PICCART 2007). Hence, it is not surprising that the set of genes repressed by radiation in our study is able to predict breast cancer outcome, since this gene set is enriched in genes involved in cell cycle progression/proliferation (Table 4). We suggest that the reason most breast outcomes signatures to date focus on proliferation is that they were trained on gene expression array datasets from human tumors, in which the strongest transcriptional program driving this clustering is one associated with a singular biological property: proliferation. However, these results do not imply that additional biological properties of breast cancers, whose transcriptional correlate is not as strong as that of the proliferation signature (and hence does not drive the hierarchical clustering of tumors), may also carry significant prognostic information.

Indeed, our finding that the set of genes induced by radiation (RI) are enriched in checkpoint/apoptotic functions and are distinct from the proliferation cluster indicates that the RI signature may contain novel predictive information, less related to high proliferation

and likely representing additional tumor properties such as genomic instability. In addition to genes involved in apoptosis and cell cycle arrest, a number of functional pathways not previously implicated in the radiation response were among the top radiation-induced pathways. Foremost among these were the categories corresponding to glycosaminoglycan, aminoglycan, and proteoglycan metabolism (Table 3). Perhaps relatedly, proteoglycans such as heparan sulfate have been shown to be linked to tumor progression (SANDERSON *et al.* 2004).

Also consistent with our observation that the RI gene set carries prognostic information, others have shown that human precancerous (and early stage cancerous) lesions consistently show constitutive activation of the DNA-damage response (DDR) pathway due to the initial replication fork breakdown to double-strand breaks (DSBs) in proliferating cells, and this activation disappears as tumors progress (Figure 5A) (BARTKOVA *et al.* 2005; GORGOULIS *et al.* 2005), suggesting that the DNA damage checkpoint acts as an anti-proliferative barrier for tumorigenesis (BARTKOVA *et al.* 2006; DI MICCO *et al.* 2006). Hence one can imagine that a lack of this checkpoint would be associated with tumor progression and poor clinical outcome. Additionally, activity of the p53 pathway (via changes in p53 or its regulator MDM2) has been associated with survival in breast cancer (BOERSMA *et al.* 2006; ISOLA *et al.* 1992; PHAROAH *et al.* 1999; THOR *et al.* 1992; THORLACIUS *et al.* 1995), although poor standardization of the p53 immunohistochemistry-based assay coupled to the complex autoregulatory feedback of this pathway have confounded the results (MCSHANE *et al.* 2000).

Because P53 is one of the main transcriptional activators in the normal radiation response, and poor-outcome tumors are commonly P53 negative, it can be hypothesized

that the RI signature's predictive power is at least partially derived from P53 status. As predicted, P53 regulated genes make up a significant component of the RI signature. However, as we showed in Table 6, many of the genes that drive the clustering into a good- and poor-outcome group are not known to be regulated by P53. This suggests that either many of these genes are actually P53 targets that have not yet been discovered, or that the RI signature's predictive capabilities are not entirely P53- dependent, representing a novel connection between the radiation response and tumor outcome. Despite an overwhelming body of evidence indicating the potential clinical prognostic utility of the DDR pathway in human breast cancer, the lack of a clinically tractable robust assay to assess the activity of this pathway has prevented its translation into clinical care of breast cancer patients (HARRIS *et al.* 2007). Because the DDR pathway contains p53-dependent and p53-independent responses, p53 status alone does not completely assess the activity or functionality of the signal transduction cascade (HARPER and ELLEDGE 2007). Hence it is likely that the (thus far) nearly exclusive focus of clinical testing on p53 has failed to fully prosecute this complex cellular pathway as a clinical marker. The RI signature, which encompasses multiple facets of the DDR pathway, serves as an initial foray into a more robust DDR signature for prognostication, and further characterization of a number of the key drivers for this clustering may reveal the extent to which the DDR pathway is represented in the RI signature.

Of note, our radiation-responsive transcriptional study was performed in cell lines of lymphoblastoid origin, yet the signature serves as an excellent predictor of survival outcome in mammary *epithelial* tumors. This is not the first predictive signature to be derived from an entirely different cell type. The wound response signature (CHANG *et al.*

2004) is another efficient predictor of survival outcome in breast cancer, but was in fact derived from serum-stimulated fibroblast cells. The transcriptional radiation response of lymphoid cells has previously been shown to be applicable to other tissues as well, in particular for predicting radiotoxicity of normal tissues in prostate cancer patients treated with radiation therapy (SVENSSON *et al.* 2006). It is unknown how the radiation response differs among different *normal* cell types.

Like the wound response signature, the radiation signature offers additional support for the development of gene expression signatures based on known pathways whose mutations contribute to tumorigenesis. As tumor progression may proceed through a series of mutations affecting multiple pathways, one can imagine the utility of a panel of gene expression signatures for tumor diagnosis, each based on the functionality of a specific anti-tumor barrier. Such a tactic has root in the idea of the "Vogelgram," in which tumorigenesis can be understood as a multi-step genetic progression (KINZLER and VOGELSTEIN 1996). An ordered panel of pathway- specific gene expression changes may offer a complete picture of the genomic landscape for specific tumors, and could determine where each tumor sits in such a progression model. Such data would be important for both prognosis and deciding on a plan of treatment (BILD *et al.* 2006).

In a 2006 analysis, Fan et al. showed that despite minimal overlap between cancer outcome signatures, each yielded similar prognostic capabilities (FAN *et al.* 2006). Our results with the radiation-response signature agree with this assessment; for example, we show the signature has similar performance in tumor classification, and in general a low degree of overlap with other outcome signatures. The fact that all expression signatures identified a number of poor-outcome tumors that were not predicted by other

clinical parameters is particularly encouraging, but outlines a significant need for additional clinical datasets for verification. This would also allow testing of whether the misclassification of certain samples is reproducible, and help uncover a group of tumors that aren't easily classifiable by any available means. Such an investigation may help further refinement of molecular signatures to encapsulate these tumors, and a thorough study may help identify new discriminant genes, or even extrinsic factors related to early death that aren't direct properties of the tumor (overall patient health, etc.).

rank	radiation-repressed gene	symbol	Score	FDR	Feature P	Q Value	Fold Change
1	cyclin B1	CCNB1	3.02	0.002	4.00E-05	0.026	3.8
2	aurora kinase A	AURKA	2.64	0.002	4.00E-05	0.026	1.8
3	cell division cycle 20 homolog (S.	CDC20	2.45	0.002	4.00E-05	0.026	4.6
4	kinesin family member 20A	KIF20A	2.19	0.002	4.00E-05	0.026	2.2
5	polo-like kinase 1 (Drosophila)	PLK1	2.14	0.002	4.00E-05	0.026	2.1
6	ubiquitin-conjugating enzyme E2C	UBE2C	2.09	0.002	4.00E-05	0.026	1.8
7	hypothetical protein DKFZp762E1	DKFZp762E1	1.90	0.002	4.00E-05	0.026	1.4
8	cyclin B2	CCNB2	1.71	0.002	4.00E-05	0.026	1.9
9	transforming, acidic coiled-coil cor	TACC3	1.62	0.002	4.00E-05	0.026	1.6
10	TPX2, microtubule-associated, ho	TPX2	1.61	0.002	4.00E-05	0.026	1.9
11	centromere protein A	CENPA	1.55	0.002	4.00E-05	0.026	2.4
12	centromere protein F, 350/400ka (	CENPF	1.50	0.002	4.00E-05	0.026	1.9
13	aurora kinase A	AURKA	1.42	0.002	4.00E-05	0.026	1.9
14	discs, large homolog 7 (Drosophila	DLG7	1.42	0.002	4.00E-05	0.026	2.5
15	splicing factor, arginine/serine-rich	SFRS7	1.39	0.002	4.00E-05	0.026	1.3
16	cell division cycle associated 8	CDCA8	1.36	0.002	4.00E-05	0.026	1.6
17	cell division cycle associated 3	CDCA3	1.35	0.002	4.00E-05	0.026	1.6
18	trophinin associated protein (tastin	TROAP	1.33	0.002	4.00E-05	0.026	1.3
19	G-2 and S-phase expressed 1	GTSE1	1.33	0.002	4.00E-05	0.026	1.6
20	G-2 and S-phase expressed 1	GTSE1	1.31	0.002	4.00E-05	0.026	1.4
21	karyopherin alpha 2 (RAG cohort 1	KPNA2	1.30	0.002	4.00E-05	0.026	2.1
22	asp (abnormal spindle) homolog, r	ASPM	1.26	0.002	4.00E-05	0.026	1.4
23	centromere protein A	CENPA	1.26	0.002	4.00E-05	0.026	1.4
24	cyclin F	CCNF	1.21	0.002	4.00E-05	0.026	1.4
25	chromosome 13 open reading fran	C13orf34	1.18	0.002	4.00E-05	0.026	1.5
26	CDC28 protein kinase regulatory s	CKS2	1.16	0.003	8.00E-05	0.028	2.1
27	dyskeratosis congenita 1, dyskerin	DKC1	1.13	0.003	8.00E-05	0.028	1.2
28	hyaluronan-mediated motility rece	HMMR	1.11	0.005	1.20E-04	0.037	1.6
29	DEP domain containing 1	DEPDC1	1.09	0.002	4.00E-05	0.026	1.5
30	cyclin A2	CCNA2	1.08	0.005	1.20E-04	0.037	1.8
31	chromosome 15 open reading fran	C15orf23	1.08	0.002	4.00E-05	0.026	1.5
32	proline/serine-rich coiled-coil 1	PSRC1	1.05	0.002	4.00E-05	0.026	1.3
33	antigen identified by monoclonal a	MKI67	1.05	0.006	1.60E-04	0.043	1.5
34	Ran GTPase activating protein 1	RANGAP1	1.05	0.005	1.20E-04	0.037	1.3
35	unc-84 homolog B (C. elegans)	UNC84B	1.04	0.006	1.60E-04	0.043	1.4
36	antigen identified by monoclonal a	MKI67	1.04	0.005	1.20E-04	0.037	1.4
37	solute carrier family 38, member 1	SLC38A1	1.02	0.003	8.00E-05	0.028	1.4
38	G-2 and S-phase expressed 1	GTSE1	1.01	0.005	1.20E-04	0.037	1.2
39	RAD21 homolog (S. pombe)	RAD21	1.00	0.007	2.00E-04	0.049	1.5
40	cyclin-dependent kinase inhibitor 3	CDKN3	0.99	0.002	4.00E-05	0.026	1.6
41	SEC14-like 1 (S. cerevisiae)	SEC14L1	0.99	0.003	8.00E-05	0.028	1.4
42	hyaluronan-mediated motility rece	HMMR	0.97	0.005	1.20E-04	0.037	1.8
43	baculoviral IAP repeat-containing 5	BIRC5	0.96	0.006	1.60E-04	0.043	1.5
44	tumor necrosis factor (TNF superf	TNF	0.96	0.007	2.00E-04	0.049	1.4
45	centromere protein F, 350/400ka (	CENPF	0.95	0.003	8.00E-05	0.028	1.2
46	BUB1 budding uninhibited by benz	BUB1B	0.95	0.005	1.20E-04	0.037	1.6
47	DEP domain containing 1	DEPDC1	0.95	0.002	4.00E-05	0.026	1.7
48	transmembrane protein 113	TMEM113	0.95	0.013	4.00E-04	0.082	1.7
49	non-SMC condensin I complex, su	NCAPD2	0.94	0.007	2.00E-04	0.049	1.3
50	hypothetical protein HSPC111	HSPC111	0.94	0.002	4.00E-05	0.026	1.3
51	NIMA (never in mitosis gene a)-rel	NEK2	0.93	0.006	1.60E-04	0.043	1.3
52	epithelial cell transforming sequen	ECT2	0.93	0.019	6.00E-04	0.109	1.2
53	BUB1 budding uninhibited by benz	BUB1	0.92	0.006	1.60E-04	0.043	1.8
54	asp (abnormal spindle) homolog, r	ASPM	0.91	0.002	4.00E-05	0.026	2.4
55	karyopherin alpha 2 (RAG cohort 1	KPNA2	0.91	0.008	2.40E-04	0.056	1.9
56	family with sequence similarity 83,	FAM83D	0.91	0.006	1.60E-04	0.043	1.5
57	sema domain, immunoglobulin do	SEMA4D	0.90	0.030	9.20E-04	0.155	1.4
58	cell division cycle associated 2	CDCA2	0.90	0.008	2.40E-04	0.056	1.3
59	shugoshin-like 2 (S. pombe)	SGOL2	0.89	0.010	2.80E-04	0.063	1.6
60	v-myc myelocytomatosis viral onc	MYC	0.89	0.015	4.40E-04	0.089	1.9
61	cyclin F	CCNF	0.89	0.007	2.00E-04	0.049	1.3
62	cell division cycle 25 homolog B (S	CDC25B	0.89	0.008	2.40E-04	0.056	1.4
63	poliovirus receptor related immun	PVRIG	0.87	0.006	1.60E-04	0.043	1.5
64	A kinase (PRKA) anchor protein 1	AKAP1	0.87	0.019	6.00E-04	0.109	1.3
65	cytoskeleton associated protein 5	CKAP5	0.85	0.016	4.80E-04	0.096	1.2
66	kinesin family member 14	KIF14	0.85	0.019	6.00E-04	0.109	1.5
67	kinesin family member 2C	KIF2C	0.84	0.008	2.40E-04	0.056	1.6
68	peroxisome proliferator-activated r	PPRC1	0.84	0.017	5.20E-04	0.101	1.2
69	sperm associated antigen 5	SPAG5	0.84	0.017	5.20E-04	0.101	1.2
70	metadherin	MTDH	0.84	0.034	0.001079957	0.173	1.6

TABLE 1. RADIATION REPRESSED GENES IN RESPONSE TO 5 GY IR.

This table lists the transcripts repressed after radiation in response to a 5 Gy IR 5 hour exposure. Genes were determined to be enriched at a FDR cutoff of ≤ 0.05. Genes represented multiple times in this list indicate independent measurements from independent probe sets on the array.

rank	radiation-induced genes	symbol	Score	FDR	P value	Q Value	Fold Change
1	pleckstrin homology-like domain, family A	PHLDA3	-3.05	0.0019	0.0000	0.0259	2.14
2	protein phosphatase 1D magnesium-depe	PPM1D	-2.34	0.0019	0.0000	0.0259	2.40
3	damage-specific DNA binding protein 2, 4	DDB2	-2.32	0.0019	0.0000	0.0259	2.43
4	TP53 regulated inhibitor of apoptosis 1	TRIAP1	-2.18	0.0019	0.0000	0.0259	2.79
5	BTB (POZ) domain containing 10	BTBD10	-2.12	0.0019	0.0000	0.0259	1.53
6	growth arrest and DNA-damage-inducible	GADD45A	-2.12	0.0019	0.0000	0.0259	2.49
7	plexin B2	PLXNB2	-2.03	0.0019	0.0000	0.0259	2.50
8	xeroderma pigmentosum, complementati	XPC	-2.03	0.0019	0.0000	0.0259	2.26
9	chromosome 8 open reading frame 38	C8orf38	-1.98	0.0019	0.0000	0.0259	2.26
10	F-box protein 22	FBXO22	-1.97	0.0019	0.0000	0.0259	2.35
11	mitochondrial ribosomal protein L49	MRPL49	-1.93	0.0019	0.0000	0.0259	1.52
12	sestrin 1	SESN1	-1.84	0.0019	0.0000	0.0259	2.62
13	chromosome 1 open reading frame 183	C1orf183	-1.82	0.0019	0.0000	0.0259	1.42
14	zinc finger, matrin type 3	ZMAT3	-1.80	0.0019	0.0000	0.0259	2.18
15	cyclin-dependent kinase inhibitor 1A (p21	CDKN1A	-1.76	0.0019	0.0000	0.0259	2.88
16	zinc finger protein 79	ZNF79	-1.70	0.0019	0.0000	0.0259	1.42
17	MAD1 mitotic arrest deficient-like 1 (yeas	MAD1L1	-1.67	0.0019	0.0000	0.0259	1.76
18	tripartite motif-containing 22	TRIM22	-1.64	0.0019	0.0000	0.0259	1.59
19	ferredoxin reductase	FDXR	-1.64	0.0019	0.0000	0.0259	3.74
20	polymerase (DNA directed), eta	POLH	-1.64	0.0019	0.0000	0.0259	1.58
21	F-box protein 22	FBXO22	-1.57	0.0019	0.0000	0.0259	2.26
22	Notch homolog 1, translocation-associate	NOTCH1	-1.57	0.0019	0.0000	0.0259	1.37
23	zinc finger protein 337	ZNF337	-1.54	0.0019	0.0000	0.0259	1.44
24	Fas (TNF receptor superfamily, member 6	FAS	-1.53	0.0034	0.0001	0.0280	1.90
25	carboxypeptidase M	CPM	-1.52	0.0019	0.0000	0.0259	1.85
26	NA	NA	-1.51	0.0019	0.0000	0.0259	2.06
27	NA	NA	-1.49	0.0019	0.0000	0.0259	2.20
28	glutaminase 2 (liver, mitochondrial)	GLS2	-1.49	0.0019	0.0000	0.0259	2.00
29	NA	NA	-1.49	0.0019	0.0000	0.0259	1.59
30	protein kinase, AMP-activated, beta 1 non	PRKAB1	-1.48	0.0019	0.0000	0.0259	1.49
31	NA	NA	-1.47	0.0019	0.0000	0.0259	1.52
32	carboxypeptidase M	CPM	-1.41	0.0019	0.0000	0.0259	3.36
33	zinc finger protein 79	ZNF79	-1.40	0.0019	0.0000	0.0259	1.48
34	ankyrin repeat, family A (RFXANK-like), 2	ANKRA2	-1.39	0.0019	0.0000	0.0259	1.99
35	transmembrane protein 168	TMEM168	-1.39	0.0019	0.0000	0.0259	2.00
36	biogenesis of lysosome-related organelle	BLOC1S2	-1.38	0.0019	0.0000	0.0259	2.61
37	von Willebrand factor C and EGF domain	VWCE	-1.36	0.0019	0.0000	0.0259	1.65
38	transmembrane protein 142C	TMEM142C	-1.36	0.0019	0.0000	0.0259	1.65
39	Fas (TNF receptor superfamily, member 6	FAS	-1.36	0.0034	0.0001	0.0280	2.29
40	casein kinase 1, gamma 1	CSNK1G1	-1.35	0.0019	0.0000	0.0259	1.58
41	damage-regulated autophagy modulator	DRAM	-1.33	0.0019	0.0000	0.0259	1.97
42	F-box protein 22	FBXO22	-1.33	0.0034	0.0001	0.0280	2.21
43	breast cancer metastasis-suppressor 1-lik	BRMS1L	-1.32	0.0019	0.0000	0.0259	1.50
44	chromosome 12 open reading frame 5	C12orf5	-1.32	0.0019	0.0000	0.0259	3.24
45	vacuolar protein sorting 33 homolog B (ye	VPS33B	-1.30	0.0019	0.0000	0.0259	1.17
46	transmembrane 7 superfamily member 3	TM7SF3	-1.29	0.0019	0.0000	0.0259	1.51
47	RNA binding motif protein 14	RBM14	-1.28	0.0019	0.0000	0.0259	1.45
48	sestrin 2	SESN2	-1.28	0.0019	0.0000	0.0259	2.46
49	activating signal cointegrator 1 complex s	ASCC3	-1.27	0.0034	0.0001	0.0280	1.77
50	coiled-coil domain containing 90B	CCDC90B	-1.27	0.0045	0.0001	0.0365	2.27
51	CLP1, cleavage and polyadenylation facto	CLP1	-1.26	0.0019	0.0000	0.0259	1.32
52	aprataxin	APTX	-1.25	0.0019	0.0000	0.0259	1.46
53	leucine-rich repeats and death domain co	LRDD	-1.24	0.0034	0.0001	0.0280	1.26
54	FtsJ homolog 2 (E. coli)	FTSJ2	-1.24	0.0019	0.0000	0.0259	1.47
55	leucine-rich repeats and death domain co	LRDD	-1.23	0.0019	0.0000	0.0259	1.76
56	RAD51 homolog C (S. cerevisiae)	RAD51C	-1.23	0.0034	0.0001	0.0280	1.61
57	chromosome 13 open reading frame 31	C13orf31	-1.22	0.0034	0.0001	0.0280	1.39
58	astrotactin 2	ASTN2	-1.21	0.0019	0.0000	0.0259	1.52
59	phosphodiesterase 4B, cAMP-specific (ph	PDE4B	-1.20	0.0045	0.0001	0.0365	1.85
60	astrotactin 2	ASTN2	-1.20	0.0034	0.0001	0.0280	1.45
61	transducer of ERBB2, 1	TOB1	-1.18	0.0045	0.0001	0.0365	1.71
62	NA	NA	-1.18	0.0034	0.0001	0.0280	2.40
63	zinc finger protein 90 homolog (mouse)	ZFP90	-1.18	0.0019	0.0000	0.0259	1.47
64	papilin, proteoglycan-like sulfated glycopr	PAPLN	-1.18	0.0019	0.0000	0.0259	1.86
65	proliferating cell nuclear antigen	PCNA	-1.17	0.0045	0.0001	0.0365	1.86
66	polymerase (DNA directed), eta	POLH	-1.16	0.0034	0.0001	0.0280	1.71
67	cyclin G1	CCNG1	-1.16	0.0034	0.0001	0.0280	1.68
68	proline-serine-threonine phosphatase inte	PSTPIP2	-1.15	0.0045	0.0001	0.0365	1.41
69	solute carrier family 7 (cationic amino aci	SLC7A6	-1.14	0.0019	0.0000	0.0259	1.40
70	acyl-Coenzyme A binding domain contain	ACBD6	-1.12	0.0034	0.0001	0.0280	1.36

rank	radiation-induced genes	symbol	Score	FDR	Feature P	Q Value	Fold Change
71	Fas (TNF receptor superfamily, member 6	FAS	-1.12	0.0058	0.0002	0.0426	2.02
72	chromosome 1 open reading frame 183	C1orf183	-1.12	0.0019	0.0000	0.0259	1.27
73	GTP binding protein 2	GTPBP2	-1.11	0.0045	0.0001	0.0365	1.26
74	chromosome 11 open reading frame 24	C11orf24	-1.11	0.0034	0.0001	0.0280	1.35
75	IBR domain containing 3	IBRDC3	-1.11	0.0058	0.0002	0.0426	1.79
76	RAP2B, member of RAS oncogene family	RAP2B	-1.10	0.0108	0.0003	0.0700	1.39
77	solute carrier family 35 (UDP-glucuronic a	SLC35D1	-1.10	0.0019	0.0000	0.0259	1.72
78	interferon stimulated exonuclease gene 2	ISG20L1	-1.09	0.0019	0.0000	0.0259	1.54
79	AP2 associated kinase 1	AAK1	-1.09	0.0034	0.0001	0.0280	1.38
80	G protein-coupled receptor 109B	GPR109B	-1.08	0.0070	0.0002	0.0492	1.60
81	FtsJ homolog 2 (E. coli)	FTSJ2	-1.08	0.0070	0.0002	0.0492	1.67
82	transmembrane 7 superfamily member 3	TM7SF3	-1.07	0.0045	0.0001	0.0365	2.30
83	regulator of G-protein signalling 16	RGS16	-1.07	0.0019	0.0000	0.0259	1.93
84	breast cancer metastasis-suppressor 1-lik	BRMS1L	-1.06	0.0045	0.0001	0.0365	1.20
85	ribosomal protein S27-like	RPS27L	-1.06	0.0108	0.0003	0.0700	1.71
86	major histocompatibility complex, class I-	MR1	-1.06	0.0019	0.0000	0.0259	1.29
87	protein tyrosine phosphatase type IVA, m	PTP4A1	-1.05	0.0034	0.0001	0.0280	1.30
88	TAF3 RNA polymerase II, TATA box bind	TAF3	-1.05	0.0045	0.0001	0.0365	1.28
89	transmembrane protein 168	TMEM168	-1.04	0.0019	0.0000	0.0259	1.59
90	etoposide induced 2.4 mRNA	EI24	-1.04	0.0034	0.0001	0.0280	1.48
91	ribonucleotide reductase M2 B (TP53 indu	RRM2B	-1.04	0.0045	0.0001	0.0365	3.07
92	catenin (cadherin-associated protein), del	CTNND1	-1.04	0.0019	0.0000	0.0259	1.37
93	cleavage stimulation factor, 3' pre-RNA, s	CSTF3	-1.04	0.0070	0.0002	0.0492	1.36
94	CDP-diacylglycerol synthase (phosphatid	CDS2	-1.03	0.0045	0.0001	0.0365	1.26
95	tumor necrosis factor receptor superfamil	TNFRSF10B	-1.03	0.0108	0.0003	0.0700	2.06
96	carboxypeptidase M	CPM	-1.03	0.0134	0.0004	0.0819	3.45
97	lysosomal-associated membrane protein	LAMP3	-1.03	0.0045	0.0001	0.0365	1.61
98	chromosome 1 open reading frame 183	C1orf183	-1.03	0.0082	0.0002	0.0558	1.34
99	carboxypeptidase M	CPM	-1.02	0.0019	0.0000	0.0259	1.72
100	ribosomal protein S27-like	RPS27L	-1.02	0.0058	0.0002	0.0426	1.87
101	zinc finger protein 654	ZNF654	-1.02	0.0034	0.0001	0.0280	1.36
102	sestrin 2	SESN2	-1.01	0.0082	0.0002	0.0558	1.84
103	activating signal cointegrator 1 complex s	ASCC3	-1.00	0.0034	0.0001	0.0280	1.35
104	BCL2 binding component 3	BBC3	-1.00	0.0082	0.0002	0.0558	1.34
105	proliferating cell nuclear antigen	PCNA	-0.99	0.0034	0.0001	0.0280	1.15
106	polo-like kinase 3 (Drosophila)	PLK3	-0.99	0.0045	0.0001	0.0365	1.36
107	zinc finger, FYVE domain containing 1	ZFYVE1	-0.99	0.0034	0.0001	0.0280	1.36
108	solute carrier family 35 (UDP-glucuronic a	SLC35D1	-0.98	0.0019	0.0000	0.0259	1.54
109	IBR domain containing 3	IBRDC3	-0.97	0.0193	0.0006	0.1092	2.24
110	RAB, member of RAS oncogene family-li	RABL2B	-0.97	0.0070	0.0002	0.0492	1.19
111	DCP1 decapping enzyme homolog B (S.	DCP1B	-0.97	0.0045	0.0001	0.0365	1.83
112	chromosome 3 open reading frame 1	C3orf1	-0.97	0.0045	0.0001	0.0365	1.61
113	Fas (TNF receptor superfamily, member 6	FAS	-0.96	0.0082	0.0002	0.0558	2.13
114	Rab geranylgeranyltransferase, alpha sub	RABGGTA	-0.96	0.0045	0.0001	0.0365	1.48
115	nudix (nucleoside diphosphate linked moi	NUDT15	-0.95	0.0108	0.0003	0.0700	1.51
116	CD70 molecule	CD70	-0.95	0.0134	0.0004	0.0819	1.51
117	major histocompatibility complex, class I-	MR1	-0.95	0.0058	0.0002	0.0426	1.19
118	carcinoembryonic antigen-related cell adh	CEACAM1	-0.95	0.0082	0.0002	0.0558	1.40
119	phosphohistidine phosphatase 1	PHPT1	-0.94	0.0019	0.0000	0.0259	1.34
120	GPI deacylase	PGAP1	-0.94	0.0019	0.0000	0.0259	1.27
121	NA	NA	-0.94	0.0097	0.0003	0.0630	1.21
122	annexin A4	ANXA4	-0.93	0.0221	0.0007	0.1215	1.35
123	tumor necrosis factor (ligand) superfamily	TNFSF9	-0.93	0.0134	0.0004	0.0819	1.69
124	syntaxin 6	STX6	-0.92	0.0108	0.0003	0.0700	1.32
125	zinc finger CCCH-type, antiviral 1	ZC3HAV1	-0.92	0.0034	0.0001	0.0280	1.19
126	ribosomal protein S6 kinase, 90kDa, poly	RPS6KA1	-0.91	0.0123	0.0004	0.0764	1.42
127	potassium intermediate/small conductanc	KCNN3	-0.91	0.0058	0.0002	0.0426	1.41
128	tripartite motif-containing 32	TRIM32	-0.90	0.0019	0.0000	0.0259	1.30
129	lysophospholipase 3 (lysosomal phospho	LYPLA3	-0.90	0.0082	0.0002	0.0558	1.18
130	NA	NA	-0.90	0.0019	0.0000	0.0259	1.30
131	damage-specific DNA binding protein 2, 4	DDB2	-0.90	0.0045	0.0001	0.0365	1.56
132	RAN binding protein 10	RANBP10	-0.90	0.0134	0.0004	0.0819	1.10
133	TP53 activated protein 1	TP53AP1	-0.89	0.0058	0.0002	0.0426	1.47
134	Mdm2, transformed 3T3 cell double minu	MDM2	-0.89	0.0149	0.0004	0.0891	1.98
135	immediate early response 5	IER5	-0.88	0.0193	0.0006	0.1092	1.98
136	transmembrane 7 superfamily member 3	TM7SF3	-0.88	0.0184	0.0006	0.1062	1.87
137	cell growth regulator with ring finger doma	CGRRF1	-0.88	0.0045	0.0001	0.0365	1.33
138	transmembrane 7 superfamily member 2	TM7SF2	-0.88	0.0070	0.0002	0.0492	1.38
139	proline rich 14	PRR14	-0.87	0.0108	0.0003	0.0700	1.10
140	GPI deacylase	PGAP1	-0.87	0.0134	0.0004	0.0819	1.22

rank	radiation-induced genes	symbol	Score	FDR	Feature P	Q Value	Fold Change
141	galactose-3-O-sulfotransferase 4	GAL3ST4	-0.87	0.0123	0.0004	0.0764	1.27
142	E2F transcription factor 7	E2F7	-0.87	0.0058	0.0002	0.0426	2.68
143	solute carrier family 30 (zinc transporter),	SLC30A1	-0.86	0.0173	0.0005	0.1008	1.57
144	TP53 activated protein 1	TP53AP1	-0.86	0.0058	0.0002	0.0426	1.47
145	tumor protein p53 inducible protein 3	TP53I3	-0.86	0.0019	0.0000	0.0259	1.69
146	apolipoprotein B mRNA editing enzyme, c	APOBEC3G	-0.86	0.0184	0.0006	0.1062	1.65
147	inositol polyphosphate-1-phosphatase	INPP1	-0.86	0.0108	0.0003	0.0700	1.65
148	chromosome 10 open reading frame 10	C10orf10	-0.86	0.0232	0.0007	0.1264	1.30
149	scribbled homolog (Drosophila)	SCRIB	-0.86	0.0298	0.0009	0.1554	1.39
150	sorbitol dehydrogenase	SORD	-0.86	0.0123	0.0004	0.0764	1.27
151	suppressor of variegation 4-20 homolog 1	SUV420H1	-0.85	0.0108	0.0003	0.0700	1.35
152	dermatan 4 sulfotransferase 1	D4ST1	-0.85	0.0082	0.0002	0.0558	1.27
153	zinc finger protein 337	ZNF337	-0.85	0.0320	0.0010	0.1643	1.20
154	KIAA1128	KIAA1128	-0.85	0.0108	0.0003	0.0700	1.24
155	F-box protein 22	FBXO22	-0.84	0.0184	0.0006	0.1062	1.25
156	AP2 associated kinase 1	AAK1	-0.84	0.0184	0.0006	0.1062	1.43
157	hydroxysteroid dehydrogenase like 2	HSDL2	-0.84	0.0097	0.0003	0.0630	1.37
158	creatine kinase, mitochondrial 2 (sarcome	CKMT2	-0.84	0.0163	0.0005	0.0961	1.18
159	protein tyrosine phosphatase type IVA, m	PTP4A1	-0.84	0.0034	0.0001	0.0280	1.34
160	apoptotic peptidase activating factor 1	APAF1	-0.84	0.0184	0.0006	0.1062	1.33
161	leukemia inhibitory factor (cholinergic diffe	LIF	-0.83	0.0289	0.0009	0.1515	1.29
162	tumor protein p53 inducible nuclear protei	TP53INP1	-0.83	0.0070	0.0002	0.0492	2.00
163	Ras-related associated with diabetes	RRAD	-0.83	0.0173	0.0005	0.1008	1.22
164	TP53 activated protein 1	TP53AP1	-0.82	0.0045	0.0001	0.0365	1.52
165	chromosome 11 open reading frame 24	C11orf24	-0.82	0.0163	0.0005	0.0961	1.40
166	dynactin 5 (p25)	DCTN5	-0.82	0.0184	0.0006	0.1062	1.13
167	guanidinoacetate N-methyltransferase	GAMT	-0.82	0.0173	0.0005	0.1008	1.25
168	thymidylate synthetase	TYMS	-0.82	0.0207	0.0006	0.1153	1.37
169	transducer of ERBB2, 1	TOB1	-0.82	0.0407	0.0013	0.1973	1.80
170	ATG16 autophagy related 16-like 2 (S. ce	ATG16L2	-0.82	0.0108	0.0003	0.0700	1.25
171	Tax1 (human T-cell leukemia virus type I)	TAX1BP3	-0.81	0.0484	0.0016	0.2252	1.48
172	glutathione peroxidase 1	GPX1	-0.81	0.0298	0.0009	0.1554	1.32
173	chromosome 1 open reading frame 57	C1orf57	-0.81	0.0070	0.0002	0.0492	1.28
174	NA	NA	-0.81	0.0446	0.0015	0.2113	1.67
175	Pvt1 oncogene homolog, MYC activator (	PVT1	-0.81	0.0393	0.0012	0.1939	1.27
176	inositol 1,4,5-triphosphate receptor, type 2	ITPR2	-0.81	0.0407	0.0013	0.1973	2.01
177	capicua homolog (Drosophila)	CIC	-0.81	0.0419	0.0014	0.2016	1.18
178	interleukin 27 receptor, alpha	IL27RA	-0.81	0.0310	0.0010	0.1597	1.27
179	phosphatidylinositol 4-kinase, catalytic, be	PIK4CB	-0.80	0.0262	0.0008	0.1399	1.32
180	protein kinase, X-linked	PRKX	-0.80	0.0207	0.0006	0.1153	1.33
181	ATP-binding cassette, sub-family A (ABC	ABCA5	-0.80	0.0397	0.0013	0.1939	1.27
182	receptor expressed in lymphoid tissues lik	RELL1	-0.80	0.0173	0.0005	0.1008	1.57
183	vacuolar protein sorting 24 homolog (S. c	VPS24	-0.79	0.0232	0.0007	0.1264	1.25
184	chromosome 1 open reading frame 121	C1orf121	-0.79	0.0397	0.0013	0.1939	1.29
185	SMEK homolog 1, suppressor of mek1 (D	SMEK1	-0.79	0.0173	0.0005	0.1008	1.48
186	RAD51 homolog C (S. cerevisiae)	RAD51C	-0.79	0.0529	0.0018	0.2412	1.34
187	growth differentiation factor 15	GDF15	-0.79	0.0019	0.0000	0.0259	3.23
188	WAS/WASL interacting protein family, me	WIPF2	-0.78	0.0426	0.0014	0.2041	1.18
189	carboxymethylenebutenolidase homolog (	CMBL	-0.78	0.0310	0.0010	0.1597	2.21
190	Ras-related associated with diabetes	RRAD	-0.78	0.0495	0.0017	0.2289	1.42
191	SERTA domain containing 1	SERTAD1	-0.78	0.0320	0.0010	0.1643	1.34
192	abhydrolase domain containing 4	ABHD4	-0.78	0.0354	0.0011	0.1778	1.17
193	hypothetical gene supported by BC02419	LOC400099	-0.78	0.0467	0.0016	0.2189	1.17
194	transmembrane protein 30A	TMEM30A	-0.78	0.0298	0.0009	0.1554	1.51
195	myeloid leukemia factor 2	MLF2	-0.78	0.0393	0.0012	0.1939	1.32
196	phosphodiesterase 4B, cAMP-specific (ph	PDE4B	-0.78	0.0184	0.0006	0.1062	1.68
197	activating transcription factor 3	ATF3	-0.78	0.0426	0.0014	0.2041	1.79
198	RAP2B, member of RAS oncogene famil	RAP2B	-0.78	0.0354	0.0011	0.1778	1.58
199	casein kinase 1, gamma 1	CSNK1G1	-0.78	0.0221	0.0007	0.1215	1.25
200	motile sperm domain containing 1	MOSPD1	-0.78	0.0320	0.0010	0.1643	1.24
201	SEC22 vesicle trafficking protein homolog	SEC22A	-0.77	0.0446	0.0015	0.2113	1.11
202	cytochrome P450, family 4, subfamily F, p	CYP4F3	-0.77	0.0456	0.0015	0.2150	1.16
203	hydroxysteroid (17-beta) dehydrogenase 7	HSD17B7P2	-0.77	0.0741	0.0026	0.3138	1.72
204	actin, alpha 2, smooth muscle, aorta	ACTA2	-0.77	0.0397	0.0013	0.1939	1.52
205	transmembrane protein 68	TMEM68	-0.77	0.0565	0.0019	0.2542	1.74
206	NA	NA	-0.77	0.0484	0.0016	0.2252	1.14
207	tripartite motif-containing 38	TRIM38	-0.77	0.0495	0.0017	0.2289	1.28
208	nucleolar protein 14	NOL14	-0.77	0.0426	0.0014	0.2041	1.20
209	sestrin 1	SESN1	-0.76	0.0593	0.0020	0.2647	1.17
210	proline rich 14	PRR14	-0.76	0.0193	0.0006	0.1092	1.18
211	SMAD family member 5	SMAD5	-0.76	0.0354	0.0011	0.1778	1.71

TABLE 2. RADIATION-INDUCED GENES AFTER IR.

This table lists the transcripts induced after radiation in response to a 5 Gy IR 5 hour exposure. Genes were determined to be enriched at a FDR cutoff of ≤ 0.05. Genes represented multiple times in this list indicate independent measurements from independent probe sets on the array.

GO Categories Enriched in Irradiated Samples (i.e. radiation-induced)							
Category	Name	Name	SIZE	EnrichmentScore	Normalized ES	NOM.p.val	FDR.q.val
GO:0030203	Biological Process	glycosaminoglycan metabolism	34	-0.61	-2.04	0.00	0.00
GO:0006022	Biological Process	aminoglycan metabolism	35	-0.60	-2.02	0.00	0.00
GO:0006029	Biological Process	proteoglycan metabolism	24	-0.61	-1.92	0.00	0.01
GO:0006790	Biological Process	sulfur metabolism	54	-0.48	-1.89	0.00	0.01
GO:0008285	Biological Process	negative regulation of cell proliferation	130	-0.42	-1.88	0.00	0.01
GO:0007050	Biological Process	cell cycle arrest	56	-0.52	-1.80	0.00	0.02
GO:0042157	Biological Process	lipoprotein metabolism	38	-0.51	-1.77	0.00	0.03
GO:0045786	Biological Process	negative regulation of progression through cell cy	133	-0.41	-1.73	0.00	0.04
GO:0007259	Biological Process	JAK-STAT cascade	29	-0.48	-1.72	0.00	0.04
GO:0007179	Biological Process	transforming growth factor beta receptor signalin	30	-0.51	-1.71	0.01	0.04
GO:0006919	Biological Process	caspase activation	24	-0.57	-1.71	0.01	0.04
GO:0051345	Biological Process	positive regulation of hydrolase activity	24	-0.57	-1.71	0.01	0.03
GO:0043280	Biological Process	positive regulation of caspase activity	24	-0.57	-1.71	0.01	0.03
GO:0044272	Biological Process	sulfur compound biosynthesis	28	-0.52	-1.71	0.00	0.03
GO:0015630	Cellular Component	microtubule cytoskeleton	200	0.48	1.95	0.00	0.02
GO:0005819	Cellular Component	spindle	48	0.66	1.92	0.00	0.01
GO:0000785	Cellular Component	chromatin	105	0.52	1.89	0.00	0.01
GO:0005875	Cellular Component	microtubule associated complex	83	0.46	1.88	0.00	0.01
GO:0005874	Cellular Component	microtubule	145	0.45	1.83	0.00	0.02
GO:0000775	Cellular Component	chromosome, pericentric region	29	0.73	1.71	0.00	0.04
GO:0000786	Cellular Component	nucleosome	47	0.52	1.69	0.03	0.04
GO:0003777	Molecular Function	microtubule motor activity	56	0.58	2.12	0.00	0.00
GO:0003774	Molecular Function	motor activity	119	0.38	1.73	0.00	0.09
GO:0004725	Molecular Function	protein tyrosine phosphatase activity	71	0.41	1.70	0.00	0.10
GO:0004540	Molecular Function	ribonuclease activity	49	0.48	1.63	0.01	0.18
GO:0003682	Molecular Function	chromatin binding	40	0.53	1.60	0.02	0.19
GO:0005200	Molecular Function	structural constituent of cytoskeleton	81	0.38	1.56	0.02	0.27
GO:0008138	Molecular Function	protein tyrosine/serine/threonine phosphatase ac	33	0.42	1.49	0.02	0.53

TABLE 3. ENRICHMENT OF GO CATEGORIES FOR THE RADIATION-INDUCED GENES.

Gene set enrichment was calculated using GSEA for GO categories strongly associated with the irradiated samples in comparison to the unirradiated samples. The Enrichment Score (ES) was calculated using the Signal2Noise test statistic (see Methods) and 1000 permutations were used for each analysis.

GO Categories Enriched in Non-irradiated samples (i.e. radiation-repressed)							
Category		**Name**	**SIZE**	**EnrichmentScore**	**Normalized ES**	**NOM.p.val**	**FDR.q.val**
GO:0007017	Biological Process	microtubule-based process	116	0.60	2.09	0.00	0.00
GO:0007010	Biological Process	cytoskeleton organization and biogenesis	311	0.46	2.03	0.00	0.00
GO:0007018	Biological Process	microtubule-based movement	68	0.55	2.01	0.00	0.00
GO:0030705	Biological Process	cytoskeleton-dependent intracellular transport	72	0.53	1.97	0.00	0.00
GO:0000279	Biological Process	M phase	162	0.64	1.97	0.00	0.00
GO:0000226	Biological Process	microtubule cytoskeleton organization and bioge	47	0.68	1.95	0.00	0.00
GO:0051258	Biological Process	protein polymerization	35	0.58	1.86	0.00	0.01
GO:0051301	Biological Process	cell division	143	0.62	1.85	0.00	0.01
GO:0000087	Biological Process	M phase of mitotic cell cycle	128	0.68	1.85	0.00	0.01
GO:0007059	Biological Process	chromosome segregation	23	0.72	1.84	0.00	0.01
GO:0007067	Biological Process	mitosis	126	0.68	1.84	0.00	0.01
GO:0000278	Biological Process	mitotic cell cycle	188	0.59	1.76	0.00	0.03
	Cellular Component	none were significant					
	Molecular Function	none were significant					

TABLE 4. ENRICHMENT OF GO CATEGORIES IN THE UNIRRADIATED SAMPLES.

Gene set enrichment was calculated using GSEA for GO categories strongly associated with the unirradiated samples in comparison to the irradiated samples. The Enrichment Score (ES) was calculated using the Signal2Noise test statistic (see Methods) and 1000 permutations were used for each analysis.

Dataset	Phenotype	Enriched for RI	Enriched for RR
Breast cancer (van de Vijver 2002)	outcome	0.434, 0.442	**0.000, 0.001**
Breast cancer (van de Vijver 2002)	ER status	0.286, 0.310	**0.001, 0.006**
Breast cancer (West 2001)	ER status	0.789, 1	**0.004, 0.006**
Breast cancer (van de Vijver 2002)	BRCA 1/2 status	0.166, 0.455	**0.024, 0.013**
Lung (Beer 2002)	outcome	0.155, 0.191	0.315, 0.792
Lung (Bhatacharjee 2001)	outcome	0.861, 0.811	0.678, 1
Lymphoma (Monti 2001)	outcome	0.230, 0.451	0.502, 0.453
Glioma (Nutt 2003)	outcome	0.623, 0.563	0.567, 1
Medulloblastoma (Pomeroy 2002)	outcome	0.316, 0.307	0.157, 0.202
Hepatocarcinoma (Iizuka 2003)	outcome	0.519, 0.605	0.453, 1
Multiple cancers (Ramaswamy 2001)	P53 status	**0.000, 0.006**	0.113, 0.169

TABLE 5. ENRICHMENT OF CLINICAL PARAMETERS IN RADIATION-INDUCED AND RADIATION-REPRESSED GENE SETS BY GSEA.

We tested for enrichment of Radiation Induced (RI) or Radiation Repressed (RR) gene sets with respect to clinical parameters in a panel of tumor datasets, assessed by the GSEA tool. The pairs of numerical values in each row correspond to: nominal p-value, q-value. Data tested were curated from a number of expression datasets from multiple cancers. The clinical traits tested were comprised of outcome in multiple cancer types (BEER *et al.* 2002; BHATTACHARJEE *et al.* 2001; MONTI *et al.* 2005; NUTT *et al.* 2003; POMEROY *et al.* 2002; SINGH *et al.* 2002; VAN DE VIJVER *et al.* 2002), estrogen receptor status in breast cancers (VAN DE VIJVER *et al.* 2002; WEST *et al.* 2001), Brca1 status in breast cancer (VAN 'T VEER *et al.* 2002), and P53 status in multiple cancer cell lines (RAMASWAMY *et al.* 2001). Radiation-induced (RI) and radiation-repressed (RR) genes from this study were used as bait for the GSEA program (SUBRAMANIAN *et al.* 2005) in testing for correlation with the clinical parameters described above. For the GSEA settings, we used the Signal2Noise algorithm, normalization method was meandiv, permutations were done by phenotype, the scoring scheme was weighted, and 1000 permutations were used for each analysis. Results were considered to be significant (and displayed in boldface) if both the p-value ≤ 0.05 & the FDR q-value ≤ 0.05. For breast cancers, clinical outcome, ER- status, Her2-, and BRCA1/2 mutant status were significantly associated with the RR signature. The RI signature showed correlation with wildtype P53 status.

RI gene	p-value	p53 regulated?	reference
BLOC1S2	**0**	**not reported**	
BRMS1L	**0**	**not reported**	
BTBD10	**0**	**not reported**	
C12orf5	**0**	**yes**	**Jen, Cancer Res. 2005 65:7666-73**
C8orf38	**0**	**not reported**	
DRAM	**0**	**yes**	**Creighton, Cell 2006, 121-34**
FBXO22	**0**	**not reported**	
FTSJ2	**0**	**not reported**	
LRDD	**0**	**yes**	**Genome Biol. 2006; 7(3): R25.**
NOTCH1	**0**	**yes**	**Yugawa MCB 2007**
PPM1D	**0**	**yes**	**Choi, Genomics 2000**
TRIAP1	**0**	**yes**	**Park Cancer Res. 2005 65(4):1197-206.**
APTX	**1.00E-04**	**not reported**	
SESN2	**2.00E-04**	**yes**	**Budanov, Oncogene 2002, 21:6017-31.**
XPC	**5.00E-04**	**yes**	**Genome Biol. 2006; 7(3): R25.**
RBM14	**0.001**	**not reported**	
ZNF337	**0.001**	**not reported**	
CSNK1G1	**0.0012**	**yes**	**JCB, Volume 173, Number 4, 533-544**
MAD1L1	**0.0021**	**yes**	**Chun J Biol Chem. 2003**
TRIM22	**0.0029**	**yes**	**Genome Biol. 2006; 7(3): R25.**
CDKN1A	**0.0043**	**yes**	**Jen, Cancer Res. 2005 65:7666-73**
TMEM142C	**0.0084**	**not reported**	
PHLDA3	**0.0128**	**yes**	**Jen, Cancer Res. 2005 65:7666-73**
C1orf183	**0.0276**	**not reported**	
VPS33B	**0.0281**	**not reported**	
CPM	**0.0361**	**not reported**	
PRKAB1	**0.0365**	**yes**	**Jen, Cancer Res. 2005 65:7666-73**
GLS2	0.0599	yes	Genome Biol. 2006; 7(3): R25.
ZMAT3	0.0602	yes	Genome Biol. 2006; 7(3): R25.
FDXR	0.0793	yes	Liu & Chen; Oncogene 2002
ZNF79	0.0912	not reported	
TM7SF3	0.1251	not reported	
POLH	0.1358	yes	Liu & Chen MCB 2006
DDB2	0.1791	yes	Barenco Genome Biol. 2006; 7(3): R25.
MRPL49	0.286	yes	Yang, J Invest. Derm. 2006 :2490-506.
VWCE	0.4255	not reported	
ANKRA2	0.5336	not reported	
GADD45A	0.6555	yes	Genome Biol. 2006; 7(3): R25.
TMEM168	0.7914	not reported	
SESN1	0.8738	yes	Genome Biol. 2006; 7(3): R25.
ASTN2	0.8815	yes	Wei, Cell 124, pp 207-219

TABLE 6. P53-DEPENDENT TARGETS IN THE RI SET.

Only a subset of genes in the RI gene set are known to be targets of p53. For the 41 RI genes overlapping with the Loi et al. breast tumor dataset (LOI *et al.* 2007), we list the p-value for differential expression between the good- and poor-outcome clusters, along with information on whether gene expression is

known to be driven by p53. Genes with significant p-values (indicated by boldface text) showing differential expression between the two clusters are hypothesized to play a role in driving the clustering.

Gene Symbol	t-test	p-value	q-value
MMP23B	-0.181	0	0.002
DPAGT1	-0.26	0	0.009
SPTBN1	-0.26	0	0.012
LPP	-0.311	0	0.014
DCTN3	-0.294	0	0.014
ZNF318	-0.282	0	0.014
GTF2H1	-0.27	0	0.014
BTN2A1	-0.27	0	0.014
DDX12	-0.261	0	0.014
N/A	-0.248	0	0.014
N/A	-0.238	0	0.014
CLTA	-0.238	0	0.014
GALNT1	-0.237	0	0.014
DNMT1	-0.235	0	0.014
GOLGA4	-0.23	0	0.014
STK38	-0.212	0	0.014
FRG1	-0.199	0	0.014
EBP	-0.183	0	0.014
LGALS4	-0.182	0	0.014
MZF1	-0.181	0	0.014
PLOD2	-0.178	0	0.014
EIF1AP1	-0.176	0	0.014
AMPD2	-0.163	0	0.014
PA2G4	-0.162	0	0.014
PTCD3|BUB3	-0.286	0	0.015
ARID5A	-0.267	0	0.015
PRDX1	-0.266	0	0.015
CASR	-0.263	0	0.015
HIST2H2BE	-0.257	0	0.015

SNRPD2	-0.245	0	0.015
N/A	-0.242	0	0.015
GSTM5	-0.241	0	0.015
ARSB	-0.24	0	0.015
ECHS1	-0.237	0	0.015
IGHG1|EPC1	-0.225	0	0.015
PIM1	-0.224	0	0.015
LOC728643	-0.219	0	0.015
LSS	-0.218	0	0.015
GNB2L1	-0.218	0	0.015
SERPINB1	-0.218	0	0.015
HLA-DOA	-0.215	0	0.015
IREB2	-0.202	0	0.015
SLC31A2	-0.196	0	0.015
N/A	-0.186	0	0.015
KATNB1	-0.177	0	0.015
ACY1	-0.176	0	0.015
SDHD|RHCE	-0.175	0	0.015
C6orf136	-0.175	0	0.015
RPS6KA3	-0.243	0	0.016
BCL3	-0.22	0	0.016
N/A	-0.209	0	0.016
ADD2	-0.199	0	0.016
TM9SF2	-0.171	0	0.016
RAB7L1	-0.253	0	0.017
N/A|NAB1	-0.149	0	0.017
VASP	-0.3	0	0.018
SCARB1	-0.219	0	0.018
MEST	-0.292	0	0.019
DCT|EGR1	-0.234	0	0.019
SLC19A1|COL18A1	-0.233	0	0.019

N/A	-0.203	0	0.019
LOC162427|N/A	-0.189	0	0.019
U2AF1L4	-0.173	0	0.019
PAK1	-0.162	0	0.019
CYP4A11|SLC4A7	-0.273	0.001	0.02
LOC728913	-0.162	0.001	0.02

TABLE 7. DIFFERENTIAL EXPRESSION OF GENES IN BREAST TUMOR LINES BEFORE AND AFTER 8 GY OF IR.

Differential expression of genes in breast tumor cell lines before and after 8 Gy of IR from a recently published dataset from Amundson et al (AMUNDSON *et al.* 2008).

	Univariate Analysis		Multivariate Analysis			
			Model 1		Model 2	
	Hazard Ratio	P value	Hazard Ratio	P value	Hazard Ratio	P value
RI Signature	1.1	**0.04**	1.071	0.170	---	---
RR Signature	0.896	**5.61e-9**	0.940	**0.030**	---	**---**
Rad Signature (RI+RR)	0.898	**2.9e-9**	---	**---**	0.936	**0.021**
Age	0.593	**0.013**	0.652	**0.050**	0.630	**0.033**
Diameter	1.19	0.13	1.033	0.810	1.015	0.910
Lymph Node (0, 1, 2)	1.12	**0.012**	1.004	0.970	0.995	0.960
Tumor Grade (1, 2, 3)	1.98	**1.9e-5**	1.160	0.460	1.114	0.590
VascularInvasion.13	0.87	0.55	1.741	0.160	1.782	0.140
VascularInvasion.4	1.90	**0.02**	2.825	0.140	2.897	0.130
ER status (1 = pos, 0 = neg)	0.334	**2.7e-6**	0.583	0.069	0.665	0.150
Mastectomy vs conserving therapy	1.12	0.62	0.983	0.950	1.057	0.820
Chemo or hormonal therapy	0.931	0.75	0.574	0.120	0.582	0.130
Wound Response	3.67	**9.3e-8**	1.382	0.12	1.541	0.230

TABLE 8. ANALYSIS OF RISK FACTORS FOR DEATH IN BREAST CANCER PATIENTS IN THE NKI STUDY.

Univariate and Multivariate Analysis of risk factors for death in a group of breast cancer patients from the Netherland Cancer Institute (VAN DE VIJVER *et al.* 2002). The left two columns list hazard ratios and p-values from a univariate Cox analysis of survival outcome calculated independently for each parameter. The subsequent columns show two variations on a multivariate Cox analysis, using RR and RI sets as independent variables with other clinical properties (Model 1), and using the combined radiation set with the same clinical variables (Model 2).

	Univariate Analysis		Multivariate Analysis			
			Model 1		Model 2	
	Hazard Ratio	P value	Hazard Ratio	P value	Hazard Ratio	P value
RI Signature	1.09	**0.005**	1.065	0.130	--	--
RR Signature	0.946	**3e-5**	0.970	0.160	--	**--**
Rad Signature (RI+RR)	0.948	**2.6e-5**	--	**--**	0.954	**0.009**
Age	1	1	0.99	0.470	0.992	0.540
Tumor Grade (1, 2, 3)	1.56	**0.015**	1.043	0.850	1.009	0.970
Tumor Size (0— 8.2)	1.34	**0.00012**	1.218	0.071	1.182	0.110
ER status (1 = pos, 0 = neg)	0.217	**0.0097**	0.22	**0.015**	0.232	**0.019**
Lymph Node (0, 1)	1.21	0.39	1.110	0.690	1.139	0.620

TABLE 9. ANALYSIS OF RISK FACTORS FOR DEATH IN BREAST CANCER PATIENTS IN THE LOI *ET AL.* STUDY.

Univariate and Multivariate Analysis of risk factors for death in a group of breast cancer patients from Loi *et. al*. The left two columns list hazard ratios and p-values from a univariate Cox analysis of survival outcome calculated independently for each parameter. The subsequent columns show two variations on a multivariate Cox analysis, using RR and RI sets as independent variables with other clinical properties (Model 1), and using the combined radiation set with the same clinical variables (Model 2).

	Total Genes	Overlap with RR	Overlap with RI
Amsterdam 70-gene	70	1	1
76-gene	75	0	0
Wound response	512	1	2
GGI	97	34	0
PTEN	246	11	4
RS	21	3	0

TABLE 10. OVERLAP OF RR AND RI GENE SIGNATURES WITH OTHER BREAST CANCER OUTCOME SIGNATURES.

Gene set	# of Genes in Signature	Overlap between signature and genes on the NKI arrays	Error Rate	Sensitivity
Radiation Response	68 (RR) +50(RI)	34(RR)+15(RI)	30.2%	68.4%
Wound Response	512	269	28.7%	75.4%
70 gene	70	47	34.9%	63.2%
RS	20	13	28.7%	73.7%
GGI	94	60	28.7%	73.7%
76 gene	76	38	29.5%	68.4%
PTEN	246	104	28.7%	68.4%

TABLE 11. ERROR RATE AND SENSITIVITY FROM LEAVE-ONE-OUT CROSS VALIDATION.

Error rate and sensitivity from leave-one-out cross validation analysis of a panel of breast cancer outcome signatures for tumor classification using the NKI dataset (VAN DE VIJVER *et al.* 2002).

Group Index	True Survival	Predicted Survival	#of patients
1	Good	Good (at least 6 out of 7 signature)	51
2	Good	Bad (at least 6 out of 7 signature)	17
3	Bad	Good (at least 6 out of 7 signature)	10
4	Bad	Bad (at least 6 out of 7 signature)	30
0		3 signature votes for good/bad, while the other 4 votes for bad/good	21

TABLE 12. SEGREGATION OF TUMOR SAMPLES INTO 4 GROUPS BASED ON THEIR CLASSIFICATION BY GENE EXPRESSION SIGNATURES.

Group 1 represents good true survival and correctly classified; group 2 represents good survival and incorrectly classified; group 3 is bad survival and incorrectly classified; and group 4 represents bad survival and correctly classified. Samples were assigned group 0 if they were not consistently classified as good or bad by the panel of expression signatures.

	H0: no difference between Group1 and group 3	H0: no difference between Group 2 and group 4
Age	0.532	0.281
Diameter	0.922	0.749
LymphNode	0.991	0.227
Tumor Grade	**0.021**	0.293
Vascular Invasion	0.444	0.289
ER	0.253	0.066
Mastectomy vs. conserving therapy	0.283	0.515
Chemo or hormonal therapy	1	1

TABLE 13. P-VALUES FOR THE ASSOCIATION BETWEEN CLINICAL VARIABLES AND GROUP LABELS IN TABLE 12.

For the first hypothesis tested, the null indicates that there is no difference between the good survival samples that were either correctly or incorrectly classified. The second hypothesis is the same but for the true bad outcome samples. Tumor grade was significantly different between Groups 1 and 3, and thus offer additional classification information along with the gene expression signatures.

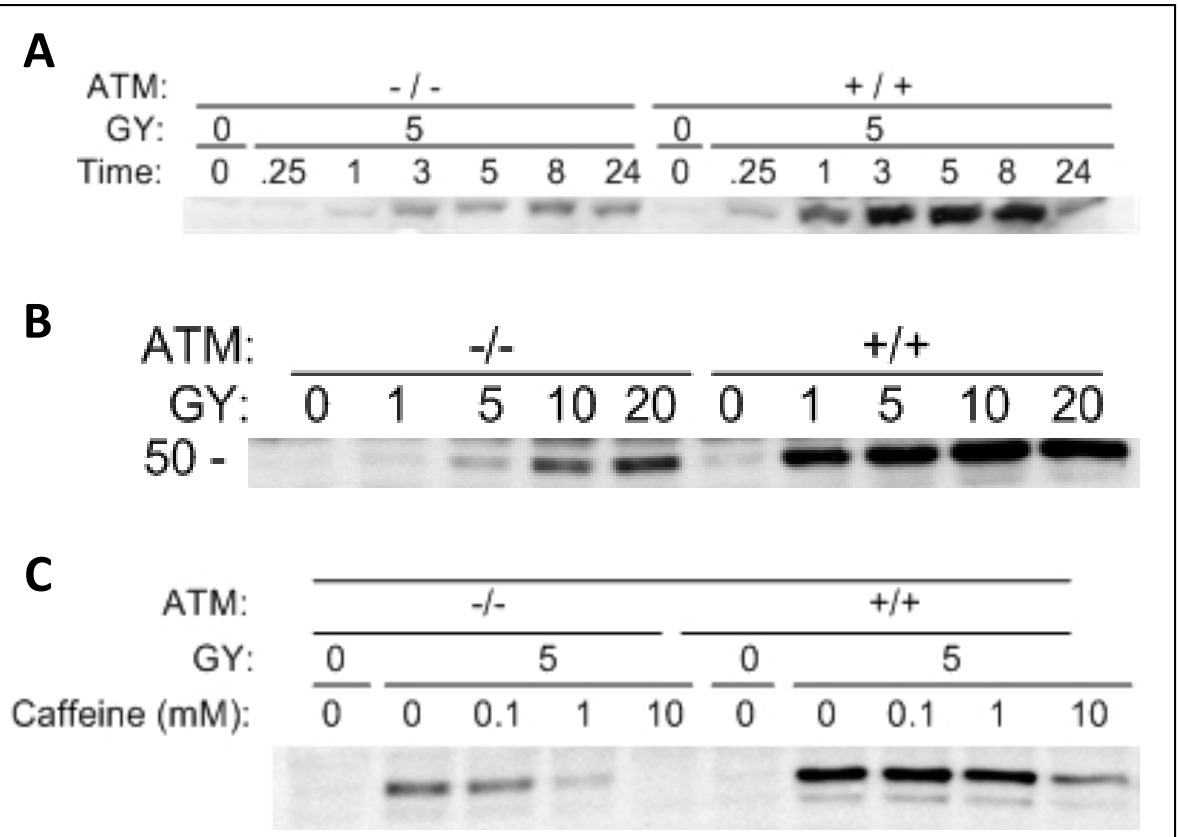

FIGURE 1. WESTERN BLOTTING FOR P53 PHOSPHORYLATION IN ATM+/+ AND ATM-/- CELLS.

A&B. Cell lines of the indicated genotype were treated with the indicated dose of ionizing radiation and harvested at the indicated time. Western blotting was performed with an antibody recognizing the S15 phosphorylation site on TP53. C. Cell lines of the indicated genotype were grown in the presence of the indicated dose of caffeine and subsequently irradiated with 5 Gy of IR. Cells were harvested 5 hours after irradiation and Western blotting was performed for phospho-P53. Blot is courtesy of Richard Ivey.

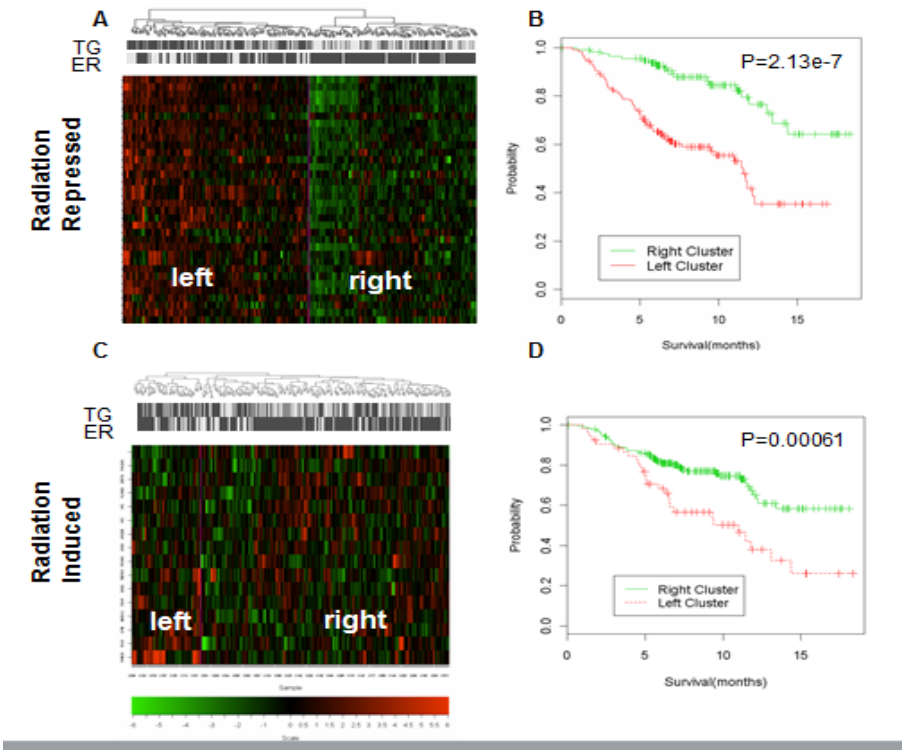

FIGURE 2. RADIATION-REPRESSED (RR) OR RADIATION–INDUCED (RI) GENE SIGNATURES CLUSTER BREAST CANCER PATIENTS FROM THE NETHERLAND CANCER INSTITUTE ACCORDING TO CLINICAL OUTCOME.

Panel A shows clustering of tumors in the space of the RR genes. The bars above the heatmap indicate clinical variables of tumor grade (black- "poorly differentiated", grey- "intermediate", white – "well differentiated"), and ER status (black- positive, white- negative). Panel B shows K-M survival analysis for the two clusters separated in A. Panels C&D show clustering analysis and survival analysis in the space of the RI genes.

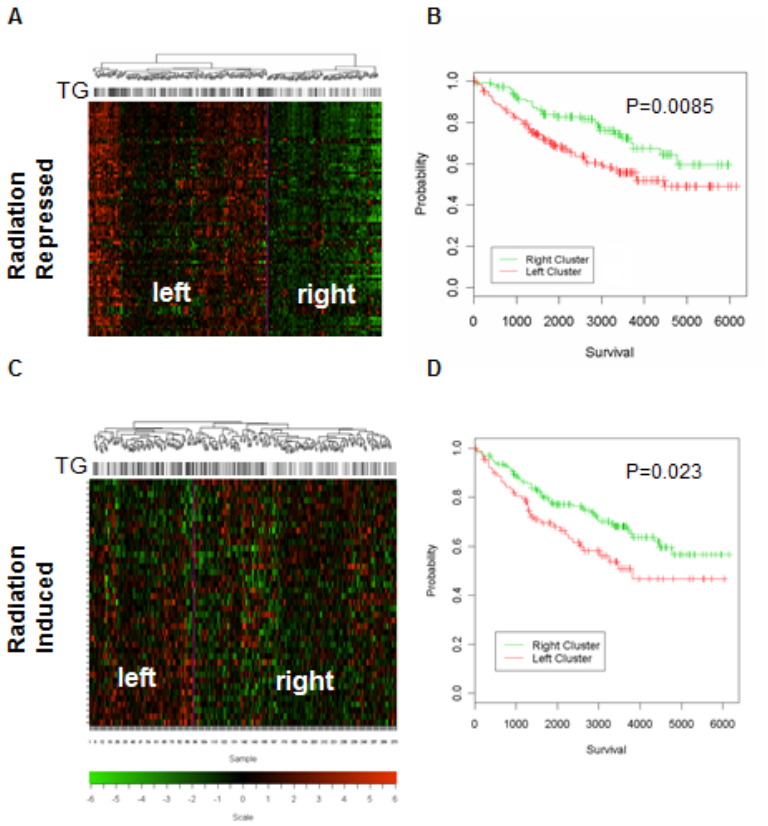

FIGURE 3. RADIATION-REPRESSED (RR) OR RADIATION–INDUCED (RI) GENE SIGNATURES CLUSTER BREAST CANCER PATIENTS FROM LOI *ET AL*. ACCORDING TO CLINICAL OUTCOME.

Panel A shows clustering of tumors in the space of the RR genes. Panel B shows K-M survival analysis for the two clusters separated in A. Panels C&D show clustering analysis and survival analysis in the space of the RI genes. The bars above the heatmap indicate clinically assessed tumor grade (black- "poorly differentiated", grey- "intermediate", white – "well differentiated").

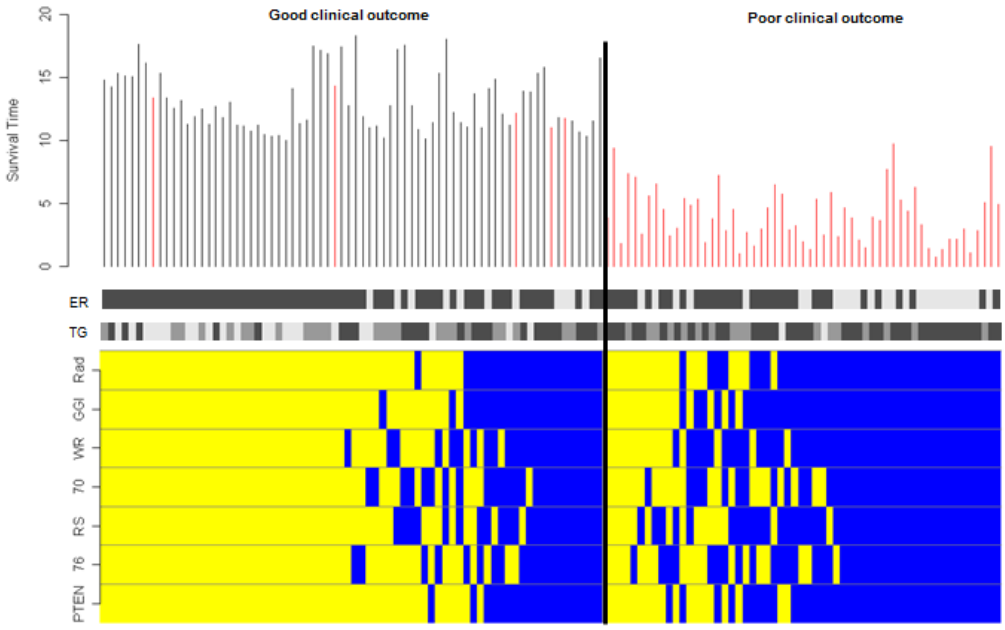

FIGURE 4. COMPARISON OF TUMOR CLASSIFICATION BY GENE EXPRESSION SIGNATURES.

Heatmap showing classification of each patient in the NKI dataset based on Cross-Validation for all the samples using the panel of gene signatures. Each column represents one patient, with yellow indicating classification to the good clinical outcome group and blue representing classification to the poor clinical outcome group. The survival time is indicated by the top bars, with red indicating a death event. Tumor grade (grade 1=white, grade 2 =grey, grade 3=black) and ER status (ER- =white, ER+ =black) are also represented by the middle bars.

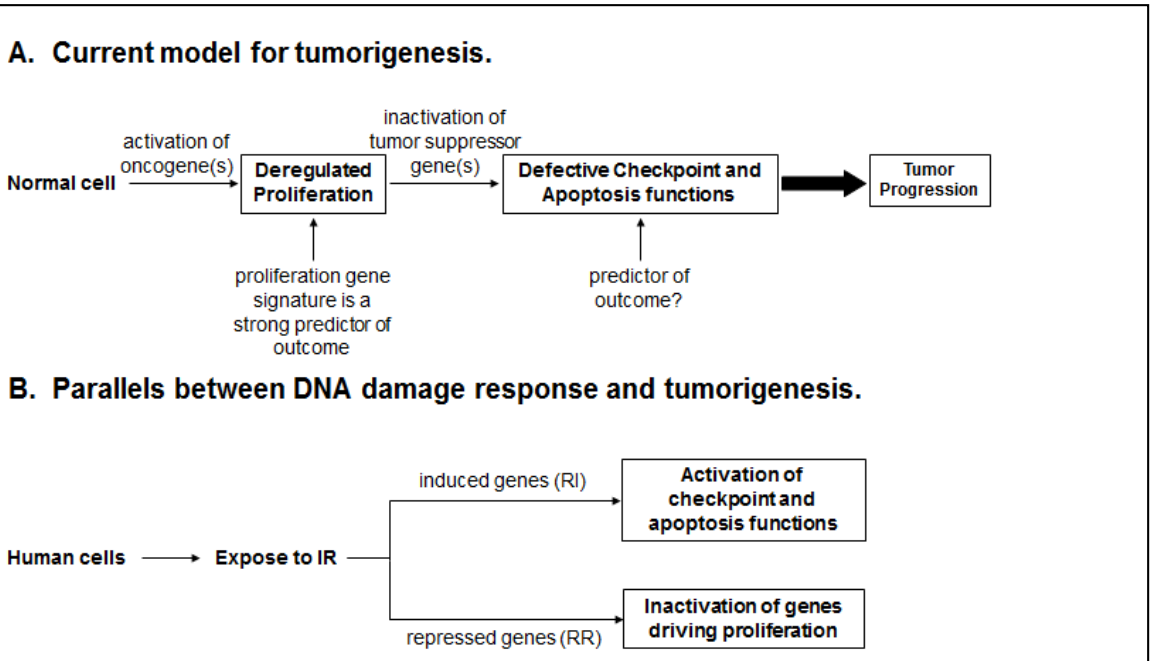

FIGURE 5. PARALLELS BETWEEN THE MOLECULAR STAGES OF TUMORIGENESIS AND THE DNA DAMAGE RESPONSE.

A. Evidence suggests that common forms of cancer may develop through a multistep process that may begin with a (dominant) mutation that results in oncogene activation and consequent aberrant proliferation. Aberrant proliferation results in replicational stress, leading to DNA double strand breaks and activation of the DNA damage response. Ultimately, mutations inactivate the DNA damage response, unleashing clonal evolution and tumor progression, leading to poor survival. It is well-established that a proliferation cluster of genes predicts outcome in breast cancer. B. Exposure to ionizing radiation activates the DNA damage response pathway, resulting in both the induction of one set and repression of a second set of genes. Pathway analysis reveals that the repressed genes function in cell cycle progression (and overlap with the proliferation cluster predicting breast cancer outcomes), whereas the induced genes function in a variety of biochemical pathways including checkpoint/cell cycle arrest and apoptosis and do not show significant overlap with the proliferation cluster., each plated two times.

CHAPTER 3: Results and characterizations from a genome-wide screen for TEL1/ATM interactions in *S. cerevisiae*

ABSTRACT

Tel1 is the budding yeast ortholog of the mammalian tumor suppressor and DNA damage response (DDR) kinase ATM. However, *tel1-Δ* cells, unlike ATM-deficient cells, do not exhibit sensitivity to DNA damaging agents, but do display shortened (but stably maintained) telomere lengths. Neither the extent to which Tel1p functions in the DDR nor the mechanism by which Tel1 contributes to telomere metabolism is well-understood. To address the first question, we present the results from a comprehensive genome-wide screen for genetic interactions with *tel1-Δ* that cause sensitivity to MMS and/or ionizing radiation, along with follow-up characterizations of the 13 interactions yielded by this screen. Surprisingly, many of the *tel1-Δ* interactions that confer DNA damage sensitivity also exacerbate the short telomere phenotype, suggesting a connection between these two phenomena. Restoration of normal telomere length in the *tel1-Δ xxx-Δ* mutants results in only minor suppression of the DNA damage sensitivity, demonstrating that the sensitivity of these mutants must also involve mechanisms independent of telomere length. In support of a model for increased replication stress in the *tel1-Δ xxx-Δ* mutants, we show that depletion of dNTP pools through pre-treatment with hydroxyurea renders *tel1-Δ* cells (but not wild-type) MMS-sensitive, demonstrating that under certain conditions, Tel1p does indeed play a critical role in the DDR.

INTRODUCTION

As discussed in Chapter 1, recent data suggest novel roles for Tel1 in the DNA damage response. In addition, the transcriptional profiling of *ATM*-deficient cell lines failed to detect an *ATM*-dependent transcriptional defect (Chapter 2). Thus we hypothesize that genetic interactions suppress the loss of *ATM/TEL1* in the DNA damage response. To comprehensively characterize the contexts by which Tel1p fits into the DDR, we performed genome-wide screens for *TEL1* genetic interactions that cause sensitivity to two different genotoxic agents, methylmethanesulfonate (MMS) and ionizing radiation (IR). From these screens, we have identified a diverse set of mutant backgrounds for which *TEL1* is required for survival upon exposure to DNA damage. We report that despite the diversity of *tel1-Δ* interactions identified here, most share an additional common phenotype of an exacerbated telomere defect.

MATERIALS AND METHODS

Media and growth conditions

YEPD and dropout media have been previously described (PAULOVICH *et al.* 1998). MMS and hydroxyurea (HU) were purchased from Sigma. YEPD and synthetic plates containing MMS were freshly prepared approximately 15 hours prior to use.

Yeast strains and plasmids

S. cerevisiae strains used in this study are listed in Table 14. Strain BY4741 and the haploid yeast knockout collection were purchased from Open Biosystems. Plasmid p4339 and strain Y7092 were gifts from Charles Boone and Brenda Andrews. Strain SLY60 was a gift from Sang Eun Lee; strain UCC3508 and plasmid pRS313-Y' were a

gift from Daniel Gottschling and plasmid pVL1107 was gifted by Vicki Lundblad. All gene disruptions were achieved by homologous recombination at their chromosomal loci by standard polymerase-chain-reaction (PCR)-based methods (BRACHMANN *et al.* 1998). Briefly, a deletion cassette with a 0.5 kb region flanking the target ORF was amplified by PCR from the corresponding *xxx*::*kanMX* strain of the deletion array (Open Biosystems) and transformed into the target strain for gene knockout. The primers used in the gene disruptions are designed using 20-23 bp sequences that are 0.5 kb upstream and downstream of the target gene. A list of primer sequences for all knockouts used in this study is available upon request.

tel1-Δ double-deletion library construction and screening

The Synthetic Gene Array (SGA) approach was used to construct a *tel1-Δ* double-deletion library following the protocol described in Tong & Boone (TONG and BOONE 2006). Library replication was performed using floating-pin manual replicators (VP Scientific). For the IR screen, the library was pin-replicated onto fresh YEPD plates and exposed to gamma irradiation using a Mark II cesium-137 irradiator (JL Shepherd & Associates) operated at varying dose rates. Plates were analyzed by manual inspection at 24 and 36 hours following IR. For the MMS screen, the library was pin-replicated onto plates containing 0.01% and 0.03% MMS, grown for two days at 30°C, and analyzed by visual inspection.

MMS/IR spot and colony assays

For serial-dilution spot assays, log-phase cells were serially diluted in PBS and spotted onto YEPD or YEPD + MMS plates using a pin replicator. A subset of the plates was immediately irradiated using the conditions described above. Plates were incubated at 30°C and analyzed by visual inspection at 24 and 36 hours.

For colony-based survival assays, three independent transformants were analyzed for each mutant, along with wild-type and *tel1-Δ* controls. Log-phase cells (~5 x 10^7 cells) were sonicated and counted using a Beckman-Dickson Coulter counter. Cells were serially diluted in PBS and plated on YEPD or YEPD + MMS plates. For analyzing radiation sensitivity, cells were spread on YEPD plates and the plates were subsequently irradiated as described above. Viability was determined by plating serial dilutions of cultures onto YEPD and scoring the number of colony-forming units (CFU) after 3-4 days at 30°C. Viability was calculated as CFU/total cells. For experiments utilizing a low dose rate (0.9 Gy/minute), cells were irradiated in 5 ml liquid cultures over a 7.5 hour period prior to plating on YEPD to assess colony-based survival. In experiments in which a hydroxyurea pretreatment was used, cells were incubated in liquid YEPD media +/- hydroxyurea (Sigma) at the indicated times. Following the incubation period, cells were washed twice with PBS, counted by Coulter counter, serially diluted and plated on YEPD or YEPD + MMS plates.

Gross Chromosomal Rearrangement (GCR) and translocation assays

For the measurement of GCR frequencies, log-phase cells grown at 30°C in YEPD were harvested, sonicated, and counted using a Coulter counter. 1 x 10^8 cells were resuspended in 20 ml YEPD and YEPD + 0.003% MMS and grown at 30°C overnight. At

15 hours, cells were washed in 5% Na_2SO_3, sonicated, and counted using a Coulter counter. 1 x 10^9 cells were plated on C-Arg-Ser + Canavanine + 5-fluororotic acid (FOA) to measure GCR events, and serial dilutions were plated on YEPD to measure cell viability. GCR plates were incubated for 4-5 days at 30°C. Viability was calculated as CFU/total cells and MMS-induced GCR frequencies were normalized to GCR frequencies from untreated cells.

The *HO*-inducible translocation assay was performed according to Lee *et al* (LEE *et al.* 2008). Briefly, log-phase cells were sonicated and cell number was determined using a Coulter counter (Beckman Dickson), and serial dilutions were plated on C-Ura dropout plates containing galactose to induce *HO* expression. Strain growth and translocations in the absence of *HO*-induced DSBs was measured on synthetic complete media and C-Ura plates containing glucose.

Southern blotting

Southern blotting for telomere lengths was carried out using a previously described DNA probe targeting telomeric Y' regions (SINGER *et al.* 1998). DIG-labeled probe synthesis was carried out by PCR using the Roche DIG Probe Synthesis Kit following the manufacturer's instructions. Genomic DNA was prepared using a Yeastar genomic DNA kit (Zymo Research). Genomic DNA preparations were digested overnight with *XhoI* (Invitrogen) and separated on 1% gels. Separated DNA molecules were transferred onto nylon membranes via blot sandwich overnight in 20X SSC buffer. DNA molecules were crosslinked onto the membrane using a UV crosslinker (Fisher Scientific) at 60 mJ/cm^2 and the membrane was incubated with the Y' telomeric DIG-labeled probe overnight.

Antibody detection of the DIG probe was performed using the DIG luminescent detection kit (Roche), and blots were imaged on a ChemiDoc XRS system (Bio-Rad).

RESULTS

A synthetic genetic array (SGA) screen for interactions with *tel1-Δ* in response to MMS and IR.

To better understand the extent of Tel1p's role in the DDR we sought to characterize mutant backgrounds in which *TEL1* is required for survival in response to MMS and/or ionizing radiation. To achieve this, we constructed a genome-wide double-deletion library by mating a *MAT*α *tel1-Δ* strain to the *MATa* haploid deletion library (WINZELER *et al.* 1999) using the Synthetic Genetic Array (SGA) procedure developed by Tong *et al* (TONG and BOONE 2006; TONG *et al.* 2001). The *tel1-Δ xxx-Δ* double-deletion library was screened for survival on YEPD plates containing either 0.01% or 0.03% MMS. Plates were examined after 24 and 48 hours by visual inspection for double mutants that exhibited MMS sensitivity. Double mutant strains exhibiting sensitivity were subsequently spotted in 10-fold serial dilutions along with the parental single mutant strains on YEPD + MMS to confirm the interaction. As an additional verification step, we re-made each single and double mutant by PCR-mediated transformation in a new BY4741 parental haploid strain. These new double-deletion mutants were then re-tested by serial-dilution spot assay on MMS plates and scored by visual inspection. Interactions passing this second criterion were then subjected to colony survival analyses to quantify the degree of interaction with *tel1-Δ* on MMS plates. After validation, 13 gene deletions showed enhanced sensitivity to MMS when paired with *tel1-Δ* (Figure 6). These genes include

multiple subunits of the 9-1-1 checkpoint clamp (*RAD17, DDC1*, ~400 fold) as well as the 9-1-1 clamp loader *RAD24* (deletion of the third subunit *mec3-Δ* grows poorly in BY4741 and was not able to be evaluated in the SGA screen), and members of the CCR4-NOT deadenylase complex (*CCR4* and *POP2*; 6- to 130-fold). Additional interactions exhibiting greater than 10-fold increases in MMS sensitivity were the base excision repair endonuclease *RAD27* (~30-fold) and a histone deacetylase (HDAC) subunit, *HDA3* (~30-fold). Additional genes exhibiting less than 10-fold interactions with *tel1-Δ* consisted of two nucleoporins (*NUP60* and *NUP133*), the non-homologous-end-joining (NHEJ) repair factor *YKU80,* a second HDAC subunit (*SAP30*), the *RAD26* ATPase, and a member of the Sm-like mRNA decay family (*LSM7*). We note that in the initial and confirmative screens, an additional *tel1-Δ* interaction with the uncharacterized *FYV4* gene exhibited a growth defect with *tel1-Δ* as well as a >10-fold increase in MMS sensitivity. However, the *FYV4* ORF is located ~200 bp upstream of the transcription start site of the essential mediator subunit *MED6.* Transforming the *fyv4-Δ tel1-Δ* strain with a plasmid containing the *MED6* gene and its promoter completely abolished the growth defect and MMS sensitivity of this strain (data not shown); leading us to conclude that the *fyv4-Δ* gene replacement exerts an off-target effect on the essential *MED6* gene. Due to these complications the *FYV4/MED6* candidate was removed from further consideration in this study.

As our MMS screen revealed a diverse set of interactions that cause enhanced MMS sensitivity with *tel1-Δ*, we asked whether a different set of mutants would interact with *tel1-Δ* in response to a different DNA damaging agent, γ-irradiation. To test for genetic interactions with *tel1-Δ* in ionizing radiation, the *tel1-Δ xxx-Δ* double-deletion

library was plated on YEPD and exposed to either 200 Gy or 400 Gy of ionizing radiation. In contrast to the MMS screen, only the 9-1-1 checkpoint genes *rad17-Δ*, *ddc1-Δ* and *rad24-Δ* exhibited interactions with *tel1-Δ* in response to IR, and these interactions were minor (<10-fold) in comparison to the *9-1-1-Δ tel1-Δ* interactions in MMS (>100-fold) (Figure 7). To confirm that the *tel1-Δ xxx-Δ* interactions identified in the MMS sensitivity screen were indeed not also sensitive to IR, we tested each of the 13 MMS sensitive *tel1-Δ xxx-Δ* strains for IR sensitivity. Consistent with the screen results, only the *9-1-1-Δ tel1-Δ* double mutants exhibited enhanced IR sensitivity (Figure 7).

As MMS is often referred to as a 'radiomimetic' agent, the finding that many of the MMS interactions were not recapitulated using IR was unexpected. One possible explanation for this is that the 400 Gy of IR was delivered as a pulse over a short period of time (8 Gy/minute), while for MMS treatment cells were grown continuously in 0.03% MMS. (DNA damage phenotypes can differ significantly when the agent is delivered as a pulse or chronic treatment (MURAKAMI-SEKIMATA *et al.* 2010).) To test this hypothesis, three of the *tel1-Δ xxx-Δ* double mutants identified in our screen (*ccr4-Δ tel1-Δ, hda3-Δ tel1-Δ* and *rad17-Δ tel1-Δ*) were examined for sensitivity to the same 400 Gy cumulative dose of IR (as in Figure 7), but this time delivered chronically over a period of 7.5 hours (0.9 Gy/minute). As seen in Figure 8, the total IR sensitivity for wild-type and single mutant strains was increased somewhat in the chronic exposure relative to the pulse of 400 Gy (Figure 7); however no additional (*i.e.* aside from 9-1-1) interactions with *tel1-Δ* were observed, and the *rad17-Δ tel1-Δ* interaction was reduced. From this, we conclude that, unlike the MMS case, *tel1-Δ* interactions in IR are limited to mutations in the 9-1-1 pathway.

Loss of telomerase is associated with a progressive increase in MMS sensitivity

Mammalian cells with shortened telomeres exhibit increased sensitivity to DNA damaging agents via an as-yet unknown mechanism (AGARWAL *et al.* 2008; DRISSI *et al.* 2011; GONZALEZ-SUAREZ *et al.* 2003; GOYTISOLO *et al.* 2000; NAKAMURA *et al.* 2005; SOLER *et al.* 2009; WONG *et al.* 2000; WOO *et al.* 2012). Based on this precedent, we hypothesized that resistance to DNA damaging agents in yeast would also be tightly linked to telomere length, and that yeast cells would become more sensitive to DNA damage in a progressive manner as telomeres shorten. To evaluate this possibility, we employed a heterozygous diploid *tlc1* strain, which upon sporulation into haploid progeny, exhibits progressive telomere shortening that leads to eventual replicative senescence (SINGER and GOTTSCHLING 1994). After inducing sporulation, we subcultured *TLC1* and *tlc1* haploid progeny over a series of days, and each day removed an aliquot of cells for testing of survival on YEPD or YEPD + MMS plates (Figure 9). In the absence of MMS, *tlc1* strains exhibited progressive telomere shortening over the three day period, while telomere lengths in the *TLC1* strains remained unchanged over the same period (Figure 10). When tested for viability on plates containing either 0.01% or 0.03% MMS, *TLC1* strains showed minimal MMS sensitivity that was unchanged over the course of the experiment (Figure 9). In contrast, the *tlc1* mutant strains exhibited a progressive and dose-dependent increase in MMS sensitivity that was most pronounced by day 3 on 0.03% MMS plates (survival rates in MMS were normalized to rates on YEPD alone to correct for MMS-independent loss of viability). As the half-life of telomerase RNA is a few hours (CHAPON *et al.* 1997) and the MMS sensitivity manifests after *days*, we conclude

that MMS sensitivity is telomere length-dependent in *tlc1* cells, rather than due to *TLC1* loss alone. These results raised the interesting possibility that the DNA damage sensitivity exhibited by the identified *tel1-Δ xxx-Δ* interactions results from an exacerbation of the well-known telomere length defect caused by loss of *TEL1*.

Many of the *tel1-Δ* MMS interactions exhibit shortened telomeres

As cellular sensitivity to MMS increases progressively with telomere shortening (Figure 9), we hypothesized that some or all of the interactions identified in the *tel1-Δ* screen exacerbate the *tel1*-mediated telomere length defect, and this may be a cause for DNA damage sensitivity in these cells. Thus we asked whether any of the *tel1-Δ xxx-Δ* double mutants exhibited telomere lengths that were significantly shorter than either corresponding single mutant. To answer this question, we isolated genomic DNA from single and double-mutants for each of the 13 *tel1-Δ xxx-Δ* interactions and analyzed *XhoI* fragments by Southern blotting with a Y' subtelomeric probe (SINGER *et al.* 1998). As expected (GREENWELL *et al.* 1995; LUSTIG and PETES 1986; MORROW *et al.* 1995), the *tel1-Δ* single mutant exhibited shorter telomere lengths relative to a wild-type strain (Figure 11). Additionally, a number of the other single mutants exhibited shorter telomere lengths relative to the wild type, including *yku80-Δ, rad27-Δ* and *sap30-Δ*, with the *yku80-Δ* mutant being the only single-mutant exhibiting a shorter telomere length than *tel1-Δ* (Figure 11). Notably, the *9-1-1* checkpoint factors *ddc1-Δ* and *rad17-Δ* strains were shown in a previous study to exhibit a minor telomere defect (LONGHESE *et al.* 2000). However, we did not observe discernible shortening of these mutants relative to the wild type (Figure 11 and 12); this may reflect differences in the strain background used between these

studies. Notably, the *9-1-1-Δ tel1-Δ* double mutants (*rad24-Δ tel1-Δ, rad17-Δ tel1* and *ddc1-Δ tel1-Δ*) exhibited very short telomeres relative to *tel1-Δ*, and a second class consisting of *sap30-Δ tel1-Δ, ccr4-Δ tel1-Δ, pop2-Δ tel1-Δ, hda3-Δ tel1-Δ, nup133-Δ tel1-Δ, nup60-Δ tel1-Δ*, *rad27-Δ tel1-Δ* and *yku80-Δ tel1-Δ* also exhibited shorter telomeres relative to *tel1-Δ*. The *rad26-Δ tel1-Δ* and *lsm7-Δ tel1-Δ* double mutants exhibited telomere lengths that were identical to *tel1-Δ.* Our finding that eleven of the thirteen *tel1-Δ xxx-Δ* interactions exhibited decreased telomere lengths relative to *tel1-Δ* is unexpected, since many of identified genes play no known role in telomere metabolism. To exclude the possibility that the *tel1-Δ xxx-Δ* short telomere phenotype was not merely an artifact due to a previously-characterized phenotypic lag for *tel1* telomeres (~150 generations (LUSTIG and PETES 1986)), we examined telomere lengths for a selection of single- and double-mutants over additional sub-culturing for a period of five days. During the repeated subculturing, we did not observe any further changes in telomere length by Southern blot (Figure 12). From these data, we conclude that the majority of *tel1-Δ* interactions identified in the MMS sensitivity screen also confer shorter telomeres, suggesting a possible connection between the two phenotypes.

Artificial elongation of telomeres in *tel1-Δ 9-1-1-Δ* mutants partially suppresses MMS sensitivity

As telomere shortening was shown to be causative for MMS sensitivity in the *tlc1* case (Figure 9), we next hypothesized that the exacerbated telomere defect exhibited by the majority of *tel1-Δ xxx-Δ* strains (Figure 11) may be causative for enhanced MMS sensitivity. Thus, reversal of the telomere length defect would also reduce the MMS

sensitivity of these mutants. To test this, we transformed each of the *tel1-Δ xxx-Δ* single- and double-mutants with a plasmid expressing a fusion of the Cdc13 capping protein to the Est2 subunit of telomerase (EVANS and LUNDBLAD 1999). This fusion has been previously shown to alleviate the short telomere phenotype in a *tel1* mutant (TSUKAMOTO *et al.* 2001). A panel of *tel1-Δ xxx-Δ* mutant strains with and without the *CDC13-EST2* plasmid was screened for sensitivity by spotting cells on MMS plates (Figure 13). Of the tested *tel1-Δ xxx-Δ* interactions, the *rad24-Δ tel1-Δ* strain exhibited a visible increase in survival on MMS plates when transformed with the *CDC13-EST2* fusion plasmid (and not the vector). None of the other *tel1-Δ xxx-Δ* interactions exhibited any change in MMS sensitivity upon transformation with *CDC13-EST2.* We confirmed the suppression of MMS sensitivity in *rad24-Δ tel1-Δ* as well as a second 9-1-1 component (*rad17-Δ tel1-*Δ) by a quantitative colony forming assay (Figure 14), and again the fusion plasmid conferred discernible (but not total) resistance to MMS (11-fold for *rad24-Δ tel1-Δ* and 4-fold for *rad17-Δ tel1-Δ* versus the vector). Telomeres in these strains were significantly elongated to wild-type levels by addition of the *CDC13-EST2* fusion and were hyper-elongated in wild-type and *tel1-Δ* strains (Figure 14). (*CDC13-EST2* was able to elongate telomeres to an identical degree in other non-9-1-1-related *tel1-Δ xxx-Δ* interactions (not shown) despite having no effect on MMS resistance.) While expression of *CDC13-EST2* suppresses the strong (>100-fold) MMS sensitivity in *9-1-1-Δ tel1-Δ* interactions by ~10-fold (Figure 14), the fact that this suppression is not total, nor does *CDC13-EST2* expression affect the MMS sensitivity of the other *tel1-Δ xxx-Δ* interactions suggests that there are additional telomere-length-independent defects that contribute to the MMS sensitivity of *tel1-Δ xxx-Δ* interactions.

tel1-Δ xxx-Δ interactions do not affect the frequency of NHEJ-mediated translocations

Lee and colleagues previously described an 11-fold increase in the frequency of DSB-induced NHEJ-mediated translocations for a *tel1-Δ* mutant, reflecting a role for *TEL1* in preventing deleterious chromosomal fusions through an as-yet undefined mechanism (LEE *et al.* 2008). That a *tel1-Δ* strain is not sensitive to DNA damaging agents despite this defect suggests that the occurrence of these events even in the presence of DNA damaging agents is a rarity. Thus, one possibility is that the *tel1-Δ xxx-Δ* interactions identified here may increase cellular dependence on *TEL1* to prevent deleterious chromosomal fusions. We tested this possibility by determining whether the *tel1-Δ xxx-Δ* double mutants experience enhanced frequencies (compared to *tel1*) of chromosomal translocations. We cloned each of the 13 single mutants and *tel1-Δ xxx-Δ* double mutants into a strain background harboring the translocation assay construct (LEE *et al.* 2008) that employs two *GAL*-inducible *HO* cuts on chromosomes V and VII, where each breakpoint contains a nonfunctional fragment of the *URA3* gene. Translocations are measured by the reconstitution of a functional *URA3* allele, which is dependent on Ku70/80-mediated NHEJ (LEE *et al.* 2008). We measured the frequency of translocations after the induction of *GAL-HO* for the panel of *tel1-Δ xxx-Δ* interaction strains (Figure 15). While we were able to reproduce the Ku-dependent increase in Ura^+ translocations for *tel1-Δ*, none of the other double mutants exhibited frequencies that differed from *tel1-Δ*. From this we conclude that an increased frequency of DSB-induced chromosomal translocations is unlikely to be the cause of the MMS sensitivity exhibited by *tel1-Δ xxx-Δ* interactions. This

is supported by the fact that the *tel1-Δ xxx-Δ* MMS interactions were also largely insensitive to IR (Figure 7), which directly induces DSBs (whether or not MMS produces DSBs is a current source of controversy (LUNDIN *et al.* 2005)).

Gross chromosomal rearrangements in *tel1-Δ xxx-Δ* strains

Kolodner and colleagues have previously shown that one double mutant identified in this screen (*rad24 tel1*) causes an increased frequency of spontaneous chromosome breakage and rearrangement involving the left arm of chromosome V (the gross chromosomal arrangement (GCR) assay) (MYUNG and KOLODNER 2002). As MMS has also been shown to induce higher GCR frequencies (MYUNG and KOLODNER 2003; STELLWAGEN *et al.* 2003), we asked whether the MMS sensitivity exhibited by the *tel1-Δ xxx-Δ* double mutants may reflect an increased frequency of MMS-induced genome rearrangements. To do this, we grew single- and double-mutant strains in the presence of 0.003% MMS for 15 hours to induce GCR events, which were detected by selecting for the loss of two nearby markers (*CAN1* and *URA3*) on the left arm of chromosome V, as previously described (CHEN and KOLODNER 1999). The 0.003% MMS exposure resulted in a ~10-fold induction of GCR events for wild-type cells. For the *tel1-Δ xxx-Δ* double mutants, members of the 9-1-1 complex showed a ~300 fold induction of MMS-induced GCR events when combined with *tel1-Δ* (Figure 16). The *rad27-Δ tel1-Δ* mutant and *nup60-Δ tel1-Δ* each showed a minor ~5-fold increase in MMS-induced GCR. None of the other double mutants exhibited an increased GCR frequency (Figure 16a). From these data, we conclude that a subset of *tel1-Δ xxx-Δ* interactions (*rad17-Δ tel1-Δ, ddc1-*

Δ tel1-Δ, rad24-Δ tel1-Δ, rad27-Δ tel1-Δ and *nup60-Δ tel1-Δ*) exhibit increased genome instability as measured by the GCR assay.

As restoration of telomere lengths through addition of the *CDC13-EST2* fusion plasmid restored a proportion of MMS resistance to the *9-1-1-Δ tel1-Δ* mutant strains, we asked whether the *CDC13-EST2* fusion would also suppress the increased MMS-induced GCR frequency of a *9-1-1-Δ tel1-Δ* mutant as well. We tested a *rad17-Δ tel1-Δ* mutant along with the corresponding single mutants for the induction of GCR events with or without the fusion construct. As can be seen in Figure 16b, the *rad17-Δ tel1-Δ* double-mutant strain harboring the fusion plasmid had a reduced GCR frequency relative to the same strain carrying an empty vector. Consistent with a partial reduction in MMS sensitivity, the *CDC13-EST2* fusion did not completely abolish MMS-induced gross chromosomal rearrangements in the *rad17-Δ tel1-Δ* strain. From these data, we conclude that a proportion of the MMS sensitivity exhibited by *9-1-1-Δ tel1-Δ* strains is due to MMS-induced genomic instability that is caused by telomere shortening. However, much of the increased GCR in *9-1-1-Δ tel1-Δ* is unexplained by telomere length effects; thus additional mechanisms (*i.e.* aside from altered telomere length) contribute to the sensitivity of *tel1-Δ xxx-Δ* interactions.

A *tel1-Δ* strain is rendered sensitive to MMS by pre-depletion of nucleotide pools

Prior studies have implicated both the *9-1-1* complex and CCR4-NOT complex as key regulators of ribonucleotide reductase, and mutants in these pathways exhibit depleted nucleotide pools and are sensitive to replication stress (MULDER *et al.* 2005; TRAVEN *et al.* 2005; WESTMORELAND *et al.* 2004; WOOLSTENCROFT *et al.* 2006; ZHAO *et al.*

2001). Moreover, a *ccr4-Δ tel1-Δ* strain has been previously shown to exhibit enhanced sensitivity to the ribonucleotide reductase inhibitor hydroxyurea (WOOLSTENCROFT *et al.* 2006). Thus we hypothesized that a decrease in dNTP pools in *9-1-1-Δ tel1-Δ* and *ccr4-Δ / pop2-Δ tel1-Δ* may contribute to the MMS sensitivity exhibited by these strains. From this, we predicted that depletion of nucleotide pools (e.g. by pretreating cells with hydroxyurea) in *tel1-Δ* cells should phenocopy deletion of *CCR4* in a *tel1-Δ* background, thus sensitizing *tel1-Δ* cells to MMS. To test this prediction, wild-type and *tel1-Δ* cells were cultured in rich medium with 0, 50 or 150 mM HU for a period of four hours, after which the HU was removed, and cells were plated onto MMS plates to assess viability. As expected, the MMS sensitivity of a wild-type strain does not change, regardless of whether the cells were pretreated with HU (Figure 17). In contrast, while a *tel1-Δ* strain is insensitive to the HU pretreatment alone, when HU pretreatment is followed by plating on MMS plates, *tel1-Δ* cells exhibit enhanced MMS sensitivity in a dose-dependent manner, with the greatest MMS sensitivity observed in 150 mM HU (Figure 17). From this we conclude that depletion of nucleotide pools renders *tel1-Δ* sensitive to the DNA damaging agent MMS, consistent with a model in which increased replication stress contributes to the MMS sensitivity exhibited by the *9-1-1-Δ tel1-Δ* and ccr4-*Δ tel1-Δ / pop2-Δ tel1-Δ* mutants (and possibly other *tel1-Δ xxx-Δ* double mutants isolated in the screen; see Discussion).

DISCUSSION

Categorizing the *tel1-Δ* interactions

While a *tel1-Δ* mutant exhibits interactions with a diverse set of 13 mutants, we found that these interactions fell into three phenotypic classes based upon our follow-up characterizations (Table 15). The first class is comprised of mutants in the 9-1-1 complex (*rad17-Δ* and *ddc1-Δ*) and the 9-1-1 clamp loader (*rad24-Δ*); these *tel1-Δ* interactions conferred a rather large (>100-fold) increase in MMS sensitivity (Figure 6), cross-sensitivity to IR (Figure 7 and 8), a pronounced telomere defect (Figure 11) and a synergistic increase in GCR events (Figure 16). For this class, the DNA damage sensitivity and the increase in GCR frequencies were partially suppressed by elongating telomeres using the *CDC13-EST2* fusion construct (Figure 14 & 16b). The second class of interactions comprises *ccr4-Δ, pop2-Δ, sap30-Δ, hda3-Δ, yku80-Δ, rad27-Δ, nup133-Δ* and *nup60-Δ* (Table 15); these exhibited a somewhat milder interaction with *tel1-Δ* in MMS, no cross-sensitive interactions to IR, but exhibited a discernible telomere length defect with *tel1-Δ* (Figure 11). The third class of mutants, *rad26-Δ* and *lsm7-Δ* showed similar characteristics to class 2, but did not exhibit any discernible telomere length defect (Figure 11). There is likely some overlap between these classes in the mechanism causing their interactions with *tel1-Δ,* discussed below.

A replication defect underlies sensitivity to MMS in multiple classes of *tel1-Δ* interactions

While the *tel1-Δ* interactions comprising classes 1 and 2 (Table 15) exhibit shortened telomeres relative to the corresponding single mutants, only in the class 1 case is MMS sensitivity suppressed by telomere elongation (Figure 14), and even in this class of double mutants the suppression is modest. While it is formally possible that telomere

elongation due to the expression of the *CDC13-EST2* fusion creates a structure that is somehow physiologically different from a natural telomere and thus is not a good substitute, a more straightforward model is that only a minor proportion of MMS sensitivity is directly caused by telomere shortening in class 1 mutants, while the majority of MMS sensitivity in these and other *tel1-Δ xxx-Δ* interactions reflects an underlying replication defect that manifests a dual-pronged effect on telomere metabolism and MMS resistance.

Our data (and other studies) support a model in which increased replication stress, combined with a *tel1-Δ*-mediated defect in replication fork stability causes both MMS sensitivity and telomere shortening in *tel1-Δ xxx-Δ* interactions. First, aside from a modest effect in the class 1 mutants, none of the identified in *tel1-Δ xxx-Δ* interactions exhibit cross-sensitivity to ionizing radiation, regardless of whether the IR was administered as a pulse (Figure 7) or chronic treatment (Figure 8). Unlike MMS treatment, IR does not induce detectable replication fork stalling (MERRICK *et al.* 2004), so while there is a minor IR interaction in *tel1-Δ 9-1-1-Δ* cells (Figure 7) (likely through an additive defect in Mec1/Tel1 DSB sensing), replication fork stalling/collapse is the likely major lethal lesion in *tel1-Δ xxx-Δ* interactions. Additionally, recent studies have uncovered a *TEL1*-dependent role in the preservation of fork stability through the prevention of fork reversion and degradation into abnormal cruciform structures (DOKSANI *et al.* 2009). Consistent with this, Kaochar *et al.* showed that *tel1-Δ* exhibits an increased frequency of dicentric chromosomes due to the fusion of inverted repeats likely due to fork reversion (KAOCHAR *et al.* 2010). As the reason why *tel1-Δ* cells exhibit short telomeres is poorly understood, it is formally possible that a failure to preserve fork stability in telomeric regions in *tel1-Δ*

cells is causative for the short telomere phenotype (telomeres are enriched for replication pause sites such as G-quadruplex structures (BOCHMAN *et al.* 2012; IVESSA *et al.* 2002)).

Many of the *tel1-Δ* interactions identified in the MMS screen fit a model for increased replication stress. Members of class 1 (9-1-1 components) (Table 15) are required for the *MEC1*-dependent degradation of the ribonucleotide reductase inhibitor Sml1 following MMS treatment (CHABES *et al.* 2003; ZHAO *et al.* 2001); the resultant increase in dNTP production following this process is thought to facilitate DNA synthesis at stalled forks to prevent fork collapse (FASULLO *et al.* 2010). In addition, members of class 2 (*CCR4* and *POP2*, members of the CCR4-NOT deadenylation complex) are known regulators of ribonucleotide reductase, and mutants in *ccr4-Δ* and *pop2-Δ* are sensitive to replication inhibitors such as hydroxyurea (MULDER *et al.* 2005; TRAVEN *et al.* 2005; WESTMORELAND *et al.* 2004; WOOLSTENCROFT *et al.* 2006). As telomere shortening has recently been shown to occur upon dNTP depletion (GUPTA *et al.* 2013), it is likely that the short telomeres in CCR4-NOT and 9-1-1 mutants are at least partially due to this mechanism. Consistent with a model for increased replication stress in *tel1-Δ xxx-Δ* cells, depleting nucleotide pools by pretreatment with hydroxyurea (effectively phenocopying the loss of *9-1-1* or *CCR4/POP2*) sensitizes *tel1-Δ* cells to MMS in a dose-dependent manner, whereas a wild-type strain is unaffected by the HU pretreatment (Figure 17).

Other mutants comprising class 2 are also linked to preventing replication stress via counteracting fork regression (*RAD27* (KANG *et al.* 2010)) or stabilizing sites of active transcription (*NUP60/NUP133* (BERMEJO *et al.* 2011; PALANCADE *et al.* 2007)). Additionally, the mutants comprising class 3 (Table 15) are linked to increased replication stress due to defects in histone regulation (*LSM7* (HERRERO and MORENO 2011; TKACH *et*

al. 2012)) or through defective targeting of transcription-coupled repair (*RAD26* (KAPITZKY *et al.* 2010; MALIK *et al.* 2010)).

Progressive telomere shortening is a cause for MMS sensitivity

Recently, numerous studies have described a connection between short telomeres and enhanced sensitivity to DNA damaging agents across a variety of organisms (DRISSI *et al.* 2011; LIN *et al.* 2009; SOLER *et al.* 2009; WONG *et al.* 2000); the reason for this relationship is poorly understood. Here, we show that in yeast, cellular sensitivity to MMS progressively increases as telomeres shorten (Figure 9), suggesting that the progressive loss of telomere protection renders cells sensitive to MMS. In concordance with this, a proportion of MMS sensitivity and genome instability can be suppressed in *9-1-1-Δ tel1-Δ* mutants by alleviating the short telomere phenotype in these cells (Figures 14).

There are multiple possible mechanisms for how short telomeres cause MMS sensitivity. Loss of telomeric protection can render telomeres targets for the DDR and the loss of telomerase activity is associated with a gradual increase in constitutive Rad53 phosphorylation (GRANDIN *et al.* 2005); accordingly in telomerase-deficient cells telomeres are enriched for DDR proteins while non-telomeric DSBs exhibit reduced binding of DDR factors (LIN *et al.* 2009). Thus, the recruitment of DDR factors to short telomeres may interfere with the ability of the cell to cope with MMS-induced stress elsewhere in the genome. Alternatively, de-protected telomeres themselves may be problematic in the presence of MMS due to the potential for lethal chromosomal fusions with DSBs resulting from MMS-induced collapsed forks. Supporting this, a subset of GCR events can be suppressed by elongating telomeres in *9-1-1-Δ tel1-Δ* (Figure 16), and a

previous study has shown that a *9-1-1-Δ tel1-Δ* double-mutant exhibits an increased frequency of spontaneous telomere-telomere fusions that can also be suppressed by elongating telomeres (MIECZKOWSKI *et al.* 2003).

For the other identified interactions, (Class 2, Table 15) despite a lack of MMS suppression by *CDC13-EST2*, the telomere defect in these cells may still be a cause for MMS sensitivity. For example, an increase in ssDNA at telomeres would create a structure that is more susceptible to MMS-induced lesions (fork-blocking lesions occur predominantly in ssDNA in MMS (SHRIVASTAV *et al.* 2010)). Accordingly, a *rad27* mutant is associated with abnormally large regions of ssDNA in telomeres (PARENTEAU and WELLINGER 1999). As DNA damage in telomeres has recently been shown to be uniquely irreparable (FUMAGALLI *et al.* 2012), it is likely that telomeres exhibiting abnormal structures are both more susceptible to MMS-induced damage and less able to survive it.

***Saccharomyces cerevisiae* Strains**

Strain	Genotype	Source
BY4741	*MATa his3Δ1 leu2Δ0 met15Δ0 ura3Δ0*	Open Biosystems
Y7092	MATα *can1Δ::STE2pr-Sp_his5 lyp1Δ his3Δ1 leu2delta0 ura3Δ0 met15Δ0*	Tong & Boone 2007
UCC3508	*MATa/MATα ura3-52/ura3-52 lys2-801/lys2-801 ade2-101/ade2-101 his3-Δ200/his3-Δ200 trp1-Δ1/TRP1 leu2-Δ1/leu2-Δ1 adh4::URA3-TEL/adh4::URA3-TEL DIA5-1/DIA5-1 ppr1::HIS3/ppr1::LYS2 TLC1/tlc1:LEU2*	Singer *et al.* 1998
SLY60	*MATΔ3':intron:ura3Δ5' hoΔ hmlΔ:ADE1 hmrΔ:ADE1 ade1-100 leu2-3,112 lys5 trp1:hisG ura3Δ3':intron:HOcs ade3:GAL:HO*	Lee *et al.* 2008
yBP1020-22	*MATα can1Δ::STE2pr-Sp_his5 lyp1Δ his3Δ1 leu2delta0 ura3Δ0 met15Δ0 tel1::NATMX*	This study
yBP1406-08	*MATa his3Δ1 leu2Δ0 met15Δ0 ura3Δ0 hxt3::URA3*	This study
yBP1416-18	*MATΔ3':intron:ura3Δ5' hoΔ hmlΔ:ADE1 hmrΔ:ADE1 ade1-100 leu2-3,112 lys5 trp1:hisG ura3Δ3':intron:HOcs ade3:GAL:HO tel1:NATMX*	This study
yBP1423	*MATa his3Δ1 leu2Δ0 met15Δ0 ura3Δ0 hxt3::URA3 tel1::NATMX*	This study
yBP1490-91	*MATa his3Δ1 leu2Δ0 met15Δ0 ura3Δ0 hxt3::URA3 pop2::KANMX*	This study
yBP1502-04	*MATa his3Δ1 leu2Δ0 met15Δ0 ura3Δ0 hxt3::URA3 sap30::KANMX*	This study
yBP1505-07	*MATΔ3':intron:ura3Δ5' hoΔ hmlΔ:ADE1 hmrΔ:ADE1 ade1-100 leu2-3,112 lys5 trp1:hisG ura3Δ3':intron:HOcs ade3:GAL:HO tel1::NATMX rad17::KANMX*	This study
yBP1508-10	*MATΔ3':intron:ura3Δ5' hoΔ hmlΔ:ADE1 hmrΔ:ADE1 ade1-100 leu2-3,112 lys5 trp1:hisG ura3Δ3':intron:HOcs ade3:GAL:HO tel1::NATMX ddc1::KANMX*	This study
yBP1511-13	*MATΔ3':intron:ura3Δ5' hoΔ hmlΔ:ADE1 hmrΔ:ADE1 ade1-100 leu2-3,112 lys5 trp1:hisG ura3Δ3':intron:HOcs ade3:GAL:HO tel1::NATMX nup60::KANMX*	This study
yBP1517-19	*MATΔ3':intron:ura3Δ5' hoΔ hmlΔ:ADE1 hmrΔ:ADE1 ade1-100 leu2-3,112 lys5 trp1:hisG ura3Δ3':intron:HOcs ade3:GAL:HO tel1::NATMX nup133::KANMX*	This study
yBP1520-21	*MATΔ3':intron:ura3Δ5' hoΔ hmlΔ:ADE1 hmrΔ:ADE1 ade1-100 leu2-3,112 lys5 trp1:hisG ura3Δ3':intron:HOcs ade3:GAL:HO tel1::NATMX lsm7::KANMX*	This study
yBP1524-26	*MATΔ3':intron:ura3Δ5' hoΔ hmlΔ:ADE1 hmrΔ:ADE1 ade1-100 leu2-3,112 lys5 trp1:hisG ura3Δ3':intron:HOcs ade3:GAL:HO tel1::NATMX sap30::KANMX*	This study
yBP1527-29	*MATΔ3':intron:ura3Δ5' hoΔ hmlΔ:ADE1 hmrΔ:ADE1 ade1-100 leu2-3,112 lys5 trp1:hisG ura3Δ3':intron:HOcs ade3:GAL:HO tel1::NATMX hda3::KANMX*	This study
yBP1550-52	*MATa his3Δ1 leu2Δ0 met15Δ0 ura3Δ0 hxt3::URA3 rad17::KANMX*	This study

yBP1553-55	*MATa his3Δ1 leu2Δ0 met15Δ0 ura3Δ0 hxt3::URA3 nup60::KANMX*	This study
yBP1558-60	*MATa his3Δ1 leu2Δ0 met15Δ0 ura3Δ0 hxt3::URA3 tel1::NATMX rad17::KANMX*	This study
yBP1564-66	*MATa his3Δ1 leu2Δ0 met15Δ0 ura3Δ0 hxt3::URA3 tel1::NATMX nup60::KANMX*	This study
yBP1576-78	*MATa his3Δ1 leu2Δ0 met15Δ0 ura3Δ0 hxt3::URA3 tel1::NATMX sap30::KANMX*	This study
yBP1585-87	*MATa his3Δ1 leu2Δ0 met15Δ0 ura3Δ0 hxt3::URA3 tel1::NATMX hda3::KANMX*	This study
yBP1608-10	*MATa his3Δ1 leu2Δ0 met15Δ0 ura3Δ0 hxt3::URA3 nup133::KANMX*	This study
yBP1611-13	*MATa his3Δ1 leu2Δ0 met15Δ0 ura3Δ0 hxt3::URA3 tel1::NATMX nup133::KANMX*	This study
yBP1622-23	*MAT∆3':intron:ura3∆5' ho∆ hml∆:ADE1 hmr∆:ADE1 ade1-100 leu2-3,112 lys5 trp1:hisG ura3∆3':intron:HOcs ade3:GAL:HO tel1::NATMX pop2::KANMX*	This study
yBP1630-32	*MATa his3Δ1 leu2Δ0 met15Δ0 ura3Δ0 hxt3::URA3 rad26::KANMX*	This study
yBP1633-35	*MATa his3Δ1 leu2Δ0 met15Δ0 ura3Δ0 hxt3::URA3 tel1::NATMX rad26::KANMX*	This study
yBP1636-38	*MAT∆3':intron:ura3∆5' ho∆ hml∆:ADE1 hmr∆:ADE1 ade1-100 leu2-3,112 lys5 trp1:hisG ura3∆3':intron:HOcs ade3:GAL:HO tel1::NATMX rad26::KANMX*	This study
yBP1669-71	*MATa his3Δ1 leu2Δ0 met15Δ0 ura3Δ0 hxt3::URA3 ccr4::KANMX*	This study
yBP1672-74	*MATa his3Δ1 leu2Δ0 met15Δ0 ura3Δ0 hxt3::URA3 tel1::NATMX ccr4::KANMX*	This study
yBP1681-83	*MATa his3Δ1 leu2Δ0 met15Δ0 ura3Δ0 hxt3::URA3 lsm7::KANMX*	This study
yBP1684-86	*MATa his3Δ1 leu2Δ0 met15Δ0 ura3Δ0 hxt3::URA3 tel1::NATMX lsm7::KANMX*	This study
yBP1714-16	*MATa his3Δ1 leu2Δ0 met15Δ0 ura3Δ0 hxt3::URA3 hda3::KANMX*	This study
yBP1717-19	*MATa his3Δ1 leu2Δ0 met15Δ0 ura3Δ0 hxt3::URA3 ddc1::KANMX*	This study
yBP1720-22	*MATa his3Δ1 leu2Δ0 met15Δ0 ura3Δ0 hxt3::URA3 tel1::NATMX ddc1::KANMX*	This study
yBP1738-40	*MATa his3Δ1 leu2Δ0 met15Δ0 ura3Δ0 hxt3::URA3 tel1::NATMX pop2::KANMX*	This study
yBP1787-89	*MATa his3Δ1 leu2Δ0 met15Δ0 ura3Δ0 hxt3::URA3 fyv4::KANMX*	This study
yBP1790-92	*MATa his3Δ1 leu2Δ0 met15Δ0 ura3Δ0 hxt3::URA3 tel1::NATMX fyv4::KANMX*	This study
yBP1793-95	*MATa his3Δ1 leu2Δ0 met15Δ0 ura3Δ0 hxt3::URA3 yku80::KANMX*	This study

yBP1796-98	*MATa his3Δ1 leu2Δ0 met15Δ0 ura3Δ0 hxt3::URA3 tel1::NATMX yku80::KANMX*	This study
yBP1799-1801	*MATa his3Δ1 leu2Δ0 met15Δ0 ura3Δ0 hxt3::URA3 rad27::KANMX*	This study
yBP1802-04	*MATa his3Δ1 leu2Δ0 met15Δ0 ura3Δ0 hxt3::URA3 tel1::NATMX rad27::KANMX*	This study
yBP1805-07	*MATa his3Δ1 leu2Δ0 met15Δ0 ura3Δ0 hxt3::URA3 rad24::KANMX*	This study
yBP1808-10	*MATa his3Δ1 leu2Δ0 met15Δ0 ura3Δ0 hxt3::URA3 tel1::NATMX rad24::KANMX*	This study
yBP1838-40	*MAT∆3':intron:ura3∆5' ho∆ hml∆:ADE1 hmr∆:ADE1 ade1-100 leu2-3,112 lys5 trp1:hisG ura3∆3':intron:HOcs ade3:GAL:HO tel1::NATMX ccr4::KANMX*	This study
yBP1841-43	*MAT∆3':intron:ura3∆5' ho∆ hml∆:ADE1 hmr∆:ADE1 ade1-100 leu2-3,112 lys5 trp1:hisG ura3∆3':intron:HOcs ade3:GAL:HO yku80::KANMX*	This study
yBP1844-46	*MAT∆3':intron:ura3∆5' ho∆ hml∆:ADE1 hmr∆:ADE1 ade1-100 leu2-3,112 lys5 trp1:hisG ura3∆3':intron:HOcs ade3:GAL:HO tel1::NATMX yku80::KANMX*	This study
yBP1847-49	*MAT∆3':intron:ura3∆5' ho∆ hml∆:ADE1 hmr∆:ADE1 ade1-100 leu2-3,112 lys5 trp1:hisG ura3∆3':intron:HOcs ade3:GAL:HO rad27::KANMX*	This study
yBP1850-52	*MAT∆3':intron:ura3∆5' ho∆ hml∆:ADE1 hmr∆:ADE1 ade1-100 leu2-3,112 lys5 trp1:hisG ura3∆3':intron:HOcs ade3:GAL:HO tel1::NATMX rad27::KANMX*	This study
yBP1859-61	*MAT∆3':intron:ura3∆5' ho∆ hml∆:ADE1 hmr∆:ADE1 ade1-100 leu2-3,112 lys5 trp1:hisG ura3∆3':intron:HOcs ade3:GAL:HO rad24::KANMX*	This study
yBP1862-64	*MAT∆3':intron:ura3∆5' ho∆ hml∆:ADE1 hmr∆:ADE1 ade1-100 leu2-3,112 lys5 trp1:hisG ura3∆3':intron:HOcs ade3:GAL:HO tel1::NATMX rad24::KANMX*	This study

TABLE 14. *SACCHAROMYCES CEREVISIAE* STRAINS USED IN THIS STUDY.

	strain	MMS interaction	IR interaction	GCR	short telomere	*CDC13-EST2* rescue	Description
CLASS 1	***rad24-Δtel1-Δ***	++	+	++	++	+/-	*9-1-1 complex*
	rad17-Δtel1-Δ	++	+	++	++	+/-	*9-1-1 complex*
	ddc1-Δtel1-Δ	++	+	++	++	+/-	*9-1-1 complex*
CLASS 2	***nup60-Δtel1-Δ***	+	-	+	+	-	*nucleoporin*
	rad27-Δtel1-Δ	+	-	+	+	-	*flap endonuclease*
	sap30-Δtel1-Δ	+	-	-	+	-	*deacetylase*
	pop2-Δtel1-Δ	+	-	-	+	-	*deadenylase*
	ccr4-Δtel1-Δ	+	-	-	+	-	*deadenylase*
	hda3-Δtel1-Δ	+	-	-	+	-	*deacetylase*
	yku80-Δtel1-Δ	+	-	-	+	-	*NHEJ*
	nup133-Δtel1-Δ	+	-	-	+	-	*nucleoporin*
CLASS 3	***lsm7-Δtel1-Δ***	+	-	-	-	-	*mRNA decap*
	rad26-Δtel1-Δ	+	-	-	-	-	*TCR*

TABLE 15. TABULATION OF PHENOTYPES UNCOVERED IN THIS STUDY.

For each of the *tel1-Δ xxx-Δ* genetic interactions identified in the MMS screen a '+' indicates whether a double mutant exhibited a positive result in each of the assays tested (e.g. increased GCR frequency, shorter telomere etc.; a '++' indicates a more severe phenotype and '+/-' indicates partial suppression). For the abbreviations listed, NHEJ = non-homologous end joining, TCR = transcription-coupled repair.

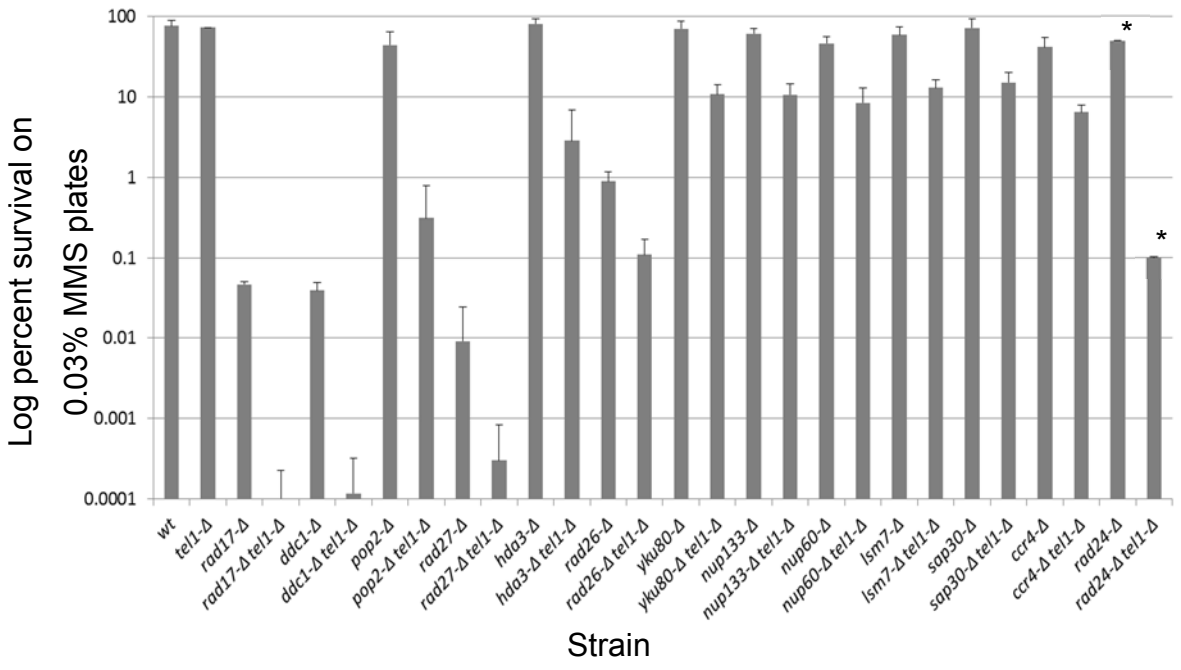

FIGURE 6. QUANTITATIVE SURVIVAL ANALYSIS FOR *TEL1* INTERACTIONS IN MMS VIA COLONY-FORMING ASSAY.

Quantitative survival analysis in MMS. Log-phase cultures for three independent transformants of each single and double mutant were serially diluted in PBS and spread on YEPD or YEPD + 0.03% MMS plates (asterisks indicate that screening was done in 0.015% MMS due to extreme MMS sensitivity). Viable cells were determined by the number of colony-forming units (CFU) after 3 days at 30ºC.

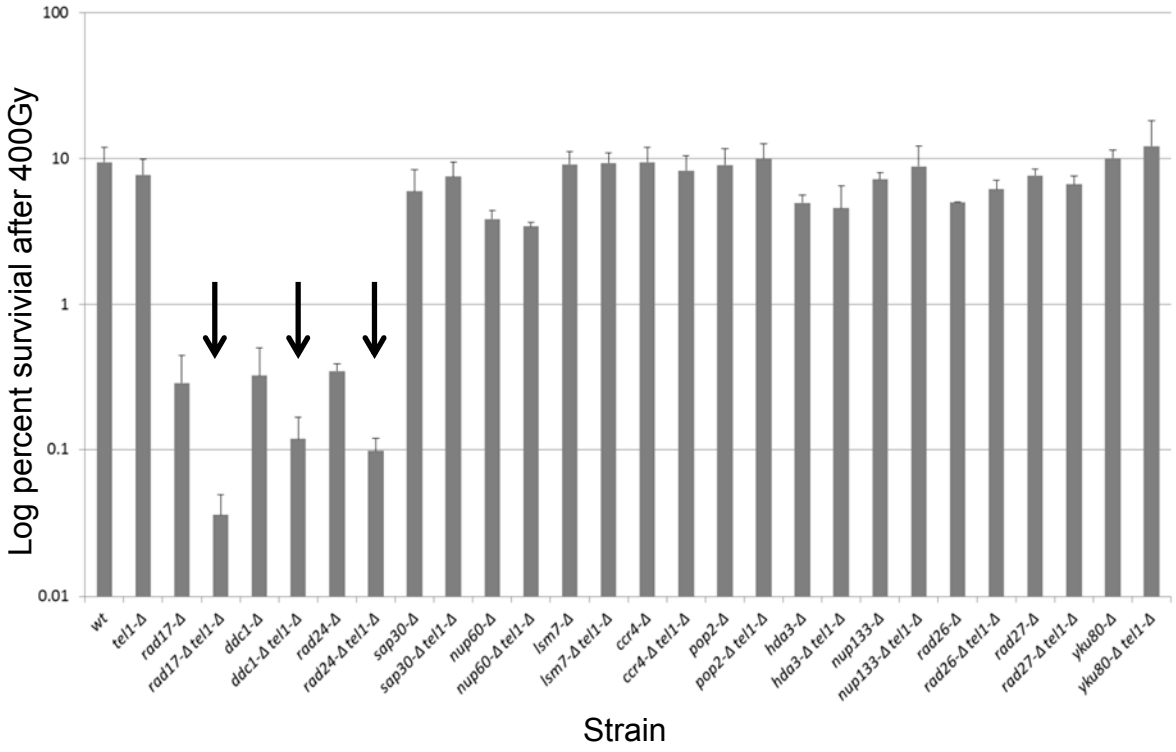

FIGURE 7. QUANTITATIVE SURVIVAL ANALYSIS IN IR.

Log-phase cultures for three independent transformants of each single and double mutant were serially diluted in PBS and spread on YEPD plates and irradiated at 400 Gy at 8 Gy/min. Viable cells were determined by the number of colony-forming units (CFU) after 3 days at 30ºC. Arrows indicate interactions identified in the genome-wide screen. Error bars represent the standard deviation of values from three independent transformants.

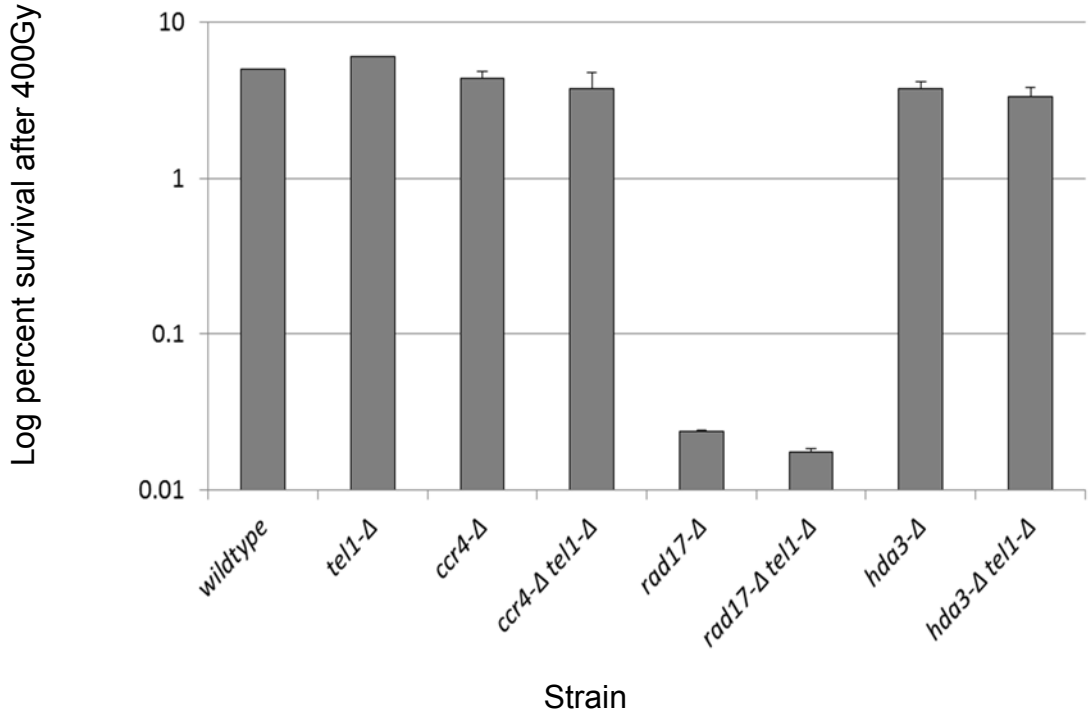

FIGURE 8. QUANTITATIVE SURVIVAL ANALYSIS USING CONTINUOUS LOW DOSE-RATE IR.

Log-phase cultures for two independent transformants of each single and double mutant were diluted into YEPD in 15 ml tubes and irradiated with 400 Gy delivered at a continuous dose rate of 0.9 Gy/minute over 7.5 hours. Following delivery of IR, cells were counted, serially diluted and plated for colony survival analysis. Error bars show the range of values for two independent transformants.

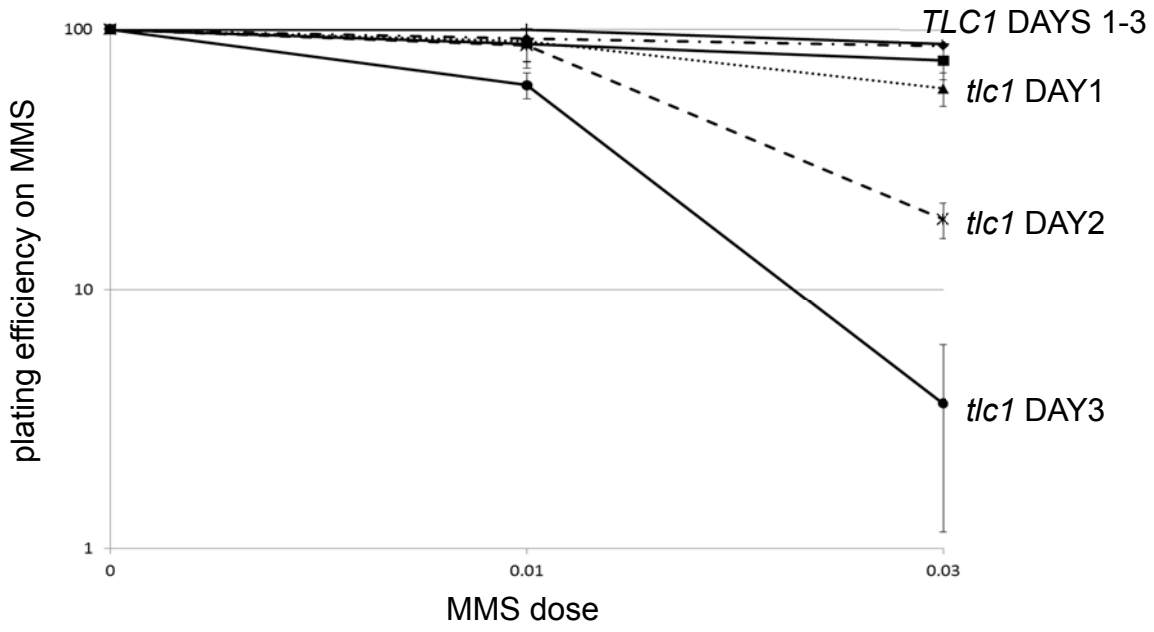

FIGURE 9. TELOMERASE-NULL CELLS EXHIBIT A PROGRESSIVE INCREASE IN MMS SENSITIVITY.

TLC1 and *tlc1* haploid spores from freshly dissected tetrads were subcultured in YEPD over multiple days. Each day, an aliquot was removed and assayed for MMS sensitivity by colony forming assay. Error bars represent the standard deviation of values from three independent spores.

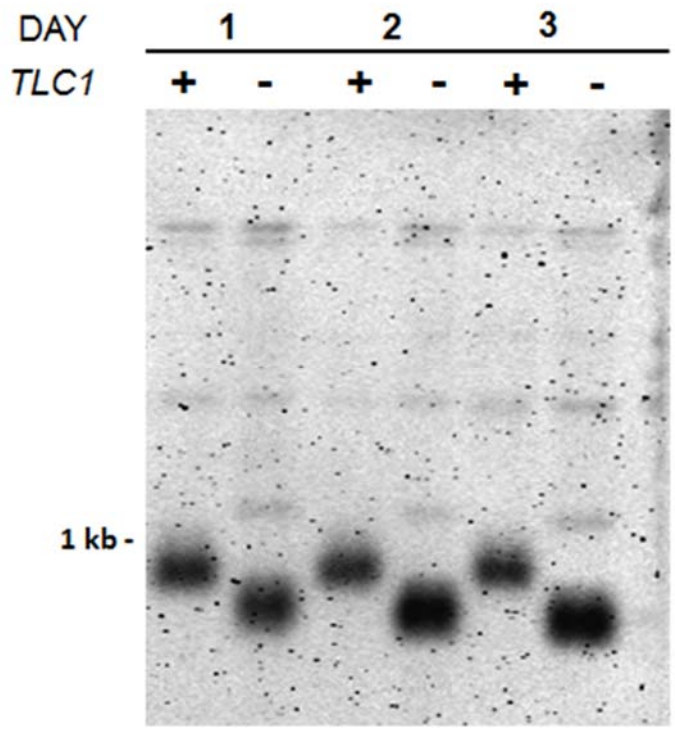

FIGURE 10. SOUTHERN BLOT FOR TELOMERE LENGTHS OF TLC1 AND TLC1 HAPLOID SPORES.

Genomic DNA from spores with or without a functional *TLC1* gene was isolated over three consecutive days of subculturing. DNA were separated by electrophoresis, blotted onto membranes and probed with a labeled DNA fragment complementary to the Y' subtelomere.

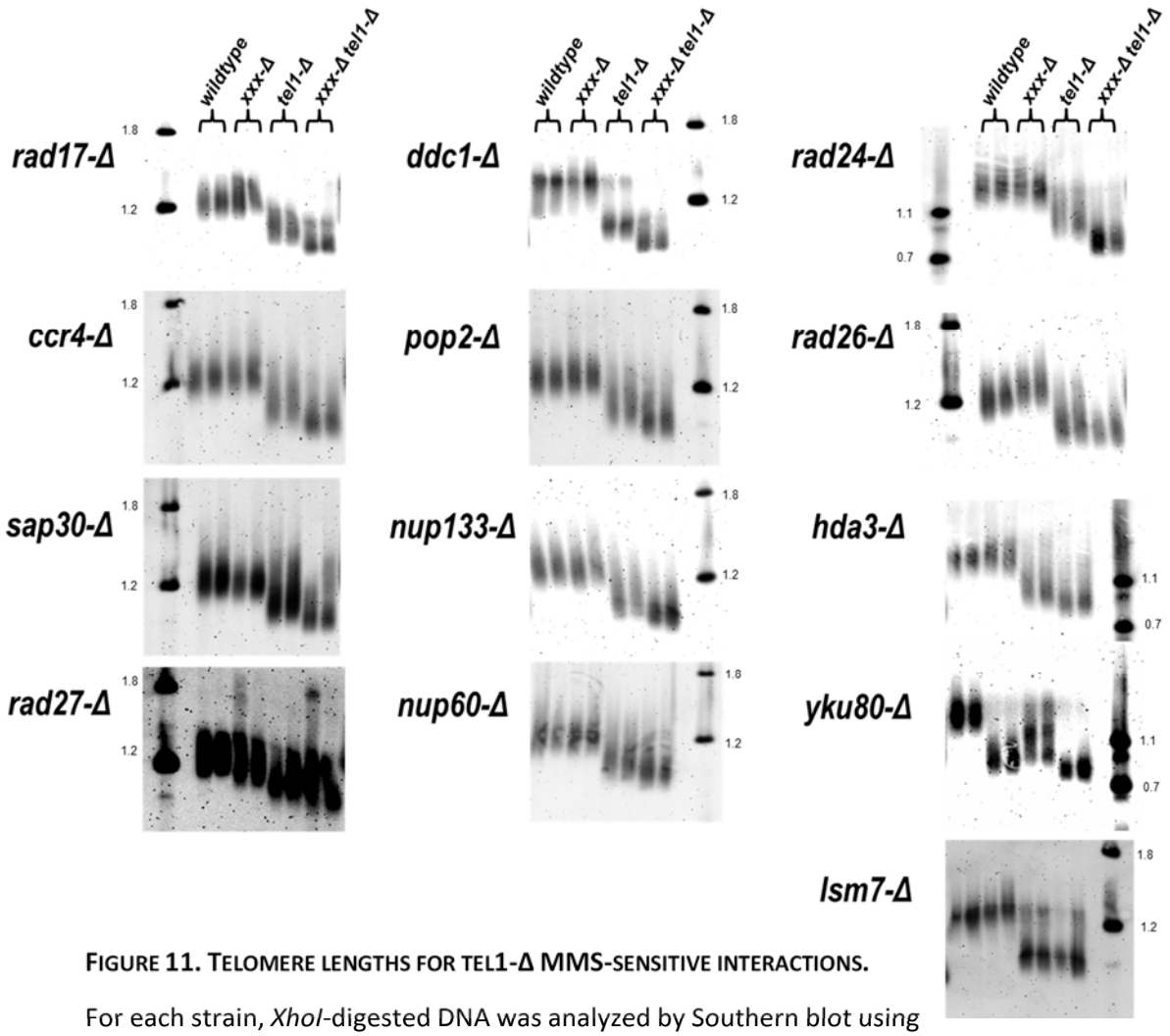

FIGURE 11. TELOMERE LENGTHS FOR TEL1-Δ MMS-SENSITIVE INTERACTIONS.

For each strain, *XhoI*-digested DNA was analyzed by Southern blot using a probe complementary to the Y' subtelomere. Each *xxx-Δ* mutant is listed to the left of each corresponding blot, and duplicates representing independent transformants for each strain are loaded side-by-side (duplicates are indicated by the brackets above). DNA ladders (in kb) are indicated in the far left or right lane of each blot.

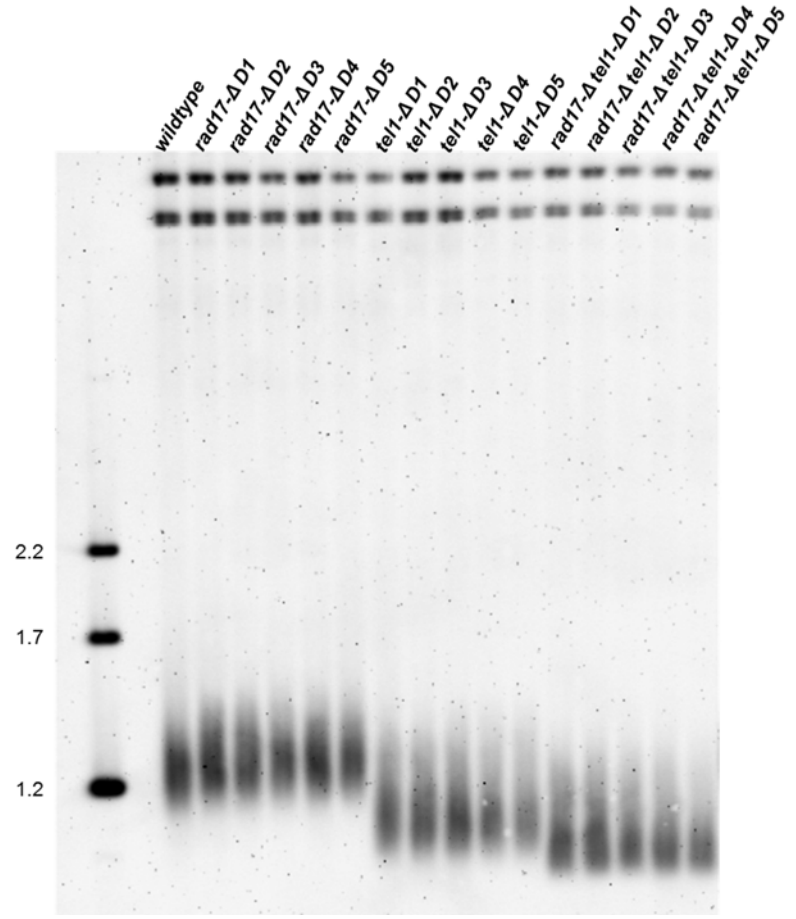

FIGURE 12. REPEATED SUBCULTURING DOES NOT ALTER TELOMERE LENGTHS.

Wildtype, *tel1-Δ*, *rad17-Δ* and *rad17-Δ tel1-Δ* cultures were diluted into fresh YEPD media and grown overnight. Genomic DNA was harvested the following day and a portion of the cells was diluted in to fresh medium and cultured overnight. The process was repeated over a period of five days (D1-D5). *Xho*I-digested DNA was analyzed by gel electrophoresis and Southern blotting with a probe recognizing subtelomeric Y' sequence. Molecular weight markers are indicated on the left (kb).

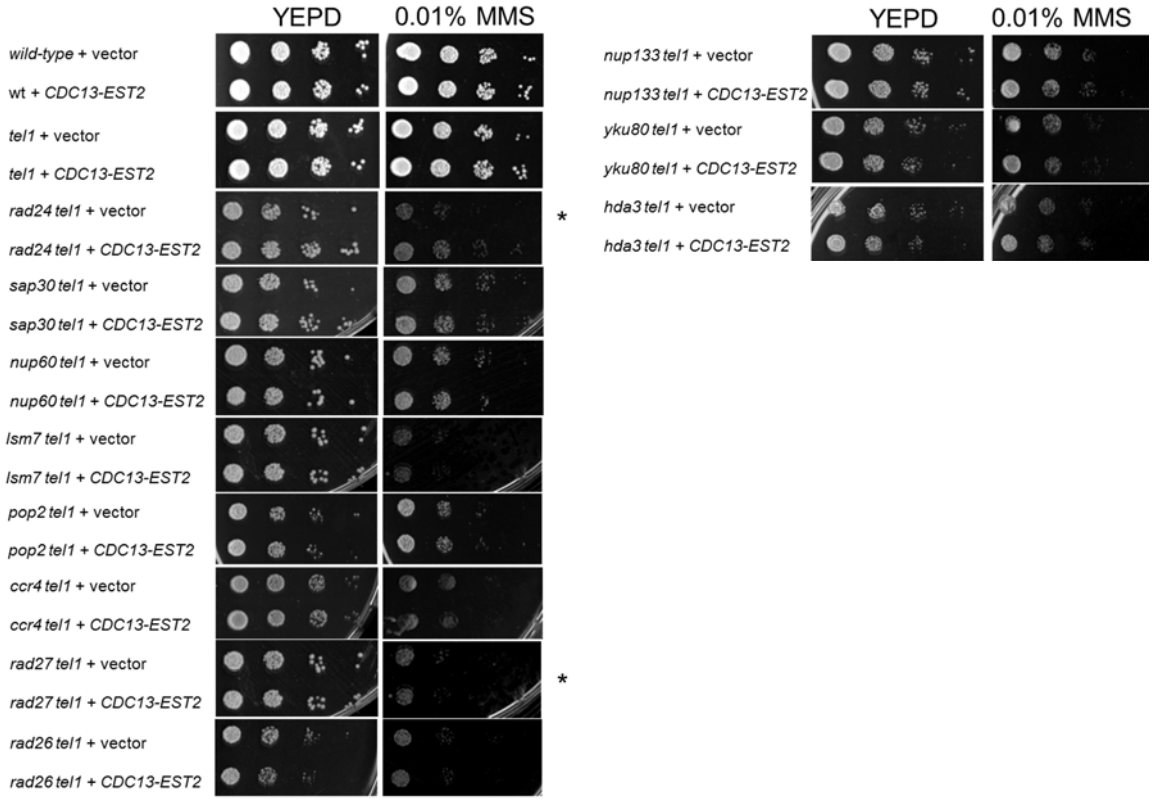

FIGURE 13. MMS SENSITIVITY WITH OR WITHOUT THE CDC13-EST2 FUSION CONSTRUCT.

Strains containing either an empty vector or a *CDC13-EST2* fusion plasmid were cultured in selective media, serially diluted and spotted onto YEPD+/- MMS plates. An asterisk indicates that 0.005% MMS plates were used due to strain sensitivity.

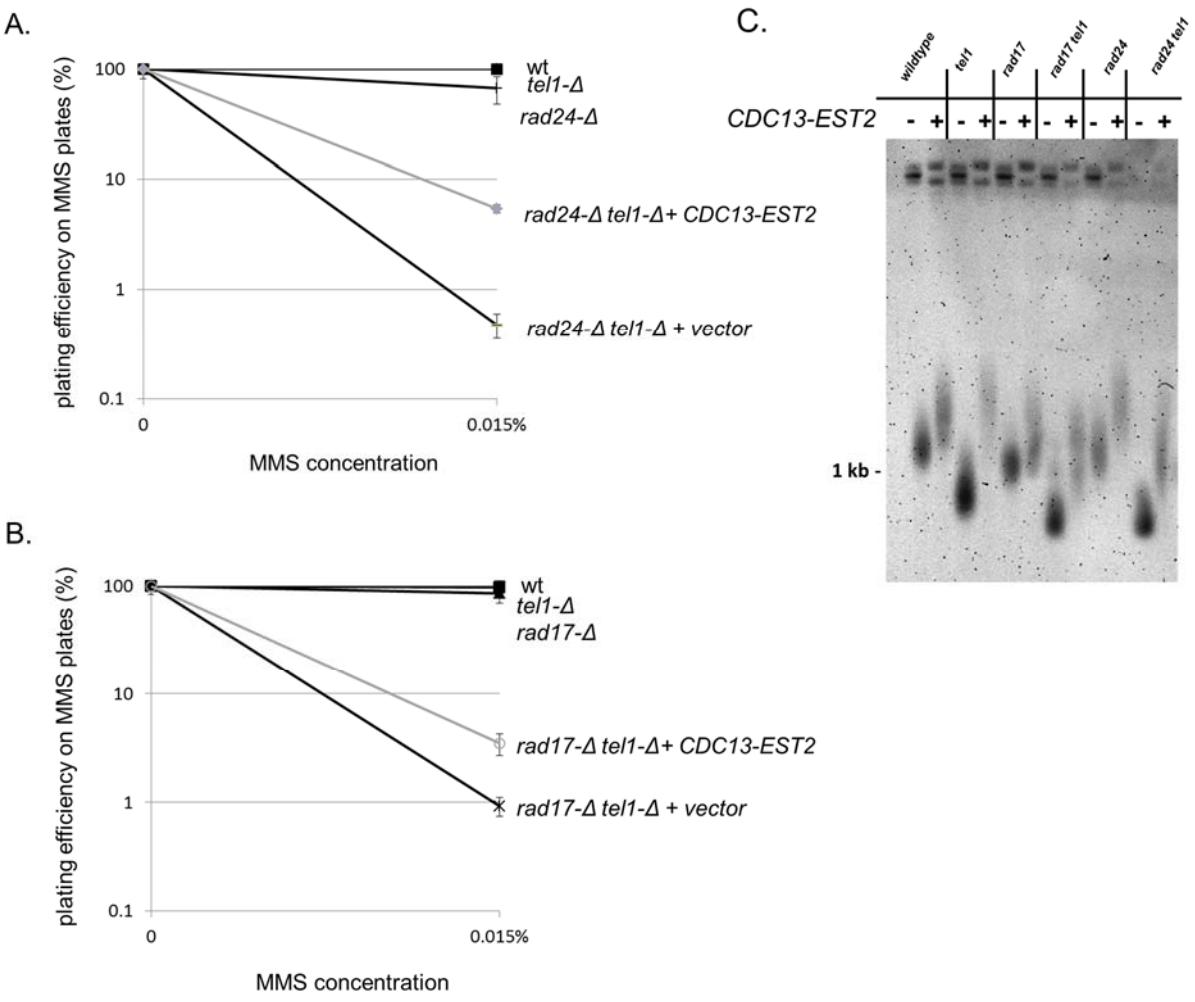

FIGURE 14. SUPPRESSION OF MMS SENSITIVITY IN RAD24-Δ TEL1-Δ AND RAD17-Δ TEL1-Δ BY A CDC13-EST2 FUSION PLASMID.

(A) & (B) Strains of the indicated genotype were transformed either with an empty vector or with a *CDC13-EST*2 fusion plasmid (pVL1107) and screened for MMS sensitivity by colony-forming assay on MMS plates. Error bars represent the standard deviation of values from three independent transformants. (C) Telomere lengths for *tel1-Δ* interactions with or without the *CDC13-EST2* fusion plasmid. Cells with the *CDC13-EST2* fusion plasmid or empty vector were propagated on –Leu media and diluted into fresh rich medium overnight. Genomic DNA was harvested the following day and analyzed by electrophoresis and Southern blotting. The blot was probed with sequence complementary to a region in the Y' subtelomeric element.

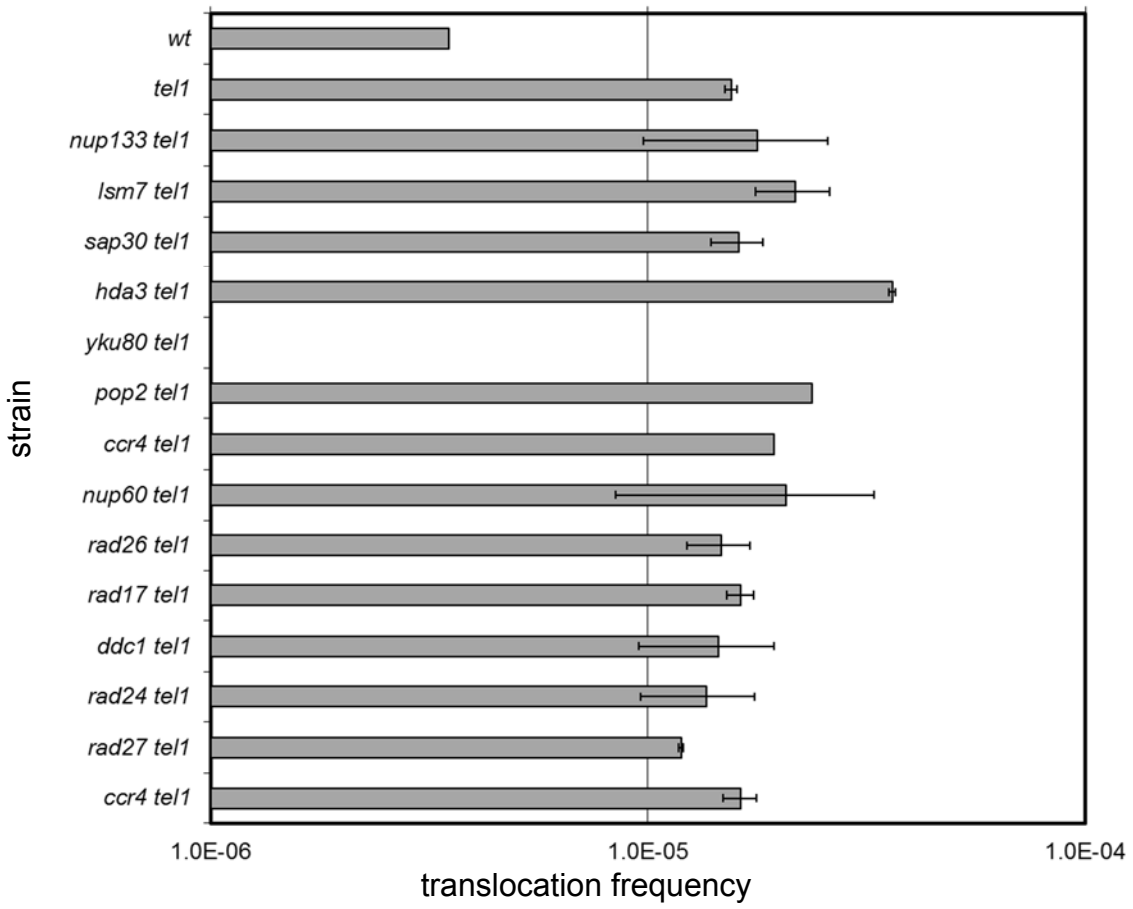

FIGURE 15. HO-INDUCED TRANSLOCATION FREQUENCY FOR TEL1-Δ INTERACTIONS.

NHEJ-mediated translocation frequency for *tel1-Δ* double mutants following *GAL-HO* induction of double strand breaks on Ch V and Ch VII. Frequencies are measured as the fraction of colonies that survive on -Ura plates. Error bars indicate the standard deviation of values from three independent transformants.

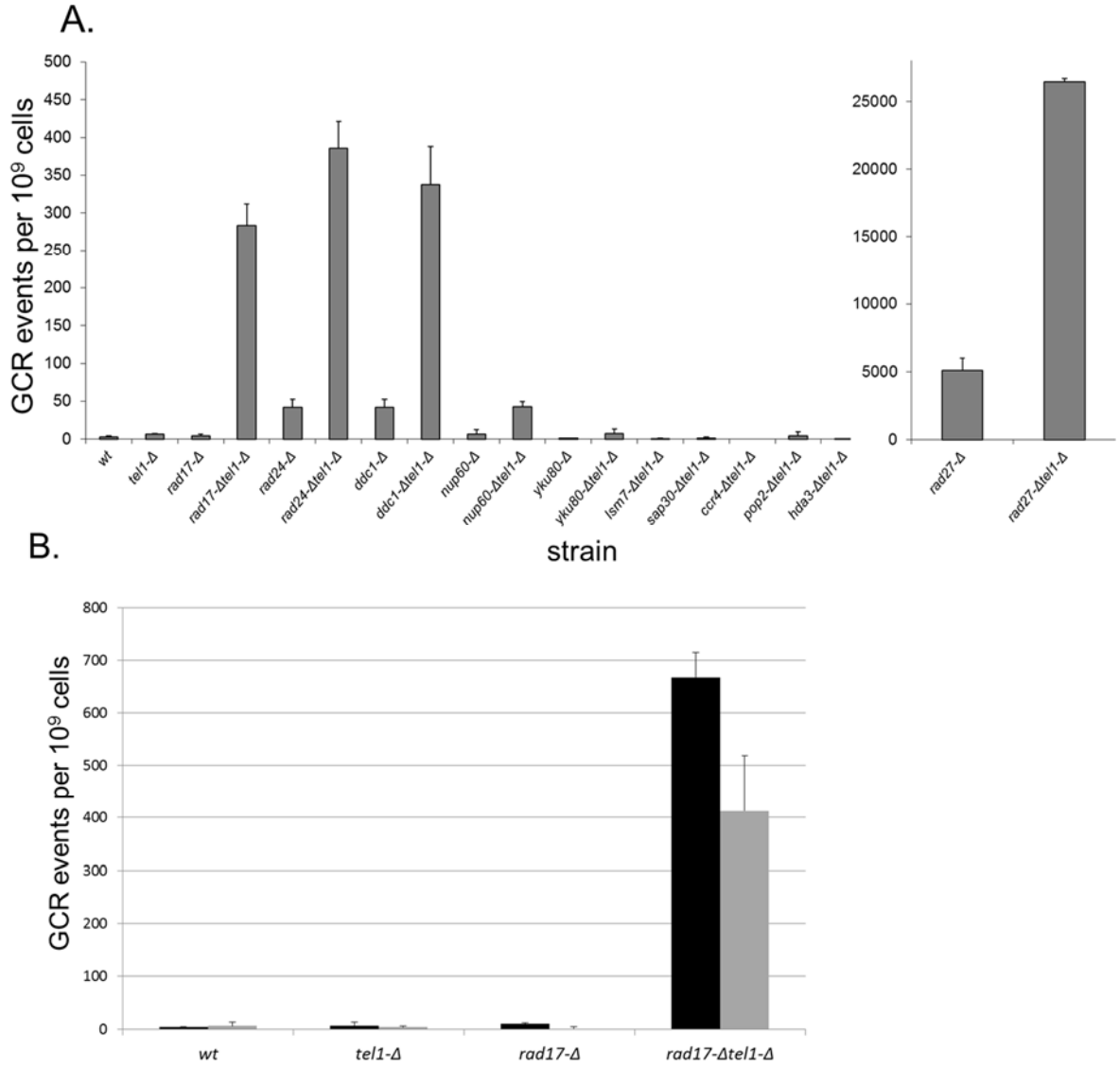

FIGURE 16. GROSS CHROMOSOMAL REARRANGEMENT (GCR) FREQUENCY IN 0.003% MMS.

(A) GCR frequency for *tel1-Δ* interactions. Strains were grown in YEPD + 0.003% MMS for 15 hours and subsequently plated on C-Arg-Ser + Canavanine + 5-FOA to simultaneously select for the loss of *CAN1* and *URA3* markers on the left end of chromosome V. Error bars represent standard deviations from two independent cultures per strain, each plated two times. The *rad27-Δ* mutants are plotted separately due to scale. (B) Gross chromosomal rearrangement (GCR) frequency in 0.003% MMS with or without the *CDC13-EST2* fusion plasmid. The indicated strains containing either an empty vector (black bars) or the *CDC13-EST2* fusion (grey bars) were grown in YEPD + 0.003% MMS for 15 hours and subsequently plated on C-Arg-Ser + Canavanine + 5-FOA to select for simultaneous loss of *CAN1* and *URA3* markers. Error bars represent standard deviations from two independent cultures per strain, each plated two times.

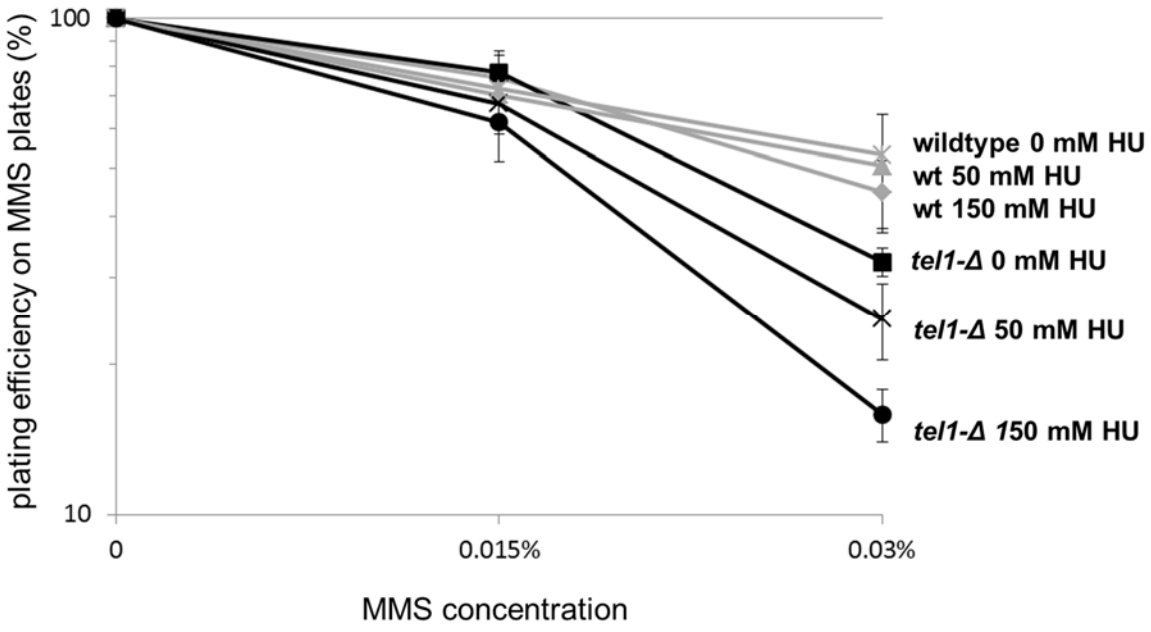

FIGURE 17. MMS SENSITIVITY FOLLOWING PRETREATMENT WITH HYDROXYUREA.

The indicated strains were grown in the presence of the indicated dose of hydroxyurea for 4 hours to deplete nucleotide pools. Cells were then washed 2x and plated on MMS plates to assay MMS sensitivity by colony forming assay. The error bars indicate the standard deviation of values from three independent cultures.

CHAPTER 4: Conclusions and future directions

OVERVIEW

The genesis of the reasoning that led to the yeast *TEL1* interaction screen and my characterization of the relationship between short telomeres and MMS sensitivity had its surprising beginning in a human microarray study. In this study, we found that *ATM-/-* lymphoblast cells exhibited a robust transcriptional response to 5 Gy of IR that was indistinguishable from *ATM+/+* cells (Chapter 2). Moreover, we detected radiation-induced S15 phosphorylation (an ATM target site) of the TP53 transcription factor in *ATM-/-* cells, and this phosphorylation was significantly reduced upon treatment with the phosphoinositide 3-kinase related kinase (PIKK) inhibitor caffeine (Figure 1). These data are consistent with the overlap in substrate specificity for PIKKs (ABRAHAM 2001) and point to a model in which other PIKKs buffer the loss of *ATM* in the DNA damage response. A clear analog for this in *Saccharomyces cerevisiae* is the well-characterized interaction between *TEL1* and *MEC1,* in which loss of both PIKKs leads to synergistic DNA damage sensitivity and a progressive loss of telomere protection (CRAVEN *et al.* 2002; MORROW *et al.* 1995; RITCHIE *et al.* 1999; SANCHEZ *et al.* 1996). My intellectual curiosity led me to ask what other genetic mutations may cause an interaction effect with *tel1-Δ* in response to DNA damage, and I began the large-scale screening for *tel1-Δ* interactions with some trepidation that *TEL1* interaction effects may not extend past its redundancy with *MEC1.* This turned out to not be the case however, as a diverse set of thirteen mutants conferred an increase in MMS and/or IR sensitivity with *tel1-Δ* (Figures

6 and 7). The connection between MMS sensitivity and short telomeres for many of the *tel1-Δ xxx-Δ* interactions (Figure 11) and the inability of *tel1-Δ* cells to deal with replication stress (Figure 17) suggest a novel and complex role for Tel1p in the DNA damage response that could be further elucidated by future experiments (Figure 18 and see below).

SHORT TELOMERES AND DNA DAMAGE SENSITIVITY

A significant conclusion of this work is that I have shown in two different genetic contexts (via progressive shortening in *tlc1* cells and via the *CDC13-EST2*-reversible *9-1-1-Δ tel1-Δ* interaction) that MMS sensitivity is telomere-length dependent. Characterization of the mechanism(s) underlying this connection will be an important direction for future studies. One possible (and testable) mechanism for the MMS sensitivity exhibited by *9-1-1-Δ tel1-Δ* is that this phenotype results from a loss of telomere protection rendering ends susceptible to detection by DNA repair enzymes (Figure 18). In this case, MMS sensitivity may result from the sequestration of DNA repair enzymes at telomeres (and away from MMS-induced lesions elsewhere in the genome) or may be due to the fusion of unprotected telomeres with MMS-induced DSBs. The former case has been observed for post-senescent yeast telomeres maintained by recombination (LIN *et al.* 2009) however it is important to note that *9-1-1-Δ tel1-Δ* telomeres are short but stably maintained (Figure 12). To test this model, ChIP could be used to measure the binding of DNA repair proteins to telomeres in *9-1-1-Δ tel1-Δ* cells. The alternative model (increased fusion of telomeres to DSBs in *9-1-1-Δ tel1-Δ*) could be tested using the HO-

inducible telomere capping assay (DUBOIS *et al.* 2002) that has been modified for the detection of telomere-DSB fusions (CHAN and BLACKBURN 2003).

EXPLORING THE ROLE OF Tel1p IN RESPONSE TO REPLICATION STRESS

As much of the DNA damage sensitivity observed for *tel1-Δ xxx-Δ* interactions could not be suppressed by *CDC13-EST2*-mediated elongation of telomeres (Figures 13 & 14), I propose that a general increase in replication stress may underlie the DNA damage sensitivity of a number of *tel1-Δ xxx-Δ* mutants (Figure 18). This is supported by the fact that a *tel1-Δ* strain (and not wild-type) is rendered sensitive to MMS by pre-depletion of nucleotide pools via hydroxyurea treatment (Figure 17). The mechanism for this is unclear and further studies may focus on elucidating the role of Tel1p in preventing replication stress. One possibility is that *tel1-Δ* combined with other mutations (*ccr4-Δ, rad24-Δ etc.*) leads to a synergistic decrease in dNTP pools, an idea that is supported by the fact that Mec1/Tel1-mediated phosphorylation targets multiple ribonucleotide reductase inhibitors for degradation in response to DNA damage (HUANG *et al.* 1998; ZHAO and ROTHSTEIN 2002). Thus one prediction is that deletion of one or multiple RNR inhibitors (*SML1, CRT1*) or overexpression of *RNR3* (DESANY *et al.* 1998) may suppress the MMS sensitivity of *tel1-Δ xxx-Δ* double-mutants. Moreover, chromatographic separation and detection (*i.e.* via HPLC) could be used to directly assess whether levels of dNTPs are significantly reduced in *tel1-Δ xxx-Δ* strains (FASULLO *et al.* 2010).

An alternative hypothesis is that Tel1p may prevent replication fork collapse in response to MMS treatment, and an increase in fork stalling (via the identified interacting mutants) may increase the importance of Tel1p's role here. Doksani *et al.* has previously

shown that in *tel1-Δ* cells, a terminal replication fork (a fork encountering a DNA break or chromosome end) exhibits an increased tendency to revert into a cruciform structure, a precursor to fork collapse (DOKSANI *et al.* 2009). The combination of MMS treatment added to a preexisting state of replication stress may serve to increase the probability of these events. Such structures in MMS-treated *tel1-Δ xxx-Δ* strains could be detected by 2D gel electrophoresis (BREWER and FANGMAN 1987). In addition, the observation that *tel1-Δ* is required for terminal fork integrity suggests that these events could occur specifically or predominantly at telomeres (DOKSANI *et al.* 2009). The location of such events could be mapped using the recently developed strategy of Break-chip (FENG *et al.* 2011), which involves labeling of broken DNA ends from intact chromosomal DNA preparations and hybridization to a microarray. Alternately, ChIP-chip or ChIP-Seq could be performed via the immunoprecipitation of a double-strand-break-associated protein (Rad52p for example) in order to determine whether DNA damage in MMS-treated *tel1-Δ xxx-Δ* occurs in a site-specific manner.

In addition, it would be worthwhile to ask whether a novel molecular function of Tel1p contributes to MMS resistance. This could be assessed by verifying that the MMS-sensitive interactions we see for *tel1-Δ* can be recapitulated with a kinase-dead form of Tel1p (MALLORY and PETES 2000). Moreover, as Tel1p binding at DNA ends occurs via an interaction with the MRX complex (NAKADA *et al.* 2003) it would be worthwhile to ask which (if any) of the thirteen genes identified in the *tel1-Δ* screen also exhibit an interaction effect with an MRX mutant such as *xrs2-Δ*.

CONSERVATION OF *ATM/TEL1* INTERACTIONS IN MAMMALIAN CELLS

One possible future direction for this project is the assessment of whether the *tel1-Δ* gene-gene interactions observed in yeast can be recapitulated in human cells. The identification of novel *ATM* interactions in human cells may offer significant predictive and therapeutic potential. For example, as discussed in Chapter 2, the functionality of the DNA damage response (*i.e.* the radiation-induced gene set) is a strong predictor of breast tumor outcome (Table 2 and Figure 3), and the ability to search for *ATM*-interacting alleles in breast cancer GWAS data may result in the identification of novel risk factors for breast cancer development and/or outcome.

Thus, follow-up studies may ask whether knockdowns of human orthologs of the 13 *tel1-Δ* interactions confer MMS sensitivity with *ATM* depletion. One strategy would be to combine treatment with the specific ATM inhibitor KU55933 (HICKSON *et al.* 2004) with siRNA-mediated knockdowns of additional targets such as 9-1-1 components followed by testing for MMS sensitivity. Intriguingly, a recent study found that the specific combination of KU55933 combined with a telomerase inhibitor rendered MCF-7 tumor cells extremely sensitive to the chemotherapy agent etoposide (TAMAKAWA *et al.* 2010), suggesting that such a strategy may be feasible. However, as these techniques result in transient gene inhibition, and we expect that in at least a subset of cases the MMS-sensitivity is partly telomere-length dependent, generation of *ATM-/- XXX-/-* double-mutant cell lines may be necessary to observe an MMS-dependent interaction. Such a line might be generated utilizing recently developed genome editing strategies (TALENs, etc.) (JOUNG and SANDER 2013) in a cell line derived from an AT patient. Testing for conservation of these interactions in mammalian cells may give some indication of the utility of yeast-based DNA damage interaction screens for mapping out the mammalian interactome.

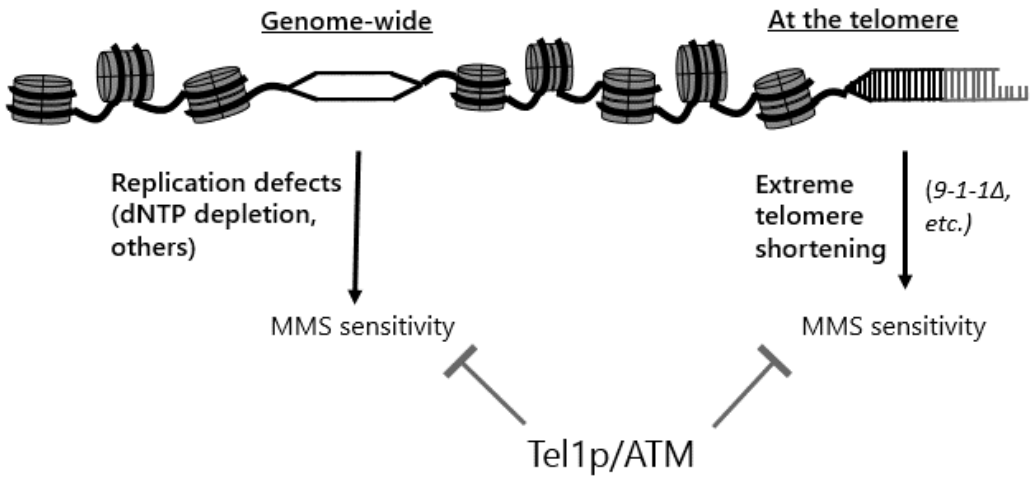

FIGURE 18. A MODEL FOR TEL1P/ATM-MEDIATED SUPPRESSION OF MMS SENSITIVITY.

The results of the *tel1-Δ* interaction screen suggest a model in which Tel1p suppresses DNA damage sensitivity in a telomere-specific fashion and in response to genome-wide replication stress.

REFERENCES

ABRAHAM, R. T., 2001 Cell cycle checkpoint signaling through the ATM and ATR kinases. Genes Dev **15:** 2177-2196.

AGARWAL, M., S. PANDITA, C. R. HUNT, A. GUPTA, X. YUE *et al.*, 2008 Inhibition of telomerase activity enhances hyperthermia-mediated radiosensitization. Cancer Res **68:** 3370-3378.

AMUNDSON, S. A., K. T. DO, L. C. VINIKOOR, R. A. LEE, C. A. KOCH-PAIZ *et al.*, 2008 Integrating global gene expression and radiation survival parameters across the 60 cell lines of the National Cancer Institute Anticancer Drug Screen. Cancer research **68:** 415-424.

ARNERIC, M., and J. LINGNER, 2007 Tel1 kinase and subtelomere-bound Tbf1 mediate preferential elongation of short telomeres by telomerase in yeast. EMBO Rep **8:** 1080-1085.

ASHBURNER, M., C. A. BALL, J. A. BLAKE, D. BOTSTEIN, H. BUTLER *et al.*, 2000 Gene ontology: tool for the unification of biology. The Gene Ontology Consortium. Nature genetics **25:** 25-29.

BAKKENIST, C. J., and M. B. KASTAN, 2003 DNA damage activates ATM through intermolecular autophosphorylation and dimer dissociation. Nature **421:** 499-506.

BANIN, S., L. MOYAL, S. SHIEH, Y. TAYA, C. W. ANDERSON *et al.*, 1998 Enhanced phosphorylation of p53 by ATM in response to DNA damage. Science **281:** 1674-1677.

BARRIER, A., A. LEMOINE, P. Y. BOELLE, C. TSE, D. BRAULT *et al.*, 2005 Colon cancer prognosis prediction by gene expression profiling. Oncogene **24:** 6155-6164.

BARTKOVA, J., Z. HOREJSI, K. KOED, A. KRAMER, F. TORT *et al.*, 2005 DNA damage response as a candidate anti-cancer barrier in early human tumorigenesis. Nature **434:** 864-870.

BARTKOVA, J., N. REZAEI, M. LIONTOS, P. KARAKAIDOS, D. KLETSAS *et al.*, 2006 Oncogene-induced senescence is part of the tumorigenesis barrier imposed by DNA damage checkpoints. Nature **444:** 633-637.

BEER, D. G., S. L. KARDIA, C. C. HUANG, T. J. GIORDANO, A. M. LEVIN *et al.*, 2002 Gene-expression profiles predict survival of patients with lung adenocarcinoma. Nature medicine **8:** 816-824.

BERMEJO, R., T. CAPRA, R. JOSSEN, A. COLOSIO, C. FRATTINI *et al.*, 2011 The replication checkpoint protects fork stability by releasing transcribed genes from nuclear pores. Cell **146:** 233-246.

BHATTACHARJEE, A., W. G. RICHARDS, J. STAUNTON, C. LI, S. MONTI *et al.*, 2001 Classification of human lung carcinomas by mRNA expression profiling reveals distinct adenocarcinoma subclasses. Proceedings of the National Academy of Sciences of the United States of America **98:** 13790-13795.

BILD, A. H., G. YAO, J. T. CHANG, Q. WANG, A. POTTI *et al.*, 2006 Oncogenic pathway signatures in human cancers as a guide to targeted therapies. Nature **439:** 353-357.

BLOOM, J. S., I. M. EHRENREICH, W. T. LOO, T. L. LITE and L. KRUGLYAK, 2013 Finding the sources of missing heritability in a yeast cross. Nature.

BOCHMAN, M. L., K. PAESCHKE and V. A. ZAKIAN, 2012 DNA secondary structures: stability and function of G-quadruplex structures. Nat Rev Genet **13:** 770-780.

BOERSMA, B. J., T. M. HOWE, J. E. GOODMAN, H. G. YFANTIS, D. H. LEE *et al.*, 2006 Association of breast cancer outcome with status of p53 and MDM2 SNP309. Journal of the National Cancer Institute **98:** 911-919.

BRACHMANN, C. B., A. DAVIES, G. J. COST, E. CAPUTO, J. LI *et al.*, 1998 Designer deletion strains derived from Saccharomyces cerevisiae S288C: a useful set of strains and plasmids for PCR-mediated gene disruption and other applications. Yeast (Chichester, England) **14:** 115-132.

BREWER, B. J., and W. L. FANGMAN, 1987 The localization of replication origins on ARS plasmids in S. cerevisiae. Cell **51:** 463-471.

CANMAN, C. E., D. S. LIM, K. A. CIMPRICH, Y. TAYA, K. TAMAI *et al.*, 1998 Activation of the ATM kinase by ionizing radiation and phosphorylation of p53. Science **281:** 1677-1679.

CHABES, A., B. GEORGIEVA, V. DOMKIN, X. ZHAO, R. ROTHSTEIN *et al.*, 2003 Survival of DNA damage in yeast directly depends on increased dNTP levels allowed by relaxed feedback inhibition of ribonucleotide reductase. Cell **112:** 391-401.

CHAN, S. W., and E. H. BLACKBURN, 2003 Telomerase and ATM/Tel1p protect telomeres from nonhomologous end joining. Mol Cell **11:** 1379-1387.

CHANG, H. Y., D. S. NUYTEN, J. B. SNEDDON, T. HASTIE, R. TIBSHIRANI *et al.*, 2005 Robustness, scalability, and integration of a wound-response gene expression signature in predicting breast cancer survival. Proceedings of the National Academy of Sciences of the United States of America **102:** 3738-3743.

CHANG, H. Y., J. B. SNEDDON, A. A. ALIZADEH, R. SOOD, R. B. WEST *et al.*, 2004 Gene expression signature of fibroblast serum response predicts human cancer progression: similarities between tumors and wounds. PLoS biology **2:** E7.

CHANG, M., M. ARNERIC and J. LINGNER, 2007 Telomerase repeat addition processivity is increased at critically short telomeres in a Tel1-dependent manner in Saccharomyces cerevisiae. Genes Dev **21:** 2485-2494.

CHAPON, C., T. R. CECH and A. J. ZAUG, 1997 Polyadenylation of telomerase RNA in budding yeast. RNA **3:** 1337-1351.

CHEN, C., and R. D. KOLODNER, 1999 Gross chromosomal rearrangements in Saccharomyces cerevisiae replication and recombination defective mutants. Nat Genet **23:** 81-85.

CHOMCZYNSKI, P., and N. SACCHI, 1987 Single-step method of RNA isolation by acid guanidinium thiocyanate-phenol-chloroform extraction. Analytical Biochemistry **162:** 156-159.

CHOMCZYNSKI, P., and N. SACCHI, 2006 The single-step method of RNA isolation by acid guanidinium thiocyanate-phenol-chloroform extraction: twenty-something years on. Nat Protoc **1:** 581-585.

CIMPRICH, K. A., T. B. SHIN, C. T. KEITH and S. L. SCHREIBER, 1996 cDNA cloning and gene mapping of a candidate human cell cycle checkpoint protein. Proc Natl Acad Sci U S A **93:** 2850-2855.

CRAVEN, R. J., P. W. GREENWELL, M. DOMINSKA and T. D. PETES, 2002 Regulation of genome stability by TEL1 and MEC1, yeast homologs of the mammalian ATM and ATR genes. Genetics **161:** 493-507.

DESANY, B. A., A. A. ALCASABAS, J. B. BACHANT and S. J. ELLEDGE, 1998 Recovery from DNA replicational stress is the essential function of the S-phase checkpoint pathway. Genes Dev **12:** 2956-2970.

DI MICCO, R., M. FUMAGALLI, A. CICALESE, S. PICCININ, P. GASPARINI *et al.*, 2006 Oncogene-induced senescence is a DNA damage response triggered by DNA hyper-replication. Nature **444:** 638-642.

DOKSANI, Y., R. BERMEJO, S. FIORANI, J. E. HABER and M. FOIANI, 2009 Replicon dynamics, dormant origin firing, and terminal fork integrity after double-strand break formation. Cell **137:** 247-258.

DRISSI, R., J. WU, Y. HU, C. BOCKHOLD and J. S. DOME, 2011 Telomere shortening alters the kinetics of the DNA damage response after ionizing radiation in human cells. Cancer Prev Res (Phila) **4:** 1973-1981.

DUBOIS, M. L., Z. W. HAIMBERGER, M. W. MCINTOSH and D. E. GOTTSCHLING, 2002 A quantitative assay for telomere protection in Saccharomyces cerevisiae. Genetics **161:** 995-1013.

EHRENREICH, I. M., J. BLOOM, N. TORABI, X. WANG, Y. JIA *et al.*, 2012 Genetic architecture of highly complex chemical resistance traits across four yeast strains. PLoS Genet **8:** e1002570.

EHRENREICH, I. M., N. TORABI, Y. JIA, J. KENT, S. MARTIS *et al.*, 2010 Dissection of genetically complex traits with extremely large pools of yeast segregants. Nature **464:** 1039-1042.

EVANS, S. K., and V. LUNDBLAD, 1999 Est1 and Cdc13 as comediators of telomerase access. Science **286:** 117-120.

FAN, C., D. S. OH, L. WESSELS, B. WEIGELT, D. S. NUYTEN *et al.*, 2006 Concordance among gene-expression-based predictors for breast cancer. The New England journal of medicine **355:** 560-569.

FASULLO, M., O. TSAPONINA, M. SUN and A. CHABES, 2010 Elevated dNTP levels suppress hyper-recombination in Saccharomyces cerevisiae S-phase checkpoint mutants. Nucleic Acids Res **38:** 1195-1203.

FENG, W., S. C. DI RIENZI, M. K. RAGHURAMAN and B. J. BREWER, 2011 Replication stress-induced chromosome breakage is correlated with replication fork progression and is preceded by single-stranded DNA formation. G3 (Bethesda) **1:** 327-335.

FUKUNAGA, K., Y. KWON, P. SUNG and K. SUGIMOTO, 2011 Activation of protein kinase Tel1 through recognition of protein-bound DNA ends. Mol Cell Biol.

FUMAGALLI, M., F. ROSSIELLO, M. CLERICI, S. BAROZZI, D. CITTARO *et al.*, 2012 Telomeric DNA damage is irreparable and causes persistent DNA-damage-response activation. Nat Cell Biol **14:** 355-365.

GAO, H., T. B. TORO, M. PASCHINI, B. BRAUNSTEIN-BALLEW, R. B. CERVANTES *et al.*, 2010 Telomerase recruitment in Saccharomyces cerevisiae is not dependent on Tel1-mediated phosphorylation of Cdc13. Genetics **186:** 1147-1159.

GLAS, A. M., A. FLOORE, L. J. DELAHAYE, A. T. WITTEVEEN, R. C. POVER *et al.*, 2006 Converting a breast cancer microarray signature into a high-throughput diagnostic test. BMC genomics **7:** 278.

GONZALEZ-SUAREZ, E., F. A. GOYTISOLO, J. M. FLORES and M. A. BLASCO, 2003 Telomere dysfunction results in enhanced organismal sensitivity to the alkylating agent N-methyl-N-nitrosourea. Cancer Res **63:** 7047-7050.

GORGOULIS, V. G., L. V. VASSILIOU, P. KARAKAIDOS, P. ZACHARATOS, A. KOTSINAS *et al.*, 2005 Activation of the DNA damage checkpoint and genomic instability in human precancerous lesions. Nature **434:** 907-913.

GOYTISOLO, F. A., E. SAMPER, J. MARTIN-CABALLERO, P. FINNON, E. HERRERA *et al.*, 2000 Short telomeres result in organismal hypersensitivity to ionizing radiation in mammals. J Exp Med **192:** 1625-1636.

GRANDIN, N., A. BAILLY and M. CHARBONNEAU, 2005 Activation of Mrc1, a mediator of the replication checkpoint, by telomere erosion. Biol Cell **97:** 799-814.

GREENMAN, C., P. STEPHENS, R. SMITH, G. L. DALGLIESH, C. HUNTER *et al.*, 2007 Patterns of somatic mutation in human cancer genomes. Nature **446:** 153-158.

GREENWELL, P. W., S. L. KRONMAL, S. E. PORTER, J. GASSENHUBER, B. OBERMAIER *et al.*, 1995 TEL1, a gene involved in controlling telomere length in S. cerevisiae, is homologous to the human ataxia telangiectasia gene. Cell **82:** 823-829.

GREIDER, C. W., and E. H. BLACKBURN, 1985 Identification of a specific telomere terminal transferase activity in Tetrahymena extracts. Cell **43:** 405-413.

GUO, Z., R. DESHPANDE and T. T. PAULL, 2010a ATM activation in the presence of oxidative stress. Cell Cycle **9:** 4805-4811.

GUO, Z., S. KOZLOV, M. F. LAVIN, M. D. PERSON and T. T. PAULL, 2010b ATM activation by oxidative stress. Science **330:** 517-521.

GUPTA, A., S. SHARMA, P. REICHENBACH, L. MARJAVAARA, A. K. NILSSON *et al.*, 2013 Telomere Length Homeostasis Responds to Changes in Intracellular dNTP Pools. Genetics.

HANAHAN, D., and R. A. WEINBERG, 2000 The hallmarks of cancer. Cell **100:** 57-70.

HARPER, J. W., and S. J. ELLEDGE, 2007 The DNA damage response: ten years after. Molecular cell **28:** 739-745.

HARRIS, L., H. FRITSCHE, R. MENNEL, L. NORTON, P. RAVDIN *et al.*, 2007 American Society of Clinical Oncology 2007 update of recommendations for the use of tumor markers in breast cancer. Journal of clinical oncology : official journal of the American Society of Clinical Oncology **25:** 5287-5312.

HAYFLICK, L., and P. S. MOORHEAD, 1961 The serial cultivation of human diploid cell strains. Exp Cell Res **25:** 585-621.

HERRERO, A. B., and S. MORENO, 2011 Lsm1 promotes genomic stability by controlling histone mRNA decay. EMBO J **30:** 2008-2018.

HICKSON, I., Y. ZHAO, C. J. RICHARDSON, S. J. GREEN, N. M. MARTIN *et al.*, 2004 Identification and characterization of a novel and specific inhibitor of the ataxia-telangiectasia mutated kinase ATM. Cancer Res **64:** 9152-9159.

HUANG, D., B. D. PIENING and A. G. PAULOVICH, 2013 The preference for error-free or error-prone postreplication repair is cell-cycle-dependent in Saccharomyces cerevisiae in response to low-dose methylmethanesulfonate. Mol Cell Biol.

HUANG, M., Z. ZHOU and S. J. ELLEDGE, 1998 The DNA replication and damage checkpoint pathways induce transcription by inhibition of the Crt1 repressor. Cell **94:** 595-605.

IRIZARRY, R. A., B. HOBBS, F. COLLIN, Y. D. BEAZER-BARCLAY, K. J. ANTONELLIS *et al.*, 2003 Exploration, normalization, and summaries of high density oligonucleotide array probe level data. Biostatistics (Oxford, England) **4:** 249-264.

ISOLA, J., T. VISAKORPI, K. HOLLI and O. P. KALLIONIEMI, 1992 Association of overexpression of tumor suppressor protein p53 with rapid cell proliferation and poor prognosis in node-negative breast cancer patients. Journal of the National Cancer Institute **84:** 1109-1114.

IVESSA, A. S., J. Q. ZHOU, V. P. SCHULZ, E. K. MONSON and V. A. ZAKIAN, 2002 Saccharomyces Rrm3p, a 5' to 3' DNA helicase that promotes replication fork progression through telomeric and subtelomeric DNA. Genes Dev **16:** 1383-1396.

JEN, K. Y., and V. G. CHEUNG, 2005 Identification of novel p53 target genes in ionizing radiation response. Cancer research **65:** 7666-7673.

JOUNG, J. K., and J. D. SANDER, 2013 TALENs: a widely applicable technology for targeted genome editing. Nat Rev Mol Cell Biol **14:** 49-55.

KANG, M. J., C. H. LEE, Y. H. KANG, I. T. CHO, T. A. NGUYEN *et al.*, 2010 Genetic and functional interactions between Mus81-Mms4 and Rad27. Nucleic Acids Res **38:** 7611-7625.

KAOCHAR, S., L. SHANKS and T. WEINERT, 2010 Checkpoint genes and Exo1 regulate nearby inverted repeat fusions that form dicentric chromosomes in Saccharomyces cerevisiae. Proc Natl Acad Sci U S A **107:** 21605-21610.

KAPITZKY, L., P. BELTRAO, T. J. BERENS, N. GASSNER, C. ZHOU *et al.*, 2010 Cross-species chemogenomic profiling reveals evolutionarily conserved drug mode of action. Mol Syst Biol **6:** 451.

KAPP, A. V., S. S. JEFFREY, A. LANGEROD, A. L. BORRESEN-DALE, W. HAN *et al.*, 2006 Discovery and validation of breast cancer subtypes. BMC genomics **7:** 231.

KASTAN, M. B., Q. ZHAN, W. S. EL-DEIRY, F. CARRIER, T. JACKS *et al.*, 1992 A mammalian cell cycle checkpoint pathway utilizing p53 and GADD45 is defective in ataxia-telangiectasia. Cell **71:** 587-597.

KINZLER, K. W., and B. VOGELSTEIN, 1996 Lessons from hereditary colorectal cancer. Cell **87:** 159-170.

KOZLOV, S. V., M. E. GRAHAM, C. PENG, P. CHEN, P. J. ROBINSON *et al.*, 2006 Involvement of novel autophosphorylation sites in ATM activation. The EMBO journal **25:** 3504-3514.

KUHNE, M., E. RIBALLO, N. RIEF, K. ROTHKAMM, P. A. JEGGO *et al.*, 2004 A double-strand break repair defect in ATM-deficient cells contributes to radiosensitivity. Cancer Res **64:** 500-508.

LAPOINTE, J., C. LI, J. P. HIGGINS, M. VAN DE RIJN, E. BAIR *et al.*, 2004 Gene expression profiling identifies clinically relevant subtypes of prostate cancer. Proceedings of the National Academy of Sciences of the United States of America **101:** 811-816.

LAVIN, M. F., 2008 Ataxia-telangiectasia: from a rare disorder to a paradigm for cell signalling and cancer. Nat Rev Mol Cell Biol **9:** 759-769.

LEE, J. H., and T. T. PAULL, 2004 Direct activation of the ATM protein kinase by the Mre11/Rad50/Nbs1 complex. Science (New York, N.Y.) **304:** 93-96.

LEE, J. H., and T. T. PAULL, 2007 Activation and regulation of ATM kinase activity in response to DNA double-strand breaks. Oncogene **26:** 7741-7748.

LEE, K., Y. ZHANG and S. E. LEE, 2008 Saccharomyces cerevisiae ATM orthologue suppresses break-induced chromosome translocations. Nature **454:** 543-546.

LIN, Y. H., C. C. CHANG, C. W. WONG and S. C. TENG, 2009 Recruitment of Rad51 and Rad52 to short telomeres triggers a Mec1-mediated hypersensitivity to double-stranded DNA breaks in senescent budding yeast. PLoS One **4:** e8224.

LOI, S., B. HAIBE-KAINS, C. DESMEDT, F. LALLEMAND, A. M. TUTT *et al.*, 2007 Definition of clinically distinct molecular subtypes in estrogen receptor-positive breast carcinomas through genomic grade. Journal of clinical oncology : official journal of the American Society of Clinical Oncology **25:** 1239-1246.

LONGHESE, M. P., V. PACIOTTI, H. NEECKE and G. LUCCHINI, 2000 Checkpoint proteins influence telomeric silencing and length maintenance in budding yeast. Genetics **155:** 1577-1591.

LUNDBLAD, V., and E. H. BLACKBURN, 1993 An alternative pathway for yeast telomere maintenance rescues est1- senescence. Cell **73:** 347-360.

LUNDIN, C., M. NORTH, K. ERIXON, K. WALTERS, D. JENSSEN *et al.*, 2005 Methyl methanesulfonate (MMS) produces heat-labile DNA damage but no detectable in vivo DNA double-strand breaks. Nucleic Acids Res **33:** 3799-3811.

LUSTIG, A. J., and T. D. PETES, 1986 Identification of yeast mutants with altered telomere structure. Proceedings of the National Academy of Sciences of the United States of America **83:** 1398-1402.

MALIK, S., P. CHAURASIA, S. LAHUDKAR, G. DURAIRAJ, A. SHUKLA *et al.*, 2010 Rad26p, a transcription-coupled repair factor, is recruited to the site of DNA lesion in an elongating RNA polymerase II-dependent manner in vivo. Nucleic Acids Res **38:** 1461-1477.

MALLORY, J. C., and T. D. PETES, 2000 Protein kinase activity of Tel1p and Mec1p, two Saccharomyces cerevisiae proteins related to the human ATM protein kinase. Proc Natl Acad Sci U S A **97:** 13749-13754.

MANOLIO, T. A., F. S. COLLINS, N. J. COX, D. B. GOLDSTEIN, L. A. HINDORFF *et al.*, 2009 Finding the missing heritability of complex diseases. Nature **461:** 747-753.

MANTIERO, D., M. CLERICI, G. LUCCHINI and M. P. LONGHESE, 2007 Dual role for Saccharomyces cerevisiae Tel1 in the checkpoint response to double-strand breaks. EMBO reports **8:** 380-387.

MARCAND, S., E. GILSON and D. SHORE, 1997 A protein-counting mechanism for telomere length regulation in yeast. Science **275:** 986-990.

MARTINA, M., M. CLERICI, V. BALDO, D. BONETTI, G. LUCCHINI *et al.*, 2012 A balance between Tel1 and Rif2 activities regulates nucleolytic processing and elongation at telomeres. Mol Cell Biol **32:** 1604-1617.

MATSUOKA, S., B. A. BALLIF, A. SMOGORZEWSKA, E. R. MCDONALD, 3RD, K. E. HUROV *et al.*, 2007 ATM and ATR substrate analysis reveals extensive protein networks responsive to DNA damage. Science **316:** 1160-1166.

MCCULLEY, J. L., and T. D. PETES, 2010 Chromosome rearrangements and aneuploidy in yeast strains lacking both Tel1p and Mec1p reflect deficiencies in two different mechanisms. Proc Natl Acad Sci U S A **107:** 11465-11470.

MCGEE, J. S., J. A. PHILLIPS, A. CHAN, M. SABOURIN, K. PAESCHKE *et al.*, 2010 Reduced Rif2 and lack of Mec1 target short telomeres for elongation rather than double-strand break repair. Nat Struct Mol Biol **17:** 1438-1445.

MCSHANE, L. M., R. AAMODT, C. CORDON-CARDO, R. COTE, D. FARAGGI *et al.*, 2000 Reproducibility of p53 immunohistochemistry in bladder tumors. National Cancer Institute, Bladder Tumor Marker Network. Clinical cancer research : an official journal of the American Association for Cancer Research **6:** 1854-1864.

MERRICK, C. J., D. JACKSON and J. F. DIFFLEY, 2004 Visualization of altered replication dynamics after DNA damage in human cells. J Biol Chem **279:** 20067-20075.

METCALFE, J. A., J. PARKHILL, L. CAMPBELL, M. STACEY, P. BIGGS *et al.*, 1996 Accelerated telomere shortening in ataxia telangiectasia. Nat Genet **13:** 350-353.

MIECZKOWSKI, P. A., J. O. MIECZKOWSKA, M. DOMINSKA and T. D. PETES, 2003 Genetic regulation of telomere-telomere fusions in the yeast Saccharomyces cerevisae. Proc Natl Acad Sci U S A **100:** 10854-10859.

MIKI, Y., J. SWENSEN, D. SHATTUCK-EIDENS, P. A. FUTREAL, K. HARSHMAN *et al.*, 1994 A strong candidate for the breast and ovarian cancer susceptibility gene BRCA1. Science **266:** 66-71.

MILLER, L. D., J. SMEDS, J. GEORGE, V. B. VEGA, L. VERGARA *et al.*, 2005 An expression signature for p53 status in human breast cancer predicts mutation status, transcriptional effects, and patient survival. Proceedings of the National Academy of Sciences of the United States of America **102:** 13550-13555.

MONTI, S., K. J. SAVAGE, J. L. KUTOK, F. FEUERHAKE, P. KURTIN *et al.*, 2005 Molecular profiling of diffuse large B-cell lymphoma identifies robust subtypes including one characterized by host inflammatory response. Blood **105:** 1851-1861.

MORRISON, A. J., J. A. KIM, M. D. PERSON, J. HIGHLAND, J. XIAO *et al.*, 2007 Mec1/Tel1 phosphorylation of the INO80 chromatin remodeling complex influences DNA damage checkpoint responses. Cell **130:** 499-511.

MORROW, D. M., D. A. TAGLE, Y. SHILOH, F. S. COLLINS and P. HIETER, 1995 TEL1, an S. cerevisiae homolog of the human gene mutated in ataxia telangiectasia, is functionally related to the yeast checkpoint gene MEC1. Cell **82:** 831-840.

MULDER, K. W., G. S. WINKLER and H. T. TIMMERS, 2005 DNA damage and replication stress induced transcription of RNR genes is dependent on the Ccr4-Not complex. Nucleic Acids Res **33:** 6384-6392.

MURAKAMI-SEKIMATA, A., D. HUANG, B. D. PIENING, C. BANGUR and A. G. PAULOVICH, 2010 The Saccharomyces cerevisiae RAD9, RAD17 and RAD24 genes are required for suppression of mutagenic post-replicative repair during chronic DNA damage. DNA Repair (Amst) **9:** 824-834.

MYUNG, K., and R. D. KOLODNER, 2002 Suppression of genome instability by redundant S-phase checkpoint pathways in Saccharomyces cerevisiae. Proc Natl Acad Sci U S A **99:** 4500-4507.

MYUNG, K., and R. D. KOLODNER, 2003 Induction of genome instability by DNA damage in Saccharomyces cerevisiae. DNA repair **2:** 243-258.

NAKADA, D., K. MATSUMOTO and K. SUGIMOTO, 2003 ATM-related Tel1 associates with double-strand breaks through an Xrs2-dependent mechanism. Genes Dev **17:** 1957-1962.

NAKAMURA, M., K. MASUTOMI, S. KYO, M. HASHIMOTO, Y. MAIDA *et al.*, 2005 Efficient inhibition of human telomerase reverse transcriptase expression by RNA interference sensitizes cancer cells to ionizing radiation and chemotherapy. Hum Gene Ther **16:** 859-868.

NUTT, C. L., D. R. MANI, R. A. BETENSKY, P. TAMAYO, J. G. CAIRNCROSS *et al.*, 2003 Gene expression-based classification of malignant gliomas correlates better with survival than histological classification. Cancer research **63:** 1602-1607.

PACIOTTI, V., M. CLERICI, G. LUCCHINI and M. P. LONGHESE, 2000 The checkpoint protein Ddc2, functionally related to S. pombe Rad26, interacts with Mec1 and is regulated by Mec1-dependent phosphorylation in budding yeast. Genes Dev **14:** 2046-2059.

PAIK, S., S. SHAK, G. TANG, C. KIM, J. BAKER *et al.*, 2004 A multigene assay to predict recurrence of tamoxifen-treated, node-negative breast cancer. The New England journal of medicine **351:** 2817-2826.

PAINTER, R. B., and B. R. YOUNG, 1980 Radiosensitivity in ataxia-telangiectasia: a new explanation. Proc Natl Acad Sci U S A **77:** 7315-7317.

PALANCADE, B., X. LIU, M. GARCIA-RUBIO, A. AGUILERA, X. ZHAO *et al.*, 2007 Nucleoporins prevent DNA damage accumulation by modulating Ulp1-dependent sumoylation processes. Mol Biol Cell **18:** 2912-2923.

PARENTEAU, J., and R. J. WELLINGER, 1999 Accumulation of single-stranded DNA and destabilization of telomeric repeats in yeast mutant strains carrying a deletion of RAD27. Mol Cell Biol **19:** 4143-4152.

PAULOVICH, A. G., C. D. ARMOUR and L. H. HARTWELL, 1998 The Saccharomyces cerevisiae RAD9, RAD17, RAD24 and MEC3 genes are required for tolerating irreparable, ultraviolet-induced DNA damage. Genetics **150:** 75-93.

PEROU, C. M., T. SORLIE, M. B. EISEN, M. VAN DE RIJN, S. S. JEFFREY *et al.*, 2000 Molecular portraits of human breast tumours. Nature **406:** 747-752.

PETO, J., and T. M. MACK, 2000 High constant incidence in twins and other relatives of women with breast cancer. Nat Genet **26:** 411-414.

PHAROAH, P. D., N. E. DAY and C. CALDAS, 1999 Somatic mutations in the p53 gene and prognosis in breast cancer: a meta-analysis. British journal of cancer **80:** 1968-1973.

PIENING, B. D., D. HUANG and A. G. PAULOVICH, 2013 Novel Connections Between DNA Replication, Telomere Homeostasis and the DNA Damage Response Revealed by a Genome-Wide Screen for TEL1/ATM Interactions in Saccharomyces cerevisiae. Genetics.

PIENING, B. D., P. WANG, A. SUBRAMANIAN and A. G. PAULOVICH, 2009 A radiation-derived gene expression signature predicts clinical outcome for breast cancer patients. Radiat Res **171:** 141-154.

POMEROY, S. L., P. TAMAYO, M. GAASENBEEK, L. M. STURLA, M. ANGELO *et al.*, 2002 Prediction of central nervous system embryonal tumour outcome based on gene expression. Nature **415:** 436-442.

RAMASWAMY, S., P. TAMAYO, R. RIFKIN, S. MUKHERJEE, C. H. YEANG *et al.*, 2001 Multiclass cancer diagnosis using tumor gene expression signatures. Proceedings of the National Academy of Sciences of the United States of America **98:** 15149-15154.

RENWICK, A., D. THOMPSON, S. SEAL, P. KELLY, T. CHAGTAI *et al.*, 2006 ATM mutations that cause ataxia-telangiectasia are breast cancer susceptibility alleles. Nat Genet **38:** 873-875.

RITCHIE, K. B., J. C. MALLORY and T. D. PETES, 1999 Interactions of TLC1 (which encodes the RNA subunit of telomerase), TEL1, and MEC1 in regulating telomere length in the yeast Saccharomyces cerevisiae. Molecular and cellular biology **19:** 6065-6075.

SAAL, L. H., P. JOHANSSON, K. HOLM, S. K. GRUVBERGER-SAAL, Q. B. SHE *et al.*, 2007 Poor prognosis in carcinoma is associated with a gene expression signature of aberrant PTEN tumor suppressor pathway activity. Proceedings of the National Academy of Sciences of the United States of America **104:** 7564-7569.

SABOURIN, M., C. T. TUZON and V. A. ZAKIAN, 2007 Telomerase and Tel1p preferentially associate with short telomeres in S. cerevisiae. Molecular cell **27:** 550-561.

SANCHEZ, Y., B. A. DESANY, W. J. JONES, Q. LIU, B. WANG *et al.*, 1996 Regulation of RAD53 by the ATM-like kinases MEC1 and TEL1 in yeast cell cycle checkpoint pathways. Science (New York, N.Y.) **271:** 357-360.

SANDERSON, R. D., Y. YANG, L. J. SUVA and T. KELLY, 2004 Heparan sulfate proteoglycans and heparanase--partners in osteolytic tumor growth and metastasis. Matrix biology : journal of the International Society for Matrix Biology **23:** 341-352.

SAVITSKY, K., S. SFEZ, D. A. TAGLE, Y. ZIV, A. SARTIEL *et al.*, 1995 The complete sequence of the coding region of the ATM gene reveals similarity to cell cycle regulators in different species. Hum Mol Genet **4:** 2025-2032.

SHILOH, Y., 2003 ATM and related protein kinases: safeguarding genome integrity. Nat Rev Cancer **3:** 155-168.

SHRIVASTAV, N., D. LI and J. M. ESSIGMANN, 2010 Chemical biology of mutagenesis and DNA repair: cellular responses to DNA alkylation. Carcinogenesis **31:** 59-70.

SINGER, M. S., and D. E. GOTTSCHLING, 1994 TLC1: template RNA component of Saccharomyces cerevisiae telomerase. Science **266:** 404-409.

SINGER, M. S., A. KAHANA, A. J. WOLF, L. L. MEISINGER, S. E. PETERSON *et al.*, 1998 Identification of high-copy disruptors of telomeric silencing in Saccharomyces cerevisiae. Genetics **150:** 613-632.

SINGH, D., P. G. FEBBO, K. ROSS, D. G. JACKSON, J. MANOLA *et al.*, 2002 Gene expression correlates of clinical prostate cancer behavior. Cancer cell **1:** 203-209.

SMOLKA, M. B., C. P. ALBUQUERQUE, S. H. CHEN and H. ZHOU, 2007 Proteome-wide identification of in vivo targets of DNA damage checkpoint kinases. Proc Natl Acad Sci U S A **104:** 10364-10369.

SOLER, D., J. PAMPALONA, L. TUSELL and A. GENESCA, 2009 Radiation sensitivity increases with proliferation-associated telomere dysfunction in nontransformed human epithelial cells. Aging Cell **8:** 414-425.

SOTIRIOU, C., and M. J. PICCART, 2007 Taking gene-expression profiling to the clinic: when will molecular signatures become relevant to patient care? Nature reviews.Cancer **7:** 545-553.

SOTIRIOU, C., P. WIRAPATI, S. LOI, A. HARRIS, S. FOX *et al.*, 2006 Gene expression profiling in breast cancer: understanding the molecular basis of histologic grade to improve prognosis. Journal of the National Cancer Institute **98:** 262-272.

STELLWAGEN, A. E., Z. W. HAIMBERGER, J. R. VEATCH and D. E. GOTTSCHLING, 2003 Ku interacts with telomerase RNA to promote telomere addition at native and broken chromosome ends. Genes Dev **17:** 2384-2395.

STOREY, J. D., and R. TIBSHIRANI, 2003 Statistical significance for genomewide studies. Proc Natl Acad Sci U S A **100:** 9440-9445.

SUBRAMANIAN, A., P. TAMAYO, V. K. MOOTHA, S. MUKHERJEE, B. L. EBERT *et al.*, 2005 Gene set enrichment analysis: a knowledge-based approach for interpreting genome-wide expression profiles. Proceedings of the National Academy of Sciences of the United States of America **102:** 15545-15550.

SUN, Y., X. JIANG, S. CHEN, N. FERNANDES and B. D. PRICE, 2005 A role for the Tip60 histone acetyltransferase in the acetylation and activation of ATM. Proceedings of the National Academy of Sciences of the United States of America **102:** 13182-13187.

SUN, Y., X. JIANG and B. D. PRICE, 2010 Tip60: connecting chromatin to DNA damage signaling. Cell Cycle **9:** 930-936.

SUN, Y., Y. XU, K. ROY and B. D. PRICE, 2007 DNA damage-induced acetylation of lysine 3016 of ATM activates ATM kinase activity. Mol Cell Biol **27:** 8502-8509.

SUN, Z., D. S. FAY, F. MARINI, M. FOIANI and D. F. STERN, 1996 Spk1/Rad53 is regulated by Mec1-dependent protein phosphorylation in DNA replication and damage checkpoint pathways. Genes Dev **10:** 395-406.

SVENSSON, J. P., L. J. STALPERS, R. E. ESVELDT-VAN LANGE, N. A. FRANKEN, J. HAVEMAN *et al.*, 2006 Analysis of gene expression using gene sets discriminates cancer patients with and without late radiation toxicity. PLoS medicine **3:** e422.

SWIFT, M., D. MORRELL, E. CROMARTIE, A. R. CHAMBERLIN, M. H. SKOLNICK *et al.*, 1986 The incidence and gene frequency of ataxia-telangiectasia in the United States. Am J Hum Genet **39:** 573-583.

TAMAKAWA, R. A., H. B. FLEISIG and J. M. WONG, 2010 Telomerase inhibition potentiates the effects of genotoxic agents in breast and colorectal cancer cells in a cell cycle-specific manner. Cancer Res **70:** 8684-8694.

TEIXEIRA, M. T., M. ARNERIC, P. SPERISEN and J. LINGNER, 2004 Telomere length homeostasis is achieved via a switch between telomerase- extendible and -nonextendible states. Cell **117:** 323-335.

TENG, S. C., and V. A. ZAKIAN, 1999 Telomere-telomere recombination is an efficient bypass pathway for telomere maintenance in Saccharomyces cerevisiae. Mol Cell Biol **19:** 8083-8093.

THOMPSON, D., S. DUEDAL, J. KIRNER, L. MCGUFFOG, J. LAST *et al.*, 2005 Cancer risks and mortality in heterozygous ATM mutation carriers. J Natl Cancer Inst **97:** 813-822.

THOR, A. D., D. H. MOORE, II, S. M. EDGERTON, E. S. KAWASAKI, E. REIHSAUS *et al.*, 1992 Accumulation of p53 tumor suppressor gene protein: an independent marker of prognosis in breast cancers. Journal of the National Cancer Institute **84:** 845-855.

THORLACIUS, S., B. THORGILSSON, J. BJORNSSON, L. TRYGGVADOTTIR, A. L. BORRESEN *et al.*, 1995 TP53 mutations and abnormal p53 protein staining in breast carcinomas related to prognosis. European journal of cancer (Oxford, England : 1990) **31A:** 1856-1861.

TKACH, J. M., A. YIMIT, A. Y. LEE, M. RIFFLE, M. COSTANZO *et al.*, 2012 Dissecting DNA damage response pathways by analysing protein localization and abundance changes during DNA replication stress. Nat Cell Biol **14:** 966-976.

TONG, A. H., and C. BOONE, 2006 Synthetic genetic array analysis in Saccharomyces cerevisiae. Methods Mol Biol **313:** 171-192.

TONG, A. H., M. EVANGELISTA, A. B. PARSONS, H. XU, G. D. BADER *et al.*, 2001 Systematic genetic analysis with ordered arrays of yeast deletion mutants. Science (New York, N.Y.) **294:** 2364-2368.

TRAVEN, A., A. HAMMET, N. TENIS, C. L. DENIS and J. HEIERHORST, 2005 Ccr4-not complex mRNA deadenylase activity contributes to DNA damage responses in Saccharomyces cerevisiae. Genetics **169:** 65-75.

TSUKAMOTO, Y., A. K. TAGGART and V. A. ZAKIAN, 2001 The role of the Mre11-Rad50-Xrs2 complex in telomerase- mediated lengthening of Saccharomyces cerevisiae telomeres. Curr Biol **11:** 1328-1335.

TUSHER, V. G., R. TIBSHIRANI and G. CHU, 2001 Significance analysis of microarrays applied to the ionizing radiation response. Proc Natl Acad Sci U S A **98:** 5116-5121.

UZIEL, T., Y. LERENTHAL, L. MOYAL, Y. ANDEGEKO, L. MITTELMAN *et al.*, 2003 Requirement of the MRN complex for ATM activation by DNA damage. EMBO J **22:** 5612-5621.

VALENTIN-VEGA, Y. A., and M. B. KASTAN, 2012 A new role for ATM: regulating mitochondrial function and mitophagy. Autophagy **8:** 840-841.

VALENTIN-VEGA, Y. A., K. H. MACLEAN, J. TAIT-MULDER, S. MILASTA, M. STEEVES *et al.*, 2012 Mitochondrial dysfunction in ataxia-telangiectasia. Blood **119:** 1490-1500.

VAN 'T VEER, L. J., H. DAI, M. J. VAN DE VIJVER, Y. D. HE, A. A. HART *et al.*, 2002 Gene expression profiling predicts clinical outcome of breast cancer. Nature **415:** 530-536.

VAN DE VIJVER, M. J., Y. D. HE, L. J. VAN'T VEER, H. DAI, A. A. HART *et al.*, 2002 A gene-expression signature as a predictor of survival in breast cancer. The New England journal of medicine **347:** 1999-2009.

VERNON, M., K. LOBACHEV and T. D. PETES, 2008 High rates of "unselected" aneuploidy and chromosome rearrangements in tel1 mec1 haploid yeast strains. Genetics.

WANG, Y., J. G. KLIJN, Y. ZHANG, A. M. SIEUWERTS, M. P. LOOK *et al.*, 2005 Gene-expression profiles to predict distant metastasis of lymph-node-negative primary breast cancer. Lancet **365:** 671-679.

WEINERT, T. A., G. L. KISER and L. H. HARTWELL, 1994 Mitotic checkpoint genes in budding yeast and the dependence of mitosis on DNA replication and repair. Genes Dev **8:** 652-665.

WEST, M., C. BLANCHETTE, H. DRESSMAN, E. HUANG, S. ISHIDA *et al.*, 2001 Predicting the clinical status of human breast cancer by using gene expression profiles. Proceedings of the National Academy of Sciences of the United States of America **98:** 11462-11467.

WESTMORELAND, T. J., J. R. MARKS, J. A. OLSON, JR., E. M. THOMPSON, M. A. RESNICK *et al.*, 2004 Cell cycle progression in G1 and S phases is CCR4 dependent following ionizing radiation or replication stress in Saccharomyces cerevisiae. Eukaryot Cell **3:** 430-446.

WINZELER, E. A., D. D. SHOEMAKER, A. ASTROMOFF, H. LIANG, K. ANDERSON *et al.*, 1999 Functional characterization of the S. cerevisiae genome by gene deletion and parallel analysis. Science (New York, N.Y.) **285:** 901-906.

WONG, K. K., S. CHANG, S. R. WEILER, S. GANESAN, J. CHAUDHURI *et al.*, 2000 Telomere dysfunction impairs DNA repair and enhances sensitivity to ionizing radiation. Nat Genet **26:** 85-88.

WOO, S. R., J. E. PARK, K. M. JUHN, Y. J. JU, J. JEONG *et al.*, 2012 Cells with dysfunctional telomeres are susceptible to reactive oxygen species hydrogen peroxide via generation of multichromosomal fusions and chromosomal fragments bearing telomeres. Biochem Biophys Res Commun **417:** 204-210.

WOOLSTENCROFT, R. N., T. H. BEILHARZ, M. A. COOK, T. PREISS, D. DUROCHER *et al.*, 2006 Ccr4 contributes to tolerance of replication stress through control of CRT1 mRNA poly(A) tail length. J Cell Sci **119:** 5178-5192.

WOOSTER, R., G. BIGNELL, J. LANCASTER, S. SWIFT, S. SEAL *et al.*, 1995 Identification of the breast cancer susceptibility gene BRCA2. Nature **378:** 789-792.

WU, Y., P. A. DIMAGGIO, JR., D. H. PERLMAN, V. A. ZAKIAN and B. A. GARCIA, 2013 Novel Phosphorylation Sites in the S. cerevisiae Cdc13 Protein Reveal New Targets for Telomere Length Regulation. J Proteome Res **12:** 316-327.

WU, Y., S. XIAO and X. D. ZHU, 2007 MRE11-RAD50-NBS1 and ATM function as co-mediators of TRF1 in telomere length control. Nat Struct Mol Biol **14:** 832-840.

YANG, J., Y. YU, H. E. HAMRICK and P. J. DUERKSEN-HUGHES, 2003 ATM, ATR and DNA-PK: initiators of the cellular genotoxic stress responses. Carcinogenesis **24:** 1571-1580.

ZHAO, X., A. CHABES, V. DOMKIN, L. THELANDER and R. ROTHSTEIN, 2001 The ribonucleotide reductase inhibitor Sml1 is a new target of the Mec1/Rad53 kinase cascade during growth and in response to DNA damage. EMBO J **20:** 3544-3553.

ZHAO, X., and R. ROTHSTEIN, 2002 The Dun1 checkpoint kinase phosphorylates and regulates the ribonucleotide reductase inhibitor Sml1. Proc Natl Acad Sci U S A **99:** 3746-3751.

ZOU, L., and S. J. ELLEDGE, 2003 Sensing DNA damage through ATRIP recognition of RPA-ssDNA complexes. Science **300:** 1542-1548.

VITA

Brian Piening was born in Freehold, New Jersey and spent most of his formative years in the Garden State. Brian attended college at the University of Washington in Seattle where he earned a Bachelor's of Science in Physics and Astronomy. Brian's graduate training was performed at the University of Washington and Fred Hutchinson Cancer Research Center, and he was awarded the degree of Doctor of Philosophy in Molecular and Cellular Biology in 2013.